

# Force transmission in the tibio-femoral contact complex

**Citation for published version (APA):**

Schreppers, G. J. M. A. (1991). *Force transmission in the tibio-femoral contact complex*. [Phd Thesis 1 (Research TU/e / Graduation TU/e), Mechanical Engineering]. Technische Universiteit Eindhoven.  
<https://doi.org/10.6100/IR354560>

**DOI:**

[10.6100/IR354560](https://doi.org/10.6100/IR354560)

**Document status and date:**

Published: 01/01/1991

**Document Version:**

Publisher's PDF, also known as Version of Record (includes final page, issue and volume numbers)

**Please check the document version of this publication:**

- A submitted manuscript is the version of the article upon submission and before peer-review. There can be important differences between the submitted version and the official published version of record. People interested in the research are advised to contact the author for the final version of the publication, or visit the DOI to the publisher's website.
- The final author version and the galley proof are versions of the publication after peer review.
- The final published version features the final layout of the paper including the volume, issue and page numbers.

[Link to publication](#)

**General rights**

Copyright and moral rights for the publications made accessible in the public portal are retained by the authors and/or other copyright owners and it is a condition of accessing publications that users recognise and abide by the legal requirements associated with these rights.

- Users may download and print one copy of any publication from the public portal for the purpose of private study or research.
- You may not further distribute the material or use it for any profit-making activity or commercial gain
- You may freely distribute the URL identifying the publication in the public portal.

If the publication is distributed under the terms of Article 25fa of the Dutch Copyright Act, indicated by the "Taverne" license above, please follow below link for the End User Agreement:

[www.tue.nl/taverne](http://www.tue.nl/taverne)

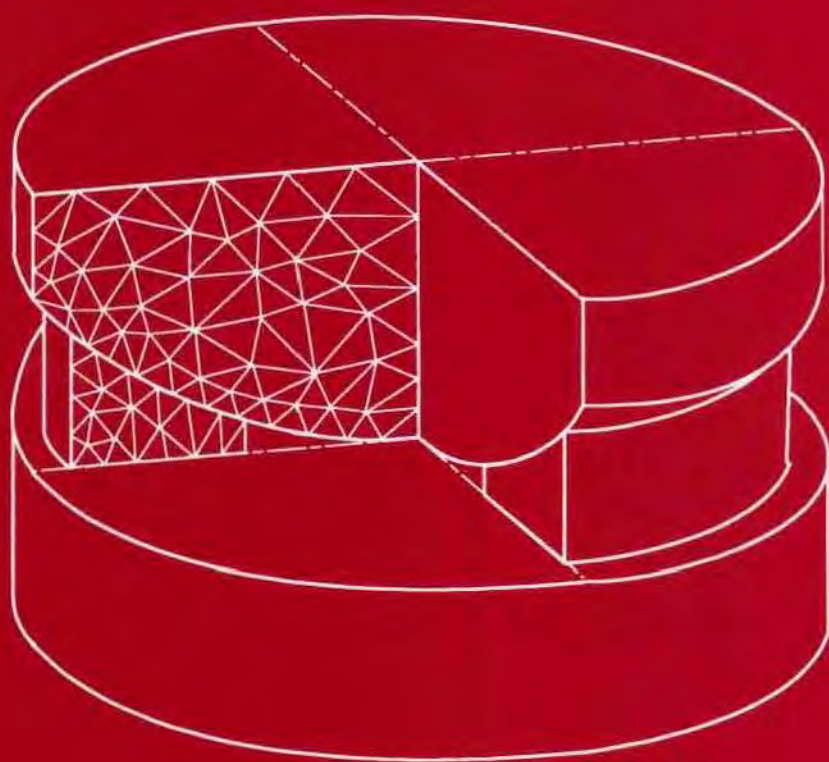
**Take down policy**

If you believe that this document breaches copyright please contact us at:

[openaccess@tue.nl](mailto:openaccess@tue.nl)

providing details and we will investigate your claim.

**FORCE TRANSMISSION IN THE  
TIBIO-FEMORAL CONTACT COMPLEX**



**Gerd-Jan Schreppers**

**FORCE TRANSMISSION IN THE  
TIBIO-FEMORAL CONTACT COMPLEX**

CIP-DATA KONINKLIJKE BIBLIOTHEEK, DEN HAAG

Schreppers, Gerd-Jan Marie Antoin

Force transmission in the tibio-femoral contact complex /

Gerd-Jan Marie Antoin Schreppers. - [S.l. : s.n.]

(Enschede : Febodruk). - I11.

Thesis Eindhoven. - With ref. - With summary in Dutch.

ISBN 90-9004229-6 bound

Subject headings: applied mechanics /

biomedical engineering.

**FORCE TRANSMISSION IN THE  
TIBIO-FEMORAL CONTACT COMPLEX**

**PROEFSCHRIFT**

ter verkrijging van de graad van doctor  
aan de Technische Universiteit Eindhoven,  
op gezag van de Rector Magnificus, prof.dr. J.H. van Lint,  
voor een commissie aangewezen door het College van Dekanen  
in het openbaar te verdedigen  
op woensdag 26 juni 1991 om 16.00 uur

door

**GERD-JAN MARIE ANTOIN SCHREPPERS**

geboren op 7 oktober 1963 te Gendringen

Dit proefschrift is goedgekeurd door de promotoren

prof.dr.ir. D.H. van Campen

en

prof.dr. A. Huson

co-promotor

dr.ir. A.A.H.J. Sauren

*To my father and mother  
and Marian*

# CONTENTS

## SUMMARY

## NOTATION

<b>1</b>	<b>INTRODUCTION</b>	<b>1</b>
1.1	<i>motivation and objectives</i>	1
1.2	<i>modelling strategy</i>	4
1.3	<i>functional description of joint elements</i>	4
1.4	<i>perspective and structure of this thesis</i>	8
1.5	<i>summary and conclusions</i>	9
<b>2</b>	<b>NUMERICAL FORMULATION</b>	<b>11</b>
2.1	<i>introduction</i>	11
2.2	<i>description and discretization of coupled sub-systems</i>	11
2.3	<i>general elaboration of solution strategies</i>	14
2.4	<i>solid-solid contact with large sliding</i>	17
2.4.1	<i>continuous formulation of contact behaviour</i>	18
2.4.2	<i>discretization and solution strategy</i>	19
2.4.3	<i>contact state transitions</i>	22
2.4.4	<i>examples</i>	24
2.5	<i>discussion</i>	28
2.6	<i>summary and conclusions</i>	29
<b>3</b>	<b>CARTILAGE AND MENISCUS</b>	<b>31</b>
3.1	<i>introduction</i>	31
3.2	<i>reference model</i>	33
3.3	<i>parameter studies</i>	36
3.3.1	<i>bony components</i>	36
3.3.2	<i>meniscal ring</i>	43
3.4	<i>model reductions</i>	46
3.5	<i>experimental analysis</i>	49
3.6	<i>summary and conclusions</i>	57

<b>4</b>	<b>FORMULATION OF MIXTURE INTERACTION</b>	<b>59</b>
4.1	<i>introduction</i>	59
4.2	<i>mixture</i>	59
4.3	<i>fluid</i>	65
4.4	<i>interface conditions</i>	67
4.4.1	<i>introduction</i>	67
4.4.2	<i>interaction between sealed mixture sub-systems</i>	68
4.4.3	<i>interaction between mixtures not being sealed</i>	69
4.4.4	<i>other interactions</i>	71
4.5	<i>summary and conclusions</i>	71
<b>5</b>	<b>INCORPORATION OF FLUID AND MIXTURES IN THE TIBIO-FEMORAL CONTACT MODEL</b>	<b>73</b>
5.1	<i>introduction</i>	73
5.2	<i>description of the model</i>	74
5.3	<i>parameter studies</i>	78
5.3.1	<i>introduction</i>	78
5.3.2	<i>interface conditions</i>	78
5.3.3	<i>loadings</i>	84
5.3.4	<i>surface geometry</i>	86
5.4	<i>summary and conclusions</i>	87
<b>6</b>	<b>CONCLUSIONS AND RECOMMENDATIONS</b>	<b>89</b>
6.1	<i>conclusions</i>	89
6.2	<i>recommendations</i>	91
	<b>REFERENCES</b>	<b>93</b>
	<b>APPENDICES</b>	<b>99</b>
<b>A</b>	<i>directly and iteratively coupled solution methods</i>	<b>99</b>
<b>B</b>	<i>constitutive behaviour of silicone rubber</i>	<b>103</b>
	<b>SAMENVATTING</b>	<b>109</b>

## SUMMARY

The objective of this study is to increase the insight into the mechanical function of the joint elements in the tibio-femoral contact complex. The relevant joint elements are tibia, femur, cartilage layers, menisci and synovial fluid. The function of the single elements is affected by interaction with other elements. A stepwise modelling approach is adopted in which it is started with simple models. During every step, parameter studies are executed to investigate the function of the relevant components. Numerical analyses, based on the finite element method, are performed and validated by experiments on physical models.

The contact problem is defined by equilibrium conditions for the set of sub-systems and the appropriate contact conditions. Both contact conditions and contact forces are generally dependent on the positions and the deformation field of all the sub-systems in the problem. For the large sliding solid-solid interaction problem a formulation is worked out for which friction is assumed to be zero. The presented algorithm proves to be quite satisfactory for general contact problems.

An axisymmetric model has been utilized for the analysis of the force transmission between the tibia-meniscus-femur connection. The model assumes linear elastic material properties, static loading and frictionless sliding contact between the components. The study explores the effects of the tibial surface geometry, of the presence of soft layers on the bony components and of anisotropic properties of the meniscus. Studies with eight combinations of parameters have been performed starting from a simple reference model. The presence of articular layers and the circumferential stiffness of the meniscus appeared to be very important for the load distribution.

The numerical formulation was extended in such a way that model components can be considered as mixtures of a solid and a fluid phase. Interaction between mixtures and interaction between mixtures and fluids can be described. In the model of the tibio-femoral contact complex the cartilage layer and the meniscus are considered as mixtures. These components interact with an ideal fluid, representing the synovia. Frictionless sliding in the contacts between these sub-systems is allowed. The response of the model for a step change in the load was calculated. Investigations are performed concerning the effects of the permeability of surfaces and of different loading magnitudes. The load distribution in the model appears to change considerably in the course of time.

## NOTATION

$a$	scalar
$\underline{a}$	column
$\underline{\underline{A}}$	matrix
$\vec{a}$	vector
$\mathbf{A}$	tensor
$\mathbf{I}$	unit tensor
$\underline{a}^T$	transpose of $\underline{a}$
$\mathbf{A}^c$	conjugate of $\mathbf{A}$
$\vec{a}\vec{b}$	dyadic product of $\vec{a}$ and $\vec{b}$
$\vec{a} \cdot \vec{b}$	inner product of $\vec{a}$ and $\vec{b}$
$\mathbf{A} : \mathbf{B}$	double inner product of $\mathbf{A}$ and $\mathbf{B}$

## INTRODUCTION

### *1.1 motivation and objectives*

The investigations presented in this thesis aim at obtaining fundamental insight into the mechanical behaviour of the tibio-femoral joint. In this joint various elements can be distinguished such as femur, tibia, articular cartilage layers, menisci, synovial fluid, joint capsule, ligaments, muscles etc.

During the past decades a large amount of literature has been published on the tibio-femoral joint. In spite of these publications the knowledge concerning the mechanical function of the distinct joint elements is limited and mainly qualitative in character. For that reason the effects of surgical and non-surgical interventions to improve joint function and the outcome of rehabilitation therapies can often be predicted and evaluated only by extrapolation from clinical experiences. A validated mathematical model of the knee joint would constitute a valuable tool for making predictions and evaluations based on fundamental insight rather than on experience.

To get insight into some mechanical characteristics of the human knee joint an exploratory experimental investigation has been carried out in our laboratory ( Dortmans ( 1988 ), Jans et al. ( 1988 ), Dortmans et al. ( 1991<sup>a+b</sup> ) ). The purpose of the experiments was twofold. Firstly, the possibility was investigated of quantifying the transmission of dynamic loads through the joint in terms of stiffness and damping characteristics that are based on linear theories. Secondly, it was examined whether changes in the load transmission, brought about by deliberately damaging of selected joint elements, may provide an indication about the function of these elements.

Experiments were carried out with cadaveric knee joint specimens, consisting of the distal part of the femur and the proximal part of the tibia. A limited number of muscle tendons were preserved but the muscular tissues had been removed entirely. At the femoral side the specimens were rigidly clamped onto a three-dimensional force

platform by means of which reaction forces and torques could be measured. Static forces were exerted on three tendons to maintain a static equilibrium configuration of the joint. Dynamic loads were applied on the distal end of the tibia. The magnitude of these loads was chosen in such a way that only small displacements of the tibia relative to the femur occurred.

The results of the experiments lead to the conclusion that the dynamic behaviour of the human knee joint is essentially non-linear. Furthermore, it was found that, although damaging a particular joint element like a meniscus or a cruciate ligament yields significant changes in the dynamic behaviour, interpretation of these changes in terms of ( changes in ) the function of that element is difficult and actually not possible if one cannot rely on a non-linear model of the joint. Such a model should comprise parameters that can be interpreted in terms of properties and functions of joint elements and their interactions. However, the development of such a model for the complete knee joint is not feasible in view of its complex structure and because of the lack of experimental data needed both in the determination of model system parameters and in the validation of the model.

As may be clear from the foregoing the complete knee joint is a very intricate structure. From a mechanical point of view the tibio-femoral joint can be considered as a complex load transmitting connection. In order to model the knee joint, it is considered to be made up of three interacting sub-connections, constituted by

- capsule and ligaments,
- muscles, tendons and related fibrous sheaths,
- the contact ( direct and indirect via both the menisci and the synovial fluid ) between the cartilage layers.

Apart from the complex structure of the tibio-femoral joint, two main problems with which one is confronted in modelling the knee joint are distinguished:

- The first problem is the determination of material characteristics of biological structures. Conventional methods take for granted that samples have a well determined geometry. A sample is isolated from the structure under consideration and it is loaded with the intention to achieve a homogeneous stress and strain distribution in at least a part of the sample. However, in biological tissues severe disturbance of the structural integrity may result from the separation of the sample from its natural surroundings. Moreover, the tissue is often highly

inhomogeneous and anisotropic. Therefore, conventional methods are in fact not suitable to assess the material properties of biological tissues. Hendriks ( 1991 ) proposed a hybrid numerical-experimental approach which is not limited to homogeneous stress and strain fields. This alternative approach seems to offer promising prospects for biological tissues.

- The other problem concerns the identification of characteristics for the contact between the cartilage layers. The available techniques for identifying of the frictional behaviour in contact surfaces start from the point that at least one contact surface is rigid ( e.g. Starmans ( 1989 ) ). In that case transducers can be integrated in the rigid component at the contact surface without disturbing the load transmission, while this is not possible in deformable bodies. As surfaces are soft and deformable in the contact between cartilage layers only global observations can be made while local effects cannot be measured. Another aspect of the identification of the contact characteristics is the hydrated character of cartilage. This is a very difficult problem as no data are available with respect to the fluid-mixture interaction because of the deficiency of suitable experimental techniques. The appropriate interface conditions can neither be fully derived from theoretical considerations. Therefore, some of these conditions are arbitrarily chosen. The relation between the tangential fluid velocity of the free fluid and the fluid bounded to the tissue is an example of a condition that cannot be deduced from theoretical considerations. Hou et al. ( 1989 ) proposed the 'pseudo-no-slip' kinematic boundary condition for this velocity, which is explained into more detail in chapter 5. They got physically likely results.

The first problem is related to all sub-connections in the tibio-femoral joint, while the second problem is affiliated with the sub-connection of the contact between the cartilage layers. With respect to these problems more fundamental research has to be performed before an experimentally validated mathematical model for describing the dynamic behaviour of the human knee joint can be achieved.

The objective of this thesis is to evaluate a model describing some essential aspects of the mechanical behaviour of the tibio-femoral joint. In particular the present study is focussed on the direct and indirect contact between the cartilage layers.

## 1.2 modelling strategy

The approach for the modelling process adopted in the present study can be characterized as follows: At first instance the sub-connections as presented in the previous section are taken into account separately. From considerations mentioned before, it is started with models which are strongly abstracted, especially concerning the material and frictional behaviour in the contacts. These models are developed step by step into more realistic models of the concerned sub-connection. A numerical-mathematical formulation is applied. The mechanical functions of the joint elements within a particular sub-connection and the interactions of these elements resulting from their structural relationships are investigated using parameter studies during every step. It has to be checked whether the mechanical characteristics, displayed by the model, suffer from artefacts which may be caused by the application of a particular numerical technique. Therefore, validation experiments are carried out on physical models. For the present, both numerical and physical models are strong simplifications of reality and thus one has to be careful translating these functions to the real knee joint. However, the explored functions of joint elements in the actual model will play an important role in choosing adaptations of the model with respect to the next step in the modelling process. After some time more realistic descriptions of the geometry, the constitutive behaviour and the interaction of the elements will be attained. When more insight into the distinct sub-connections has been achieved, they can be integrated into a model of the complete knee joint. Finally, when such a model is rather complete, validation experiments can be carried out on real biological structures.

## 1.3 functional description of joint elements

The relevant elements in the sub-connection of the direct and indirect contact are the bony ends of femur and tibia, their articular cartilage layers, the menisci and the synovial fluid. A functional description of these elements is given in the following.

### bone

By and large two forms of bony structure can be distinguished in adult bone. The more massively built and relatively rigid is called cortical bone while the more lightly built and weaker form is indicated as trabecular bone. Cortical and trabecular bone

largely differ in stiffness ( e.g. Hayes ( 1986 ) ). In comparison to other joint components the time-dependent and viscous effects of the material behaviour of the bony components may be considered as very small.

Both the femur and the tibia may be imagined as a long hollow shaft of cortical bone which ends in plugs of trabecular bone just under the pair of tibio-femoral contact surfaces. The two articular surfaces of the distal femoral end are constituted by two convex condyles while the tibial surfaces comprise convex and concave curvatures. Both pairs of contact surfaces are incongruent.

### articular cartilage

Articular cartilage is a bluish semi-transparent dense connective tissue that covers the bony articulating ends. According to Mow et al. ( 1984 ) articular cartilage may be considered as a porous composite organic solid matrix swollen by water ( Fig. 1.1 ). In the water a variety of mobile electrolytes is distributed which maintain charge neutrality of the ionized proteoglycan aggregates of the matrix.

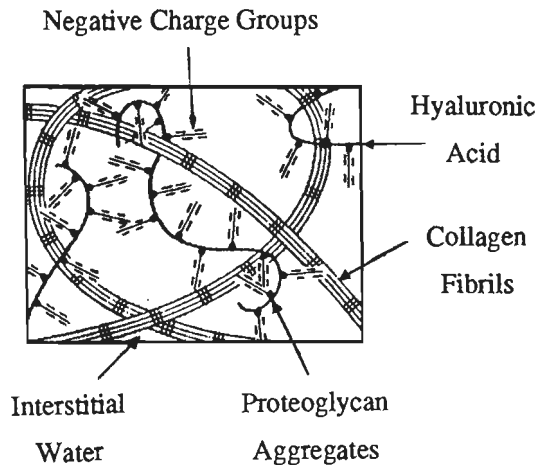


Fig. 1.1 *Schematic representation of articular cartilage as a biphasic medium. The solid matrix phase is mainly composed of a mixture of proteoglycans and a collagen network. The fluid phase is mainly water ( Mow et al. ( 1984 ) ).*

In mechanical terms it is a multi-phasic non-linearly permeable anisotropic visco-elastic material, consisting of two principal phases: A solid organic matrix, which is composed predominantly of collagen fibrils and proteoglycan macro-molecules, and a movable interstitial fluid phase, which is predominantly water.

Within the cartilage different sub-layers can be distinguished according to studies as by e.g. Minns and Steven ( 1977 ). It is generally accepted that the deepest layer consists of calcified cartilage and is fixed to the underlying bone. In the deepest and middle layer collagen fibres are lying perpendicular to the contact surface. Superficially these fibres make up a dense and irregular network and are oriented more parallel to the outer surface.

The total thickness of the cartilage layers in the tibio-femoral contact area has been measured by Swann and Seedhom ( 1989 ). They found this thickness varying from about 1.5 to 4.0 mm.

*menisci*

The menisci are semi-lunar components with wedge-shaped cross-sections. They fairly well fill the space between the incongruent articular surfaces. Posterior and anterior

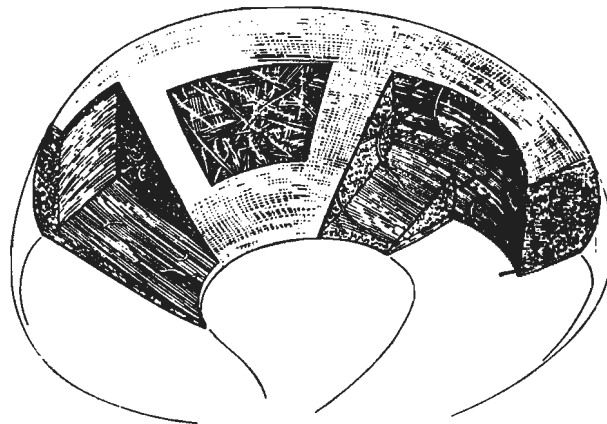


Fig. 1.2                    *Meniscal structure according to Bullough et al. ( 1970 ).*

horns of both menisci are fixed to the centre of the tibial surface. Further, some attachments to the capsule exist at the outer circumference of the menisci and the anterior horns are connected by a ligament. Likewise there are rather frequently posterior ligamentous attachments of the lateral meniscus to the femoral component. Both menisci have a fibrous structure. Bullough et al. ( 1970 ) investigated this structure ( Fig. 1.2 ) and found that the fibres were mainly oriented circumferentially. Only a few radially oriented fibres occur inside the meniscal bodies. Superficially a fibrous netting is observed which may resist longitudinal splitting of the meniscus.

In earlier years opinions have differed on the function of the menisci in the tibio-femoral joint. Fairbank ( 1948 ) indicated the relationship between the outward displacements of the loaded meniscus and its load-bearing capacity. Since then the function of the meniscus has been the subject of laboratory experiments and clinical studies ( e.g. Ahmed and Burke ( 1983 ), Kurosawa et al. ( 1980 ), Fahmy et al. ( 1983 ), Jaspers et al. ( 1980 ), Walker and Hajek ( 1972 ), Walker and Erkman ( 1975 ) ) and more and more agreement was reached with respect to the importance of the load-bearing function of the meniscus. Theoretical models for the load transmission in the meniscus will be dealt with in chapter 3.

In addition to its load transmitting function also some importance with regard to joint lubrication is attributed to the meniscus. Mac Conaill ( 1932 ) made the first attempt to develop a coherent theory about joint lubrication. He stated that the hydrodynamic action determines the friction in synovial joints. He also suggested that the menisci set themselves at a slight inclination and thus act like Mitchell tilting pads. Because of the predominantly intermittent motion of the knee joint Mac Conaill's suggestion is not very likely to apply.

According to De Keizer ( 1976 ) the enclosure by the menisci of the direct contact area in the joint prevents the synovial fluid to be squeezed out of this area.

Jaspers ( 1982 ) performed *in vitro* investigations with respect to the shock absorbing capacity of the meniscus. Porcine knee joints were used for this purpose, which generally have thicker and broader menisci than human joints. Damping of the movement resulting from the applied load was found to be larger after meniscectomy. This effect was credited to the larger sliding movements of articular contact surfaces in the case the menisci were removed.

synovial fluid

The healthy human knee joint contains only a small volume of synovial fluid. This fluid comprises a hydrated hyaluronic acid-protein complex. These large molecules cause the synovial fluid to have a viscosity that decreases with increasing shear rate ( Radin and Paul ( 1971 ), Droogendijk ( 1984 ) ).

*1.4 perspective and structure of this thesis*

As has already been stated in section 1.1, the present study is intended to provide a model of the sub-connection transmitting loads via the contact between femur and tibia, both by direct contact of the cartilage covered articular surfaces and indirectly via the menisci and the synovial fluid. Such a model should meet the following requirements:

- The final model should comprise the relevant joint elements such as bones, articular cartilage, meniscus and synovial fluid.
- These elements should be deformable while they are allowed to make large movements relative to each other.
- Simulation of solid-solid as well as fluid-solid interactions should be possible.

As an initial step a model with a straightforward geometry and material behaviour is considered. Because in future models more complex geometries and material properties will be used, the finite element method is a suitable tool for the analysis.

In chapter 2 the numerical formulation of the solid-solid interaction problem is described in such a way that several kinds of interaction between the joint elements can be taken into account. The large sliding contact interaction without friction is specified in this chapter into detail. Chapter 3 describes the first step in the modelling process. Starting from a reference model parameter studies concerning geometrical and material aspects of the bony components and the meniscal ring are performed. In chapter 4 the formulation of the solid-solid interaction problem is extended in such a way that also mixture-solid, mixture-mixture, fluid-solid and fluid-mixture contact can be described. Further, in chapter 5 the second step in the modelling process is made by taking into account the joint fluid. Finally, some conclusions and recommendations with respect to the continuation of these investigations are given in chapter 6.

### *1.5 summary and conclusions*

The objective of this study is to increase the insight into the mechanical function of the joint elements in the tibio-femoral contact complex. This insight cannot be obtained from the material and geometrical properties of the concerned elements separately, because their function is affected by interaction with other elements. These interactions make establishing the mechanical functions of joint elements a very difficult job. Therefore, a stepwise modelling approach is adopted. During every step, parameter studies are performed to investigate the function of the relevant components. Also numerical analyses are executed and validated by experiments on physical models.



## NUMERICAL FORMULATION

### 2.1 introduction

In the present study mathematical models of the load transmission in the tibio-femoral contact area will be formulated by means of the finite element method. This finite element formulation should be capable of simulating solid-solid, solid-mixture, mixture-mixture, fluid-solid and fluid-mixture interactions.

In this chapter a general approach for modelling the mechanical interaction of coupled sub-systems is described. After the definition of the problem, two different solution strategies are discussed. Further, the solid-solid interaction without friction but with large relative sliding of the contact surfaces is worked out. This interaction is a good starting point of the modelling process as the contact of the cartilage layers in the real knee joint can reasonably be characterized as frictionless ( e.g. Radin and Paul ( 1972 ) ). The elaboration of other kinds of interactions will be dealt with in chapter 4.

### 2.2 description and discretization of coupled sub-systems

Consider a mechanical system comprising several possibly interacting sub-systems, each of which can be represented as a continuum. By a continuum is meant either a solid, a fluid or a mixture of a solid phase and a fluid phase.

Both solid and mixture continua are usually described using a Lagrangian formulation while fluids are usually described using an Eulerian formulation. For the sake of simplicity both solids and mixtures will be denoted by the collective noun 'structure'.

---

*The part of this chapter concerning the solid-solid contact with large sliding has been submitted for publication.*

In the following sub-system  $j$  is assumed to be a structure and related quantities will be marked by the left subscript  $j$ . The volume of the sub-system is denoted by  ${}_jV$ . A material point  $P$  on the outer surface of this sub-system is identified by its material coordinates

$$\underset{\sim}{\xi}^P = \begin{bmatrix} \xi_1^P \\ \xi_2^P \end{bmatrix} \quad (2.1)$$

The total outer surface that comprises all material points on the boundary of the sub-system is indicated by  ${}_jA$ . It is supposed that this surface is smooth, such that the normal direction is uniquely defined. The total outer surface of the sub-system under consideration is decomposed according to

$${}_jA = {}_jA_n + {}_jA_c \quad (2.2)$$

where  ${}_jA_c$  is a fixed set of material points which are possibly interacting with points of other sub-systems or other points of  ${}_jA_c$ , and  ${}_jA_n$  is the complement of  ${}_jA$  and  ${}_jA_c$ . Points of  ${}_jA_c$  can be free or interacting. Assuming body forces to be negligible, the weak formulation of equilibrium reads

$${}_jV \int ({}_j\vec{\nabla} \cdot {}_j\vec{\sigma})^c : {}_j\sigma \, d{}_jV - \int_{{}_jA_n} {}_j\vec{w} \cdot {}_j\vec{p} \, d{}_jA - \int_{{}_jA_c} {}_j\vec{w} \cdot {}_j\vec{p}_c \, d{}_jA = 0 \quad (2.3)$$

where  ${}_j\sigma$  is the Cauchy stress tensor,  ${}_j\vec{w}$  is an arbitrary vector weighting function and  ${}_j\vec{\nabla}$  the gradient operator with respect to the actual configuration of sub-system  $j$ . The load on  ${}_jA_n$  and  ${}_jA_c$  is represented by  ${}_j\vec{p}$  and  ${}_j\vec{p}_c$  respectively, where  ${}_j\vec{p}_c$  generally will depend on the actual state of all the sub-systems under consideration.

For the field of actual position vectors a finite element discretization is introduced according to

$${}_j\vec{x} = {}_j\vec{\alpha}^T \underset{\sim}{j}x \quad (2.4)$$

$\underset{\sim}{j}x$  being the column of nodal coordinates of the sub-system  $j$  with respect to an

appropriate vector base, and  $\vec{j}\underline{\underline{\alpha}}$  being the column with vector interpolation functions expressed in material coordinates. Using a Galerkin approach for the weighting function

$$j\vec{w} = j\underline{\underline{\alpha}}^T j\underline{w} \quad (2.5)$$

with the column  $j\underline{w}$  defined analogous to  $j\underline{x}$ , it can be derived from equation ( 2.3 ) that

$$j\underline{\underline{\alpha}}^T ( j\underline{f} - j\underline{f} - j\underline{c} ) = 0 \quad (2.6)$$

The columns  $j\underline{f}$ ,  $j\underline{f}$  and  $j\underline{c}$  contain the internal nodal forces, the external nodal forces applied on  $jA_n$  and the contact forces on  $jA_c$ , respectively. These columns are defined by the equations

$$j\underline{f} = \int_{jV} ( j\underline{\vec{v}} j\underline{\underline{\alpha}} )^c : j\underline{\sigma} d_jV \quad (2.7)$$

$$j\underline{f} = \int_{jA_n} j\underline{\underline{\alpha}} \cdot j\underline{\vec{p}} d_jA \quad (2.8)$$

$$j\underline{c} = \int_{jA_c} j\underline{\underline{\alpha}} \cdot j\underline{\vec{p}}_c d_jA \quad (2.9)$$

It is supposed that the column of internal forces can be expressed in nodal coordinates of the sub-system by

$$j\underline{f} = j\underline{f}( j\underline{x} ) \quad (2.10)$$

while the column of nodal contact forces will depend on the nodal coordinates of the total system

$$j\underline{c} = j\underline{c}( j\underline{x}_1, \dots, j\underline{x}_z, \dots, z\underline{x} ) \quad (2.11)$$

where  $z$  is the number of sub-systems. The column  $j\underline{f}$  satisfies the user-supplied

dynamic boundary conditions. Corresponding components of  $j\underline{f}$  and  $j\underline{c}$  cannot both be unequal to zero.

The requirement that ( 2.6 ) applies for all arbitrary sets  $j\underline{w}$  results in the balance of nodal forces

$$j\underline{f} - j\underline{f} - j\underline{c} = \underline{0} \quad ( 2.12 )$$

The number of equations in ( 2.12 ) is defined to be  $3j_m$ ,  $j_m$  being equal to the total number of nodes in  $j\underline{V}$ . The number of non-trivial components in  $j\underline{c}$  equals  $3j_n$ ,  $j_n$  being the number of nodes on  $j\underline{A}_c$ .

Besides the equilibrium equations also contact conditions should be satisfied. These conditions control the contact behaviour and comprise both kinematical constraints to material points on the contact surfaces of the interacting sub-systems and restrictions with respect to contact forces.

### 2.3 general elaboration of solution strategies

It is assumed that the interactive behaviour in general will be history-dependent so that the column  $j\underline{c}$  will not only depend on the actual position of the sub-systems, but also on its history. Therefore, an incremental formulation is used. Contact problems will be essentially non-linear and thus for each incremental step the solution has to be calculated using an iterative procedure. The discrete contact problem is formulated by the discretized equilibrium equations with respect to the end of an increment along with the appropriate contact conditions.

Two methods for solving the interaction problem can be distinguished, i.e. the direct fully coupled solution strategy and the iteratively coupled solution strategy ( e.g. Horsten ( 1990 ) ). Both methods are explained underneath for the case where the total system comprises only two sub-systems. A detailed elaboration of a simple example using both strategies is presented in appendix A. In the case of two sub-systems the equilibrium conditions are described by

$$1\underline{f}( 1\underline{x} ) - 1\underline{f} - 1\underline{c}( 1\underline{x}, 2\underline{x} ) = \underline{0} \quad ( 2.13 )$$

$$2\underline{f}( 2\underline{x} ) - 2\underline{f} - 2\underline{c}( 1\underline{x}, 2\underline{x} ) = \underline{0} \quad ( 2.14 )$$

*the iteratively coupled solution strategy*

A summary of this algorithm is given in the flow chart ( Fig. 2.1 ). Consider the sub-systems 1 and 2. At the start of an increment the values of  ${}_1\tilde{\mathbf{x}}$  and  ${}_2\tilde{\mathbf{x}}$  for the converged situation of the previous increment are used as initial estimates.

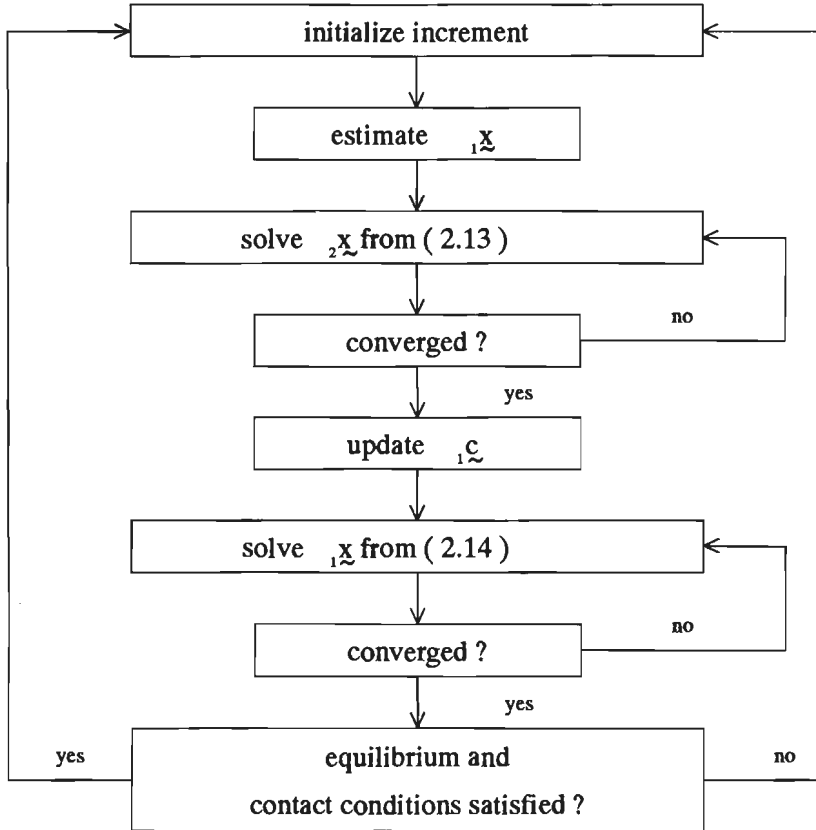


Fig. 2.1 *Flow-chart of the iteratively coupled solution strategy.*

First, with respect to sub-system 2,  ${}_1\tilde{\mathbf{x}}$  is kept constant while a new estimate for the column of coordinates of position vectors  ${}_2\tilde{\mathbf{x}}$  is calculated from the condition

$${}_2\underline{f}({}_2\underline{x}) - {}_2\underline{r} - {}_2\underline{c}({}_2\underline{x}) = \underline{0} \quad (2.15)$$

Next, with this estimate and the contact conditions, the contact forces on  ${}_1A_c$  can be updated and a new estimate for the position of sub-system 1 is calculated (  ${}_2\underline{x}$  is kept constant in the meanwhile ) from the condition

$${}_1\underline{f}({}_1\underline{x}) - {}_1\underline{r} - {}_1\underline{c}({}_1\underline{x}) = \underline{0} \quad (2.16)$$

The attained estimates of  ${}_1\underline{x}$  and  ${}_2\underline{x}$  will generally differ from the initial estimates. New estimates will be calculated starting from the former. This algorithm proceeds until the equilibrium condition as well as the contact constraints are satisfactorily met. Then the increment is considered to be converged and the next increment is started.

the direct fully coupled solution strategy

When the direct fully coupled solution strategy is used, the equilibrium equations for both coupled sub-systems are solved simultaneously under estimated contact conditions with respect to the end of the considered increment. Here,  $A$ ,  $A_n$  and  $A_c$  represent the sets comprising  ${}_jA$ ,  ${}_jA_n$  and  ${}_jA_c$  of all sub-systems, respectively, while  $V$  is the set containing the volumes  ${}_jV$  of all sub-systems. The columns  $\underline{f}$ ,  $\underline{r}$ ,  $\underline{c}$  and  $\underline{x}$  comprise respectively the internal forces, the external forces applied on  $A_n$ , the contact forces acting on  $A_c$  and the coordinates of all nodal points in the system. For every iteration new estimates for both  $\underline{x}$  and the contact conditions are obtained by solving the matrix equation that comprises both sub-systems. Eventually the equilibrium condition

$$\underline{f}(\underline{x}) - \underline{r} - \underline{c}(\underline{x}) = \underline{0} \quad (2.17)$$

for the total system must be satisfied. The number of equations in ( 2.17 ) is defined to be  $3m$ ,  $m$  equal to the total number of nodes in  $V$ . The number of non-trivial components in  $\underline{c}$  equals  $3n$ ,  $n$  being the number of nodes in  $A_c$ . A complication is the combination of the Lagrangian description for the structural system ( nodal points coincide with material points and move together with the structure ) and the Eulerian description for the fluid ( nodal points are fixed in space ).

Comparing both strategies, the direct fully coupling has the disadvantage that the number of equations and the required computer memory increase. On the other hand for the iteratively coupled strategy the number of iterations needed to obtain a solution is larger. This disadvantage is especially a serious problem if more than two sub-systems exist, because the number of iterations increases very strongly with the number of sub-systems. Therefore, we will apply the direct fully coupled solution method here for both structure-structure interaction problems and structure-fluid interaction problems with fluid sub-systems which can easily be described using a Lagrangian formulation. However, if a fluid sub-system which is described by a Eulerian formulation is incorporated in a system with more than one structural sub-system, then direct full coupling will probably be chosen for the structures while the fluid sub-system will be iteratively coupled to the structures. Such problems are not dealt with in this thesis.

#### *2.4 solid-solid contact with large sliding*

In literature ( e.g. Hughes et. al. ( 1976 ), Bathe and Chaudhary ( 1985 ) ) much attention is paid to the contact of two material points and the appropriate constraints. The ambiguity of criteria to identify sets of actual contacting material points constitutes an important aspect of the contact algorithm. This is especially the case when large sliding in the contact areas occurs. Till now relatively little attention has been paid to this point in literature. Recently, Zhong and Nilsson ( 1990 ) described a contact searching algorithm and specified contact criteria for sets of material points. However, for large sliding contacts, the actual composition of the sets of contacting points and the corresponding constraints change continuously. No special attention was given by Zhong and Nilsson ( 1990 ) to these aspects.

In this section a finite element formulation for large sliding static contact problems is presented, in which friction in the contact areas is disregarded. The formulation can easily be extended to incorporate frictional behaviour.

After the contact behaviour has been specified the solution strategy is outlined. Next the possible contact states of a material point in the discrete formulation and the modelling of the state transitions are discussed and illustrated in some examples.

2.4.1 continuous formulation of contact behaviour

With respect to an arbitrary material point P of  $A_c$  two contact states can be distinguished:

- At time  $\tau = t$  point P is contacting another material point of A. This is the case if a point Q on  $A_c$  exists, for which the position vector at time  $\tau = t$  is equal to the position vector of P

$$\vec{x}(\underline{\xi}^p, t) = \vec{x}(\underline{\xi}^q, t) \quad (2.18)$$

while at the same time the unit outward normal vectors to the outer surface at P and Q are opposite

$$\vec{n}(\underline{\xi}^p, t) = -\vec{n}(\underline{\xi}^q, t) \quad (2.19)$$

Then the contacting state with respect to the point Q is attributed to P. The principle of action and reaction has to be satisfied

$$\vec{p}_c(\underline{\xi}^p, t) = -\vec{p}_c(\underline{\xi}^q, t) \quad (2.20)$$

Because no friction is assumed in the interaction, the tangential component of the contact stress vector  $\vec{p}_c$  has to be zero. This condition is represented by

$$\vec{p}_c(\underline{\xi}^p, t) \cdot \left[ \mathbf{I} - \vec{n}(\underline{\xi}^p, t) \vec{n}(\underline{\xi}^p, t) \right] = \vec{0} \quad (2.21)$$

which describes a constitutive relationship for the contacting state. An additional constitutive relationship results from the condition that the contact stress has to be compressive

$$\vec{p}_c(\underline{\xi}^p, t) \cdot \vec{n}(\underline{\xi}^p, t) \leq 0 \quad (2.22)$$

- If point P is not coinciding with any other material point of V at time  $\tau = t$ , the free state is attributed to P. Characteristic for the constitutive behaviour of the free state is the equation

$$\vec{p}_c(\xi^p, t) = \vec{0} \quad (2.23)$$

Penetration of point P into a sub-system is not allowed.

#### 2.4.2 discretization and solution strategy

While in the continuous formulation for the contacting state attention has been focussed on a particular material point P on  $A_c$  in contact with another material point Q on  $A_c$  in the discrete formulation a nodal point P on  $A_c$  is considered to interact with several other nodes on  $A_c$ . For an adequate description the contact unit is introduced. A contact unit is defined with respect to any node P on  $A_c$  and consists of node P and a set of nodes in the part of  $A_c$  that may interact with node P. In general one node will participate in more than one contact unit.

Suppose that with respect to every node on  $A_c$  a contact unit is defined. The column  $\underline{c}$  is composed of the nodal interaction contributions of all the contact units in the system. Let  $\underline{k}_p$  ( 3 components ) be the column with the nodal force contributions on node P as a result of the interaction in the particular contact unit defined for P.

It is assumed that to every contact unit one of the following two contact states has been assigned ( the procedure to assign a certain contact state will be explained later on ):

- passive state

This state corresponds to the situation previously called free. According to equation ( 2.23 ) the contact behaviour for the contact unit is characterized by

$$\underline{k}_p = \underline{0} \quad (2.24)$$

- active state

This state is the equivalent of the contacting state of a point in the continuous formulation. Because  $\underline{k}_p$  is the force contribution on node P of the contact unit,  $-\underline{k}_p$  is the action of node P on a number of other nodes in this contact unit, according to the principle of action and reaction. The distribution of  $-\underline{k}_p$  over these nodes is formally given by

$$\Delta_p \underline{c} = -\underline{D}_p(\underline{x}) \underline{k}_p \quad (2.25)$$

where  $\underline{D}_p$  ( 3m rows, 3 columns ) is a distribution matrix, dependent on the geometry at the end of the increment as defined by the column  $\underline{x}$  with nodal coordinates. Then the total contribution to  $\underline{c}$  of the contact unit under consideration is represented by

$$\underline{c}_p = \Delta_p \underline{c} + \underline{L}_p \underline{k}_p = [ -\underline{D}_p(\underline{x}) + \underline{L}_p ] \underline{k}_p \quad (2.26)$$

with  $\underline{L}_p$  ( 3m rows, 3 columns ) being the appropriate location matrix. Because of equation ( 2.21 ) the tangential contact forces are prescribed to be zero. The corresponding conditions with respect to  $\underline{k}_p$  can be written as

$$\underline{P}_p(\underline{x}) \underline{k}_p = \underline{0} \quad (2.27)$$

with  $\underline{P}_p$  ( 2 rows, 3 columns ) the projection matrix to be derived from the actual geometry.

Finally, a kinematic condition applies for node P, taking into account that the contact unit is closed which means that node P is localized in a particular element face of  $A_c$ . This can be formulated by

$$\kappa_p(\underline{x}) = 0 \quad (2.28)$$

where  $\kappa_p$  is a scalar function of the nodal coordinates.

The set of contact units to which the active state has been assigned is denoted by S, the number of active units by s. Summation over all the active contact units in the system yields

$$\underline{c} = \sum_{p \in S} \underline{c}_p = \sum_{p \in S} [ -D_p(\underline{x}) + L_p ] \underline{k}_p = \underline{\Delta}(\underline{x}) \underline{k} \quad (2.29)$$

where the matrix  $\underline{\Delta}$  ( 3m rows, 3n columns ) controls the assemblage, whereas  $\underline{k}$  ( 3n components ) is a column with the nodal force contributions  $\underline{k}_p$  of all the contact units. The conditions ( 2.24 ), ( 2.27 ) and ( 2.28 ) are similarly denoted by

$$\underline{Z} \underline{k} = \underline{0} \quad (2.30)$$

$$\underline{P}(\underline{x}) \underline{k} = \underline{0} \quad (2.31)$$

$$\underline{\kappa}(\underline{x}) = \underline{0} \quad (2.32)$$

respectively, with  $\underline{Z}$  ( 3(n-s) rows, 3n columns ),  $\underline{P}$  ( 2s rows, 3n columns ) and  $\underline{\kappa}$  ( s components ) implicitly defined. The balance equation ( 2.17 ) and the conditions ( 2.30 ), ( 2.31 ) and ( 2.32 ) constitute a set of 3(m+n) equations, describing the discrete contact problem. In a more concise notation these can be written as

$$\begin{cases} \underline{f}(\underline{x}) - \underline{r} - \underline{c}(\underline{x}, \underline{k}) = \underline{0} \\ \underline{h}(\underline{x}, \underline{k}) = \underline{0} \end{cases} \quad (2.33)$$

This set of equations is non-linear with respect to  $\underline{x}$  and linear with respect to  $\underline{k}$ . The columns  $\underline{x}$  and  $\underline{k}$  contain the system degrees of freedom.

Because the problem formulation is essentially non-linear, an iterative solution procedure is used to calculate the system degrees of freedom at the end of each increment, starting from estimates according to the converged situation of the preceding increment. Estimates of the incremental changes for the system degrees of freedom are indicated by  $\delta \underline{x}$  and  $\delta \underline{k}$ . Incremental changes of the corresponding estimates for  $\underline{f}$ ,  $\underline{c}$  and  $\underline{h}$  are represented by  $\delta \underline{f}$ ,  $\delta \underline{c}$  and  $\delta \underline{h}$ , respectively. Linearization with respect to  $\underline{x}$  and  $\underline{k}$  yields the relationships

$${}^{i+1} \delta \underline{f} = {}^i \underline{E}_x {}^{i+1} \delta \underline{x} \quad (2.34)$$

$${}^{i+1}\delta\underline{c} = {}^i\underline{C}_x {}^{i+1}\delta\underline{x} + {}^i\underline{C}_k {}^{i+1}\delta\underline{k} \quad (2.35)$$

$${}^{i+1}\delta\underline{h} = {}^i\underline{H}_x {}^{i+1}\delta\underline{x} + {}^i\underline{H}_k {}^{i+1}\delta\underline{k} \quad (2.36)$$

with the left superscripts referring to the iteration number (  $i=1,2,\dots$  ). The matrices  ${}^i\underline{E}_x$ ,  ${}^i\underline{C}_x$ ,  ${}^i\underline{C}_k$ ,  ${}^i\underline{H}_x$  and  ${}^i\underline{H}_k$  are the derivatives of  $\underline{f}$ ,  $\underline{c}$  and  $\underline{h}$  with respect to  $\underline{x}$  and  $\underline{k}$  for  $\underline{x} = {}^i\underline{x}$  and  $\underline{k} = {}^i\underline{k}$ . Based on ( 2.33 ) the following equations to determine approximations for  $\delta\underline{x}$  and  $\delta\underline{k}$  are obtained

$$\begin{bmatrix} {}^i\underline{E}_x - {}^i\underline{C}_x & -{}^i\underline{C}_k \\ {}^i\underline{H}_x & {}^i\underline{H}_k \end{bmatrix} \begin{bmatrix} \delta\underline{x} \\ \delta\underline{k} \end{bmatrix} = \begin{bmatrix} -{}^i\underline{f} + \underline{r} + {}^i\underline{c} \\ -{}^i\underline{h} \end{bmatrix} \quad (2.37)$$

The columns  ${}^i\underline{x}$  and  ${}^i\underline{k}$  are updated according to

$${}^{i+1}\underline{x} = {}^i\underline{x} + {}^{i+1}\delta\underline{x} \quad (2.38)$$

$${}^{i+1}\underline{k} = {}^i\underline{k} + {}^{i+1}\delta\underline{k} \quad (2.39)$$

and the iteration process is continued until convergence is reached. With respect to the convergence criterion, not only the right-hand side of equation ( 2.37 ) ( the residual ) has to be negligibly small, but also the inequality conditions related to prevent penetration as well as maintaining the compressive character of interaction forces have to be satisfied. These conditions are not covered by ( 2.33 ) and they will often require changes of the initially assigned contact state. For computational reasons the contact state is allowed to change every iteration cycle. Contact state transitions, which will be specified in the next section, play an important role to achieve convergence of the iteration process.

### 2.4.3 contact state transitions

In this section the state transitions for the present algorithm are outlined. These transitions are derived from the actual estimates for the columns  $\underline{x}$  and  $\underline{k}$  every iteration again. On the basis of these estimates it is determined whether to a contact unit the passive or active state will be assigned. In case of the active state it is also

established with which element face the unit node P is in contact. It is assumed that all units have the passive state at the start of an analysis.

- transition from the passive state

If after iteration  $i$  the passive state has been assigned to the contact unit with respect to node P there is no mathematical restriction to node P against penetrating  $A_c$ . After iteration  $i+1$  it has to be checked whether this node passed any of the element faces of the contact unit. Therefore, the trajectories of the nodal points

$$\underline{x}(\mu) = \underline{x} + \mu (\underline{x}^{i+1} - \underline{x}) \quad , \quad 0 \leq \mu \leq 1 \quad (2.40)$$

from the beginning of the increment to the actual estimate are considered. All values of  $\mu$  are calculated for which node P is located exactly on an element face of the contact unit. Two cases are distinguished:

- Such a  $\mu$  does not exist, which means that node P did not penetrate any of the element faces of the contact unit and thus the passive state can be maintained.
- There are one or more values of  $\mu$  for which P is located on an element face. Then the smallest value of  $\mu$  is considered. For iteration  $i+1$  the active state with respect to the related element face is attributed in such a way that the penetration with respect to this element face is eliminated by condition ( 2.28 ).

- transition from the active state

In the active state node P is allowed to slip without friction over an element face. Starting from the active state in iteration  $i$  the following strategy is proposed:

- If the contact force is not compressive and hence ( 2.22 ) is not satisfied, the passive state is attributed.
- In all other cases ( compressive contact force ) continuation of the active state is assumed. According to this state the kinematical condition ( 2.28 ) is applied requiring node P to be coplanar to the element face to which it is coupled. If in iteration  $i+1$  node P is located on the same element face as in iteration  $i$ , P is coupled to this face. However, if node P leaves this element face during the iteration  $i+1$ , it is automatically coupled to the adjacent element face. The sliding movement from one element face to another is controlled in this way.

2.4.4 examples

To demonstrate the performance of the contact algorithm, some case-studies are discussed in the following. Because the contact algorithm is essentially the same for three- and two-dimensional analyses, for reasons of simplicity only plane examples will be presented. Consequently  $A_c$  is defined by line segments bounded by two nodes.

In the first example the process of coming into contact and the termination of contact is simulated by moving a small elastic square element in the direction of a spatially fixed rigid large square element in the first increment and pulling them apart in the second increment. Fig. 2.2a shows the reference configuration in which the prescribed

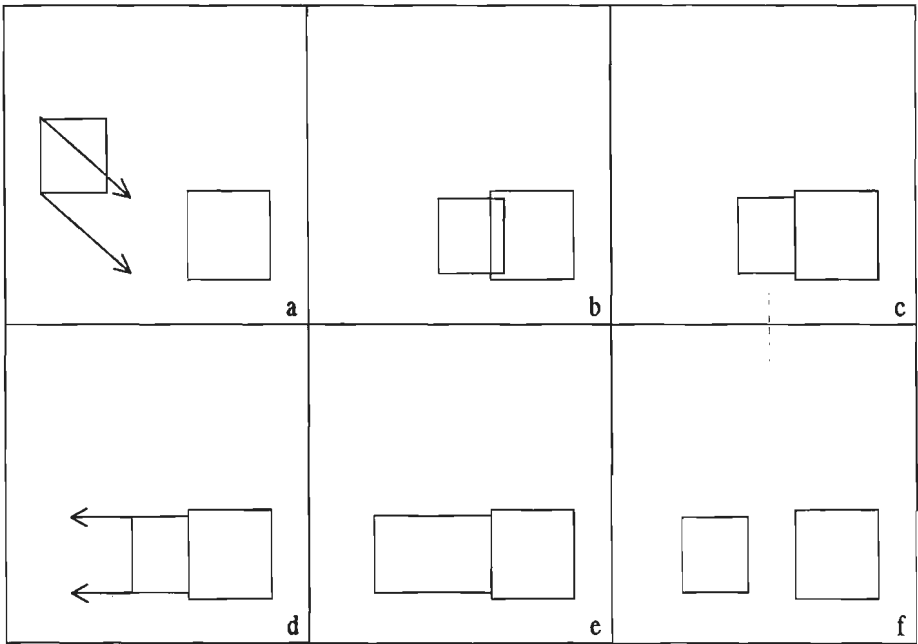


Fig. 2.2 Iteration estimates during two increments ( abc and def ).

displacements are indicated by vectors. Because the passive state is attributed to all nodes in the reference configuration, only rigid body displacements occur in the first iteration. At the end of this step ( Fig. 2.2b ) two nodes of the small square have penetrated an element face of the large square and the penetrations are calculated. In

the next iteration the active state is assigned to these nodes and penetrations are corrected as is shown in Fig. 2.2c, while equilibrium is also achieved. In the second increment the bodies are pulled apart by prescribing displacements as indicated by the vectors in Fig. 2.2d. Because at first the active state is continued, contact is maintained and tension contact forces will occur ( Fig. 2.2e ). Then the passive state takes over for the next iteration and the final situation with zero stresses is given in Fig. 2.2f.

In the second example the corner contact problem shown in Fig. 2.3a is examined. Baaijens ( 1987 ) mentioned this problem as an illustration of stability aspects in relation to choosing contact nodes and contact element faces. In this example the

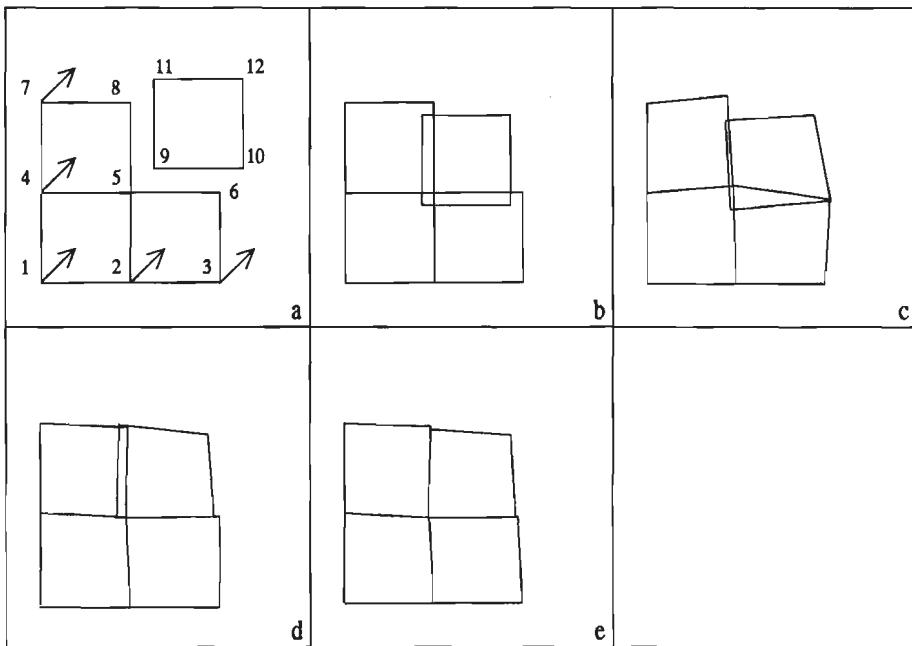


Fig. 2.3 *Corner contact problem.*

nodes 5, 6, 8, 9, 10 and 11 are considered to constitute  $A_c$ . Node 12 is fixed in space. Displacements are prescribed as indicated by the vectors in Fig. 2.3a. After a rigid-body displacement ( Fig. 2.3b ), the penetrations are calculated. Then the active state is assumed for a set of nodes according to:

node	5	6	8	9	10	11
in contact with element face	9-11	9-10	9-11	5-8	5-6	5-8

Table 2.1 *Node - element face relations.*

Node 5 is arbitrarily coupled to element face 9-11, alternatively it could be coupled to element face 9-10. Similarly node 9 can be considered contacting either face 5-6 or face 5-8. However, for the present combinations of nodes and faces, the active state constraints ( 2.28 ) for these nodes are dependent because both nodes 5 and 9 are projected onto parallel planes. This combination of active state constraints does not prevent node 9 from penetrating element face 5-6. Penetration occurs as shown in Fig. 2.3c. Now, node 9 slips off element face 5-8, and in the next iteration step the active state is assigned to node 9 ( in contact with face 5-6 ). A situation occurs in which the coinciding nodes 5 and 9 both have the active state with respect to non-parallel element faces. Constraints applied to coinciding nodes to non-parallel element faces suppress the relative motion of these nodes. In the meanwhile the nodes 8 and 6 move off their respective element faces and finally the equilibrium situation is achieved in Fig. 2.3e. The situations in Figs. 2.3c and 2.3d have to be considered as entr' actes and are avoided when the nodes 5 and 9 are bounded to orthogonal element faces in the second iteration step.

Large slidings are considered in the third example. Fig. 2.4a shows a spatially fixed point obstacle represented by node 12, and ten beam elements between the nodes 1 to 11. In node 1 the horizontal displacement is prescribed as indicated by the vector, while the vertical displacement and rotation in this point are suppressed. In the fifth increment ( Fig. 2.4f ) the beam comes into contact with the obstacle and the upper nine beam elements start bending, while the lower one is still not loaded and makes a rigid body movement. In the following increments the element faces slip over node 12, node 10 being passed in the 12th increment. In the 15th increment ( Fig. 2.4p ) the end of the beam has passed the obstacle, and an unstressed equilibrium situation results.

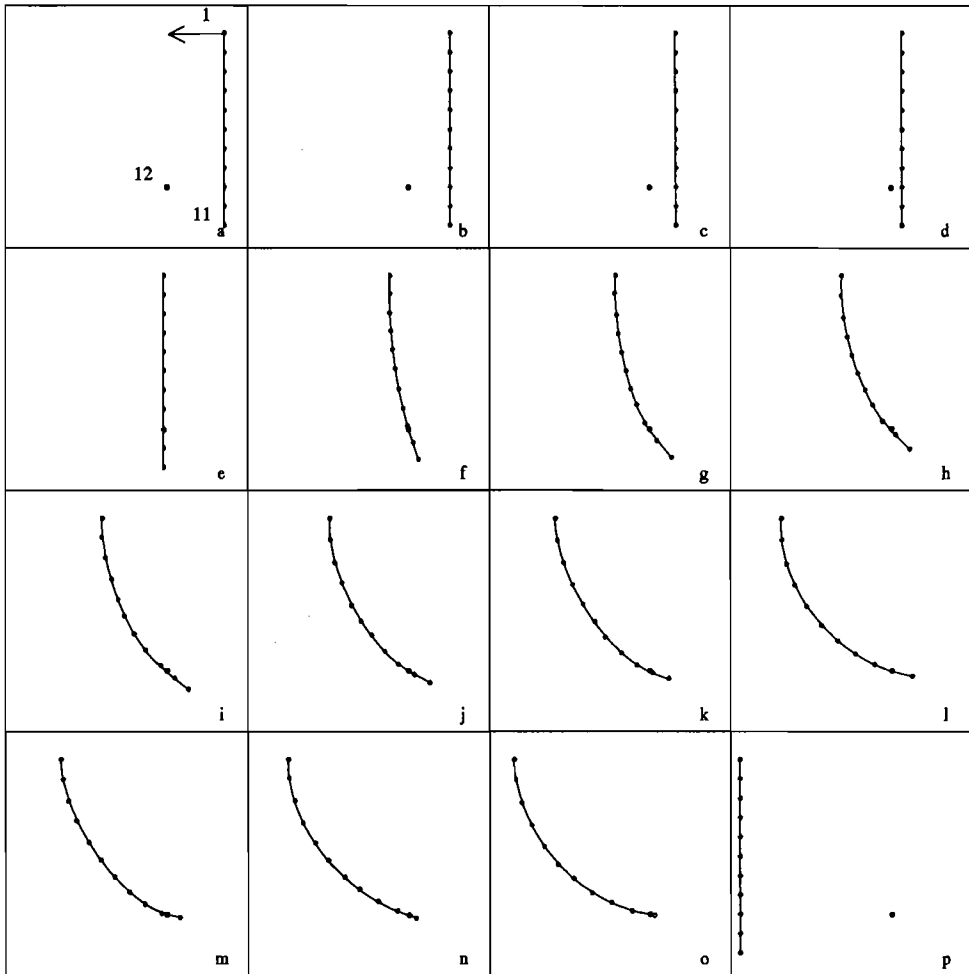


Fig. 2.4 *Beam and fixed obstacle in subsequent increments.*

### 2.5 *discussion*

Standard procedures for solving constrained problems most frequently encountered in literature are the Lagrange multiplier method, which is similar to the method presented here, and the penalty function formulation. Guerra and Browning ( 1983 ), comparing these formulations, showed that the Lagrange multiplier method satisfies the contact constraints more precisely. This method however, adds extra degrees of freedom requiring additional storage and computational effort. Further, they noticed that in most cases problems were encountered with respect to the convergence of the solution process. Using the penalty formulation implies an inaccurate formulation of the contact conditions. The resulting disturbances would affect our parameter studies in a negative way and cannot be accepted in our approach.

The examples constitute various contact problems with possible state transitions. The stability of the algorithm proves to be quite satisfactory for general contact problems.

In the actual implementation of the present algorithm in the TNO-DIANA software package all nodes of  $A_c$  are considered to constitute one element: the so-called contact interface element, containing contact units for each of the nodes. To account for the contact constraints and the internal contact forces, only the right-hand column and the tangential matrix with respect to this element have to be composed. Such a program structure offers the facility to control the element face transitions which are characteristic for this algorithm. If an iteratively coupled problem involving fluid-structure interaction has to be solved, the same TNO-DIANA basic program can be used. Starting from the element routine composing the contact forces, another element program code can be called to calculate the fluid problem.

Because in the formulation the contact is defined for every node on  $A_c$ , it is not necessary for the user to distinguish between an object body and a target body as is usually done in most formulations. However, because of possible dependences in the system of equations, emanating from the involvement of all nodes on  $A_c$ , special action has to be taken to solve these equations.

## *2.6 summary and conclusions*

In this chapter a general strategy is outlined for interaction problems. In this study two solution methods are distinguished. The direct fully coupled solution strategy is applied if all sub-systems are structures or fluids which are described using a Lagrangian formulation. If a fluid sub-system, which is described by a Eulerian formulation, interacts with one or more structures, then the structures are directly coupled to each other while the fluid is iteratively coupled to the set of structures.

The mechanical interaction problem is defined by the equilibrium conditions for the set of sub-systems and the appropriate contact conditions. These contact conditions and the contact forces are generally dependent on the positions and the deformation field of all the sub-systems in the problem. For the large sliding solid-solid interaction problem a formulation is worked out for which friction is assumed to be zero. The presented algorithm proves to be quite satisfactory for general contact problems.



## CARTILAGE AND MENISCUS

### *3.1 introduction*

Fairbank ( 1948 ) indicated the relationship between the outward displacements of the meniscus and its load bearing capacity. In later years, for example Ahmed and Burke ( 1983 ), Jaspers et al. ( 1980 ) and Walker and Erkman ( 1975 ) carried out investigations to establish the direct and indirect contact areas under different loadings. The results of these investigations confirmed Fairbank's opinion. Also physical-mathematical models of the load transmission were presented by Seedhom and Hargreaves ( 1979 ) and De Lange et al. ( 1979 ). In these models femur and tibia were considered as rigid bodies while the load was carried by two or four non-linear springs, representing the combination of meniscus and articular cartilage layers.

Recently Tissakht et al. ( 1989 ) presented a study of the stress-pattern in the menisci for different joint loads. They developed a three-dimensional non-linear finite element model incorporating the menisci and the distal femoral and proximal tibial ends, based on measurements of adult specimens. In this model the menisci were allowed to move without friction over the tibial surface while the attachments to the medial and transverse ligaments were modelled by 'cable' elements. The menisci were assumed to behave strongly anisotropic while the material properties of the bony components and articular cartilage layers were not given. Because of its complexity and the -probably-many assumptions, which were not stated explicitly, this descriptive model is in our opinion not suitable to investigate the functions of the joint components.

Other finite element analyses have been presented by Aspden ( 1985 ), Hefzy and Zoghi ( 1988 ), and Sauren et al. ( 1984 ). In these studies the meniscus was modelled as a toroid with a wedge-shaped cross-section resting on a compliant flat base.

---

*A part of this chapter has been published in Journal of Engineering in Medicine ( 1990 ) 204, 53-56.*

In the model of Aspden a prescribed load acted perpendicularly to the upper surface of a meniscus and the material behaviour was considered to be transversely isotropic. Aspden's description failed to clarify whether or not the meniscus was allowed to move with respect to the base. The model was used to provide explanations for the type and localization of meniscal lesions from the computed strain patterns.

Sauren et al. ( 1984 ) presented a more global axisymmetric model. Its main purpose was to investigate the transmission of loads through the joint both by the direct contact between the articular surfaces and by the indirect contact via the menisci. The deformations and the part of the load transmitted by the meniscus were established for three combinations of stiffness parameters and two different widths of the meniscus. The material behaviour of the meniscal ring, as well as the femoral and tibial components was homogeneous, isotropic and linearly elastic. Most important feature of this model, however, is that it allowed any of its parts to move without friction over the surfaces of any of the other parts. The meniscus appeared to transmit up to 70 % of the total load, depending on the material properties of the meniscal and bony tissues. Moreover, these properties were found to be more important than the meniscal width for the meniscal share in load transmission. The present reference model is based on the model of Sauren et al. ( 1984 ), in such a way that the numerical formulation has been improved with respect to prevention for penetrations of components and the stability of the solution process.

The model presented by Hefzy and Zoghi ( 1988 ) was identical to that of Sauren et al. ( 1984 ) as far as geometry, dimensions, and material properties are concerned. The models differed only with regard to the coarseness of the element mesh, the boundary conditions at the lower end of the tibial component and probably the contact elements. However, these differences seem to be of minor importance since the results of analyses with two combinations of material properties of meniscal and bony tissues, as reported by Hefzy and Zoghi ( 1988 ), confirmed the conclusions drawn by Sauren et al. ( 1984 ) from the same analyses.

Both the models of Hefzy and Sauren took into consideration only the meniscus and the stiff bony ends of femur and tibia, and these parts were modelled as linearly isotropic materials. Their conclusion, that the results of their analyses point to a large influence of stiffness values of the different components on the load distribution within the joint, is rather tentative, because the relatively soft articular layers on the bony ends, and the strong anisotropy of the meniscal tissue were not taken into

account. Moreover, they modelled the tibial plateau as a flat plane, thus leaving out of consideration the possible importance of local concavities and convexities in the real joint.

The overall goal of the work described in this chapter is to investigate these possible shortcomings starting from the reference model. The specific objectives are formulated as the determination of the effects of ( a ) the surface geometry of the tibial component ( that is a plane, convex or concave surface ), ( b ) the presence of a soft layer on the surfaces of the bony components, and ( c ) the anisotropy of the meniscus on the meniscal share in load transmission.

### *3.2 reference model*

The reference model ( Fig. 3.1 ) is axisymmetric and contains a planar tibial plateau, a spherical femoral condyle and, in between, a toroid with a wedge-shaped cross-section, representing the meniscus. The tibial plateau is the upper end plane of a cylinder of circular cross-section. The lower end plane rests on a rigid foundation. Except at the axis of symmetry, all points of this lower end plane are free to move radially over the rigid foundation. The spherical condylar surface is the lower end surface of a cylinder, the upper end plane of which is loaded with an axial force during the analyses. All points of the upper end plane are free to move in the radial direction, except at the axis of symmetry. The axial force is applied in such a way that the upper surface of the femoral part remains planar and perpendicular to the axis of symmetry. In the unloaded situation, the lower and upper surfaces of the meniscus match the tibial and femoral surfaces, respectively, while there is direct femorotibial contact only at the axis of symmetry. Both between the meniscal ring and the articular surfaces and in the region where the surfaces come into direct contact, relative motion of the components is allowed. No friction occurs in the contacts. By means of the finite element method, deformations and stresses of the components and the load distribution in the contact surfaces can be established. The analyses for this study have been carried out with the TNO-DIANA software package. The contacts have been modelled as described in chapter two. The three bodies in the model have been divided into isoparametric ring-shaped elements with triangular cross-sections. For these elements the displacement field is a linear function of the displacements in the

three element nodes.

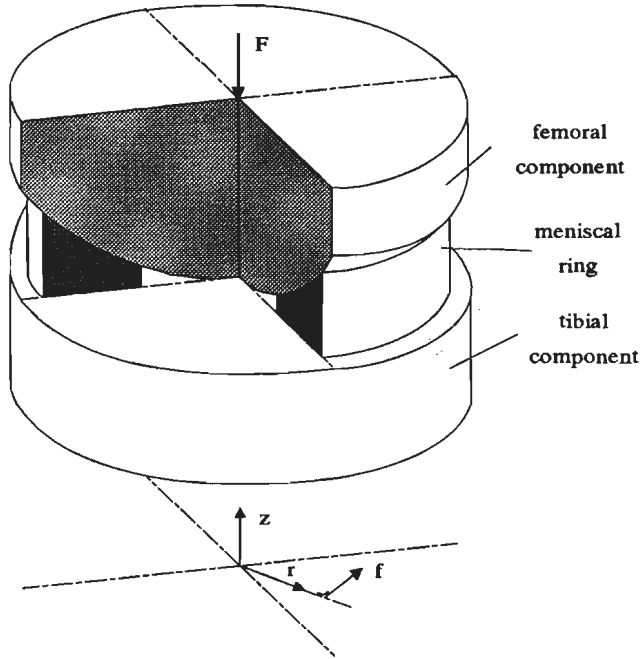


Fig. 3.1 *Outline of the reference model, where one quarter of the femoral component and the meniscus has been left out for the sake of clarity.*

The material of the components has been assumed to be homogeneous, isotropic and to behave according to Hooke's law, so that its constitutive relation is given by

$$\begin{bmatrix} \epsilon_{rr} \\ \epsilon_{rz} \\ \epsilon_{zz} \\ \epsilon_{ff} \end{bmatrix} = \frac{1}{E} \begin{bmatrix} 1 & 0 & -\nu & -\nu \\ 0 & 2(1+\nu) & 0 & 0 \\ -\nu & 0 & 1 & -\nu \\ -\nu & 0 & -\nu & 1 \end{bmatrix} \begin{bmatrix} t_{rr} \\ t_{rz} \\ t_{zz} \\ t_{ff} \end{bmatrix} \quad (3.1)$$

In this linear relationship between the second Piola-Kirchhoff stresses  $t$  and Green-Lagrange strains  $\epsilon$ , the subscripts  $r$ ,  $z$ , and  $f$  denote the radial, axial and

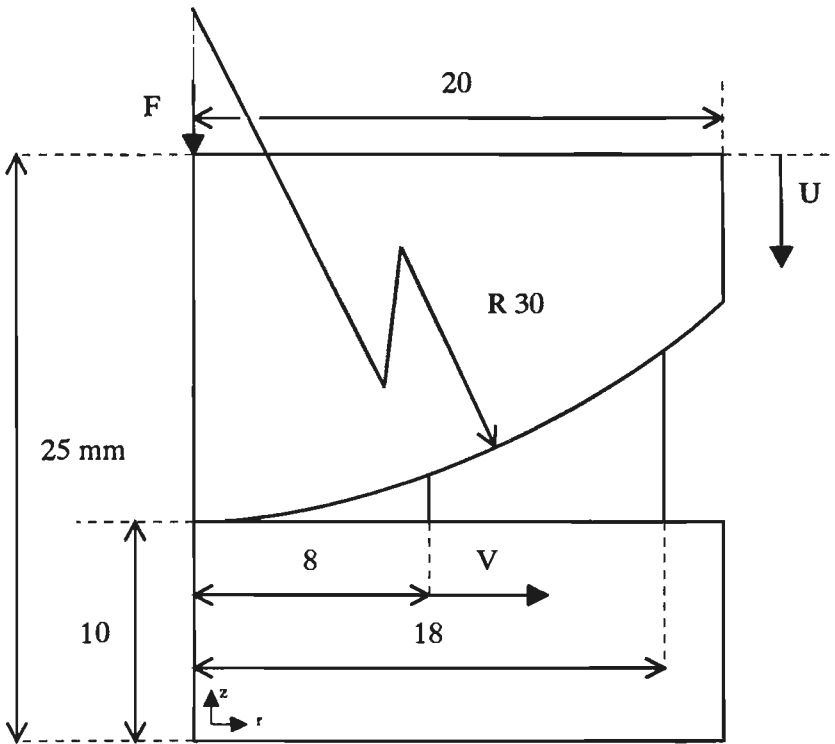


Fig. 3.2 *Half of a cross-section of the reference model in the unloaded situation, with the dimensions ( mm ). Also denoted are the axial compression  $U$  of the upper plane of the femoral component and the radial displacement  $V$  of the lower inner edge of the meniscal ring.*

circumferential direction, respectively ( Figs. 3.1 and 3.2 ). The only parameters needed are the Young modulus  $E$  and Poisson ratio  $\nu$ . In literature the values of the Young modulus and Poisson ratio for bone, articular cartilage, and menisci differ considerably. This is caused by the strongly anisotropic and inhomogeneous character of these components and their visco-elastic nature. From this point of view Hooke's law is not suitable to describe these materials. However, in this thesis it is intended to start with a simple model and therefore in the reference model for the bony

components the  $E$  and  $\nu$  values are taken 500 MPa and  $\nu = 0.2$ , respectively, while for the meniscus these values are 20 MPa and 0.3, respectively. These values are considered to represent a fair average of the values in literature. The dimensions of the reference model are given in Fig. 3.2.

The analyses have been performed for axial loads  $F$  up to 1000 N using incremental steps of 100 N. The response of the models will be given in terms of the axial compression  $U$  of the complete model, the radial displacement  $V$  of the inner lower edge of the meniscus ( Fig. 3.2 ) and the fraction  $q$  of the load transmitted by the meniscus.

Analyses of the reference model with different coarsenesses of the element mesh showed that the coarseness of the distribution of nodes on the contact surfaces influenced the results. However, the coarseness of the distribution of nodes on the contact surfaces in the reference model ( approximately 500 elements ) is such that further refinement has only minor effects on the results. In all parameter studies the distribution of the nodes on the contact surfaces was chosen similar to the reference model.

### 3.3 parameter studies

#### 3.3.1 bony components

The reference model described before deviates from reality in two important aspects: First, the tibial plateau is not a perfect plane, but locally convex and concave. Secondly, the femoral and tibial articular surfaces are covered by a soft layer of articular cartilage. Therefore, the following modifications are applied to the reference model, indicated from now on as model A ( Fig. 3.3 ):

- To account for the first aspect a convex or a concave spherical tibial plateau is incorporated ( models B and C, respectively, in Fig. 3.3 ). The radius of curvature of each plateau was 60 mm. In the unloaded configuration the radial dimensions of the meniscus remained unchanged while its lower surface was accommodated to match the tibial surface.

- To account for the second aspect, versions with soft layers of the reference model ( D ) and the models with a curved tibial surface ( models E and F ) are analysed. These layers were assumed to behave like isotropic linearly elastic material, with a Young modulus of 10 MPa and a Poisson ratio of 0.4. Their thickness was 2.5 mm, measured perpendicularly to the outer surface. The layers were incorporated in such a way that the outer dimensions of the femoral and tibial components ( layers inclusive ) remained unchanged in the stress-free situation.

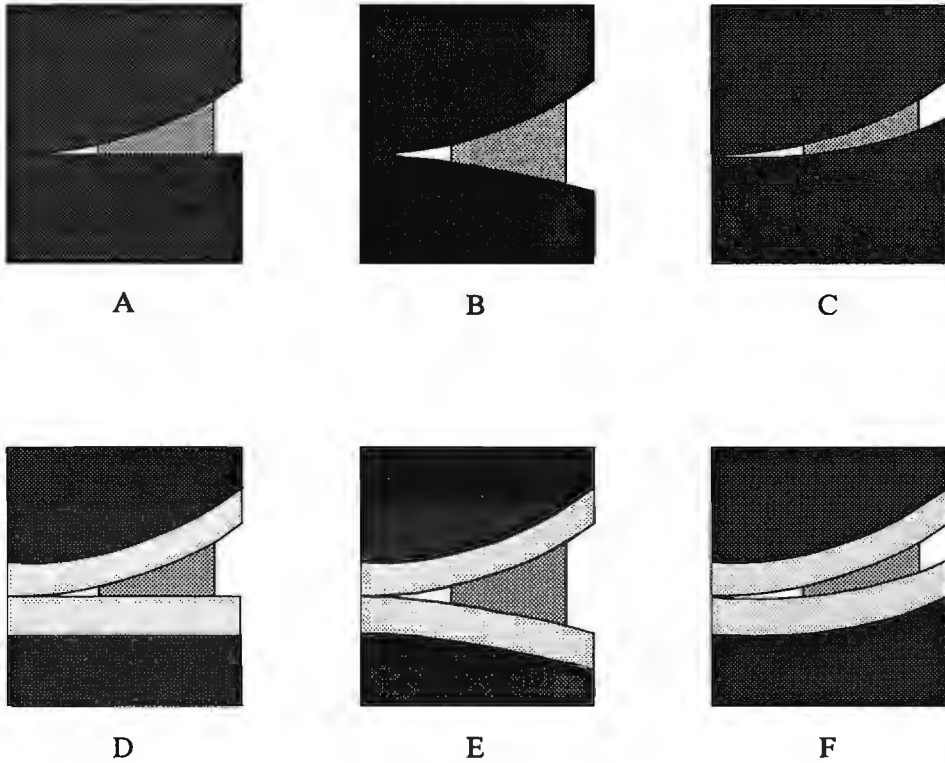


Fig. 3.3 *Halves of the cross-sections of the different models. See text for explanation.*

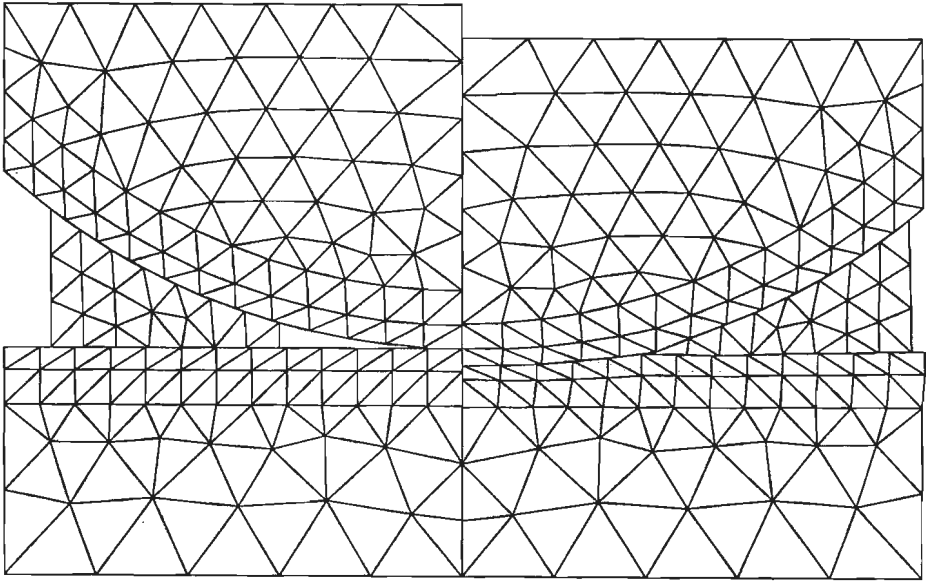


Fig. 3.4 *Element mesh of model D in the unloaded situation ( left ), and in the loaded situation with  $F=1000\text{ N}$  ( right ).*

Fig. 3.4 shows the element mesh in the undeformed and in the deformed situation ( $F = 1000\text{ N}$ ) for model D. Comparison of the two meshes clearly illustrates the axial compression, the increased area of contact between femur and tibia, and the radial displacement of the meniscus upon application of the load. It is also perceptible that the soft layers deform significantly in the neighbourhood of the direct contact area.

Fig. 3.5 shows the distribution of the contact stresses over the cross-sections just beneath the tibial contact surfaces for the models A and D at  $F = 1000\text{ N}$ . It is clear that in the model without soft layers there is a stress concentration in the neighbourhood of the direct contact while the presence of a soft layer yields smoothing of the stress distribution. This phenomenon is characteristic for all the models studied.

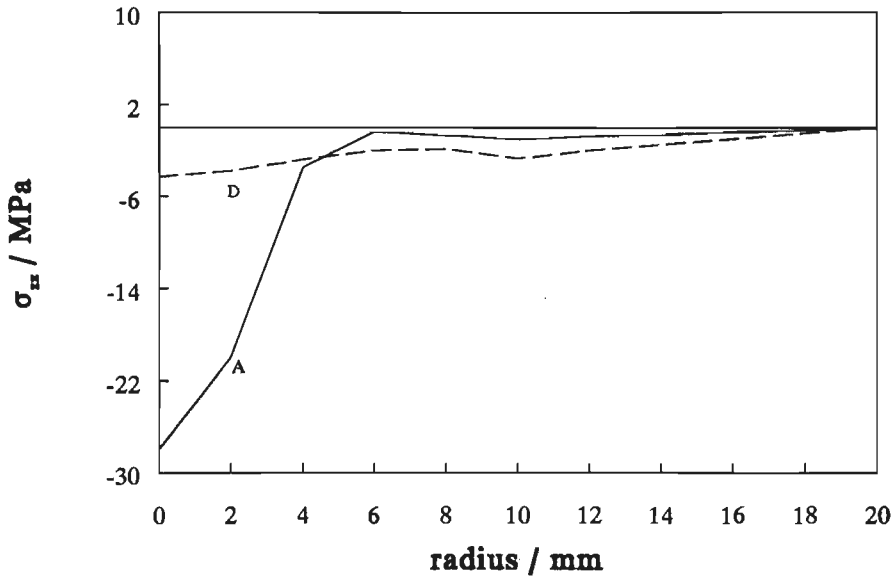


Fig. 3.5 *Paths of axial stress over cross-section just under the tibial surface of the models A and D, without and with soft layers, respectively.*

Variation of the geometry of the tibial component ( models C, A, and B ) with successively a concave, plane, and convex contact surface results in an increasing U ( Fig. 3.6 ) and a decreasing V ( Fig. 3.7 ) and q ( Fig. 3.8 ).

Incorporation of soft layers in the models A, B, and C results in the models D, E, and F, respectively. Analyses of these models yield higher values of U, V, and q for a particular load in comparison with the corresponding models without soft layers ( Figs. 3.6, 3.7, and 3.8 ). Although for the models with soft layers the variations of U are larger and those of V are smaller than for the models without layers, the effect of the geometry on the displacements U and V is qualitatively the same for both categories of models ( Figs. 3.6 and 3.7 ). However, the effect of the geometry of the tibial component on the meniscal share q in load transmission in the models A, B, and C almost disappears as soon as soft layers are applied while at the same time a significant increase of q can be seen ( Fig. 3.8 ).

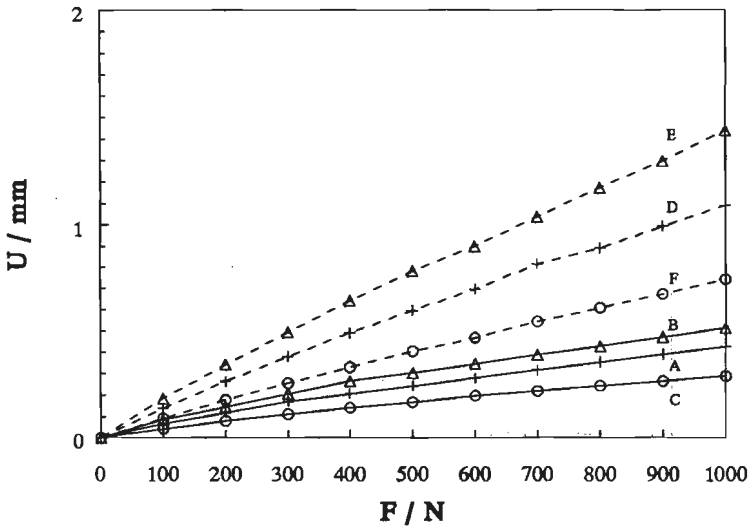


Fig. 3.6 Axial compression  $U$  versus axial load  $F$  for models A, B, C, D, E, and F

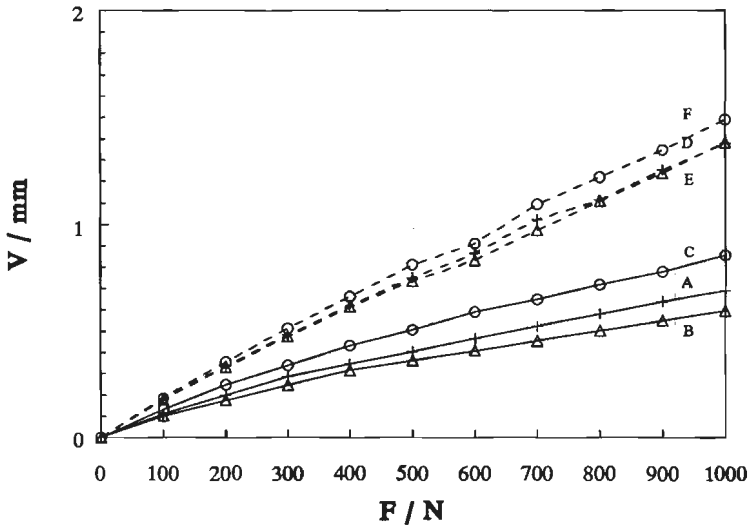


Fig. 3.7 Radial meniscal displacement  $V$  versus axial load  $F$  for models A, B, C, D, E, and F.

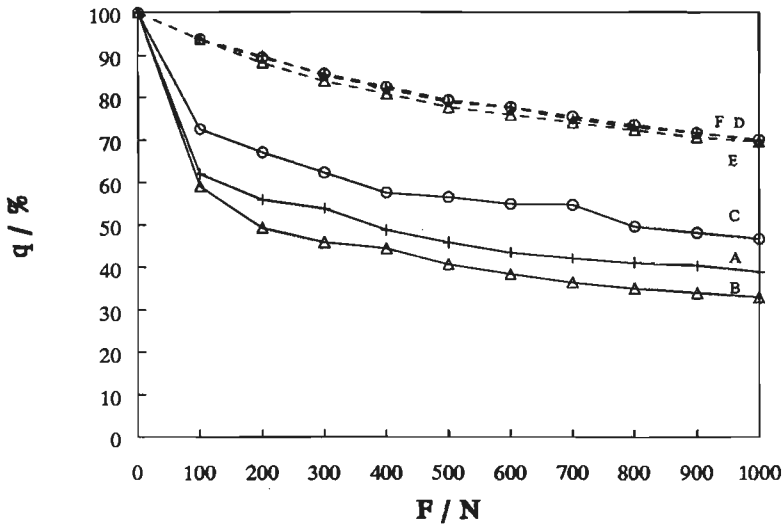


Fig. 3.8 Load transmitted by the meniscus as percentage  $q$  of the total axial load  $F$  versus  $F$  in models A, B, C, D, E, and F.

From Figs. 3.6 and 3.7, U and V can be seen to depend on the axial load  $F$  in a slightly non-linear way. The decline of the curves in Fig. 3.8 confirms the non-linear character of the load transmission for these models, because in a linear model the part of the load borne by the meniscus would be independent of the total load.

From a geometrical point of view the reference model A might be considered as an intermediate form of the models B and C with a convex and a concave tibial surface. Indeed the results for model A are in between those of the models B and C. Therefore, several effects on the load transmission are involved in changing the curvature of the tibial surface.

The first effect is the axial stiffness of the meniscus. In comparison with the reference model A, model B with a convex tibial surface has a meniscus with a larger cross-sectional area and smaller axial stiffness. If we assume, in spite of the changed curvature of the tibial plateau, that the local stiffness of the direct contact zone remains unchanged, this smaller axial stiffness will lead to a lower load fraction  $q$ . A concave tibial surface ( model C ) leads to a decrease in cross-sectional area and consequently to an increase in axial stiffness of the meniscus, yielding a higher value

of  $q$ .

The second effect is less clear. In all models the upper and lower surfaces of the meniscal ring, which are respectively in contact with the femoral and tibial surfaces, are not parallel. The meniscal wedge area is largest for model B and smallest for model C. Loadings only act on the upper and lower surfaces of the meniscal ring, and as a consequence of the assumption that no friction occurs in the contacts, these loadings are always directed normal to these surfaces. Therefore, the wedge shape of the meniscus in these models means that an axial load on the meniscus is always combined with a radial load. Radial forces can be resisted only if circumferential stresses are generated. The magnitude of the radial reaction force so created depends on the dimension of the cross-section of the meniscus and its radial displacement. Comparison of model A with model C shows that the latter has a greater axial stiffness because, as a whole, more stiff material is incorporated. Analyses indeed show a lower axial compression for model C at the same loadings ( Fig. 3.6 ). Because of the smaller cross-section of the meniscus in model C, an equivalent circumferential stress results in a lower radial reaction force in the model with a concave tibial plateau. As a consequence, the bearing capacity of the meniscus is limited because of this smaller reaction force.

In the models D, E and F, the ends of the bony parts are covered by soft layers. As could be expected, the axial stiffness of the models decreases and the radial displacement of the meniscus increases as a result of the presence of the soft layers. Especially the effect of this variation on the load of the meniscus is noteworthy. The soft layers lead to an increase of the load borne by the meniscus, while differences in the curvature of the tibial plateau seem hardly to have any effect on  $q$ . Other authors ( e.g. Wismans et al. ( 1980 ) and Huiskes et al. ( 1985 ) ), investigating the geometry of the ends of femur and tibia, go into great detail in describing the geometry of the surfaces. The results of the present analyses indicate that, in a model of the dynamic or static load transmission, the layers of articular cartilage should preferably be incorporated for modelling of the load transmission.

3.3.2 *meniscal ring*

The last class of parameter variations ( models G and H ) to be discussed took into account the anisotropic material properties of the meniscal ring. In the fibrocartilage of the meniscus the fibres run mainly in the circumferential direction ( Aspden et al. ( 1985 ), Bullough et al. ( 1970 ) ), so that the material stiffness in this direction differs considerably from the material stiffnesses in the other directions. Taking this into consideration and with Sauren's and Hefzy's conclusion in mind that the load distribution strongly depends on the global stiffnesses of the components, Hooke's law ( 3.1 ) could not be used appropriately. For the meniscal ring, in this case, the following constitutive relation was used:

$$\begin{bmatrix} \epsilon_{rr} \\ \epsilon_{rz} \\ \epsilon_{zz} \\ \epsilon_{ff} \end{bmatrix} = \begin{bmatrix} E^{-1} & 0 & -E^{-1}\nu & -E_f^{-1}\nu_f \\ 0 & 2(1+\nu)/E & 0 & 0 \\ -E^{-1}\nu & 0 & E^{-1} & -E_f^{-1}\nu_f \\ -E_f^{-1}\nu_f & 0 & -E_f^{-1}\nu_f & E_f^{-1} \end{bmatrix} \begin{bmatrix} t_{rr} \\ t_{rz} \\ t_{zz} \\ t_{ff} \end{bmatrix} \quad ( 3.2 )$$

The two analyses with transversely isotropic meniscal properties were performed using model D with a plane tibial plateau and soft layers. In these models the values applied for the Poisson ratio's were  $\nu = 0.3$  and  $\nu_f = ( E_f / E ) \nu$ . The values for E and  $E_f$  are represented in Table 3.1.

model	E ( MPa )	$E_f$ ( MPa )
D	20.0	20.0
G	10.0	35.0
H	6.0	20.0

Table 3.1 *values for moduli of the meniscal ring*

For model G the value of E is equal to the Young modulus of the cartilage layer, while  $E_f$  is larger than the Young modulus of the meniscal ring in the reference model. Because the part of the load transmitted by the meniscal ring is rather high in model D, it is interesting to find out to which degree the meniscal load decreases for model H if a smaller E is applied.

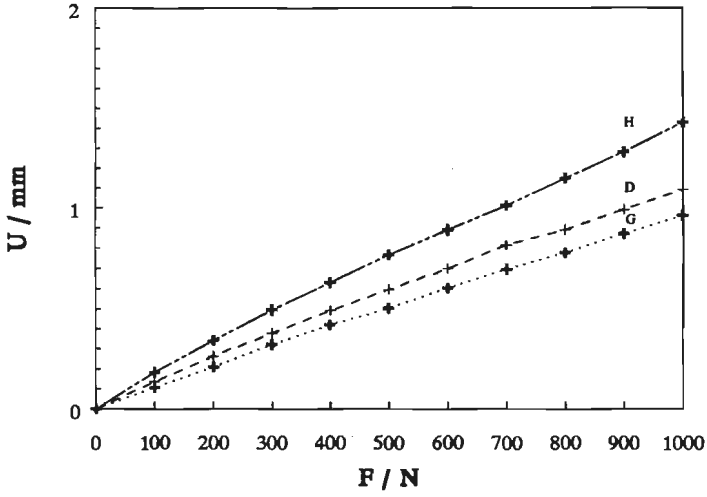


Fig. 3.9 Axial compression  $U$  versus axial load  $F$  for models  $D$ ,  $G$ , and  $H$ .

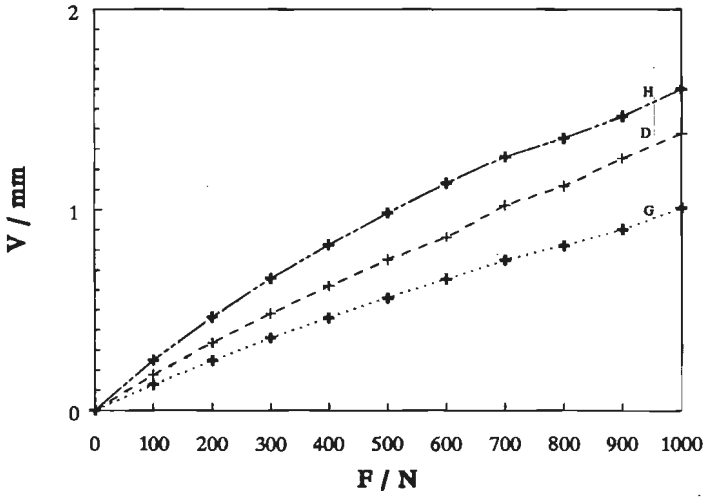


Fig. 3.10 Radial meniscal displacement  $V$  versus load  $F$  for models  $D$ ,  $G$ , and  $H$ .

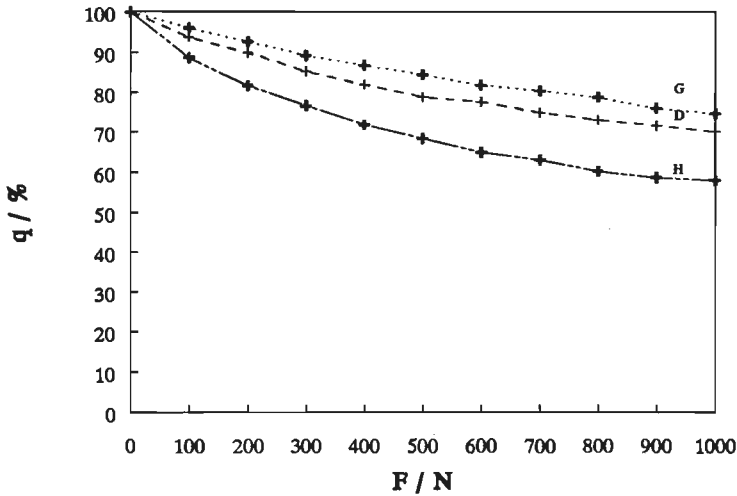


Fig. 3.11 Load transmitted by the meniscus as percentage  $q$  of the total axial load  $F$  versus  $F$  in models D, G, and H.

The two models have an anisotropic meniscus in the sense that the stiffness in circumferential direction is equal ( model H ) to the stiffness for model D, or higher than ( model G ) the one for model D. In the other directions for both models the stiffness is lower than in model D. Comparing the results of the analyses for these models with those of model D, there are two striking points. In the first place the much smaller radial displacement  $V$  ( Fig. 3.10 ) of the meniscus for model G is remarkable, because model G has a lower meniscal radial stiffness than model D and thus a larger  $V$  could be expected. Furthermore, taking into account the large differences in the axial stiffness of the meniscal ring in the models D and H, the axial compression  $U$  ( Fig. 3.9 ) and the meniscal load-fraction  $q$  ( Fig. 3.11 ) show only small deflections from model D. These results point to an important role of the circumferential stiffness of the meniscus in the load transmission through the knee joint.

### 3.4 model reductions

In the sections 3.3.1 and 3.3.2 parameter studies have been described concerning the articular joint surfaces and the meniscal ring, respectively, in both cases starting from the reference model. Comparing the results of these analyses, insight into the role of the curvature of the articular surfaces, the presence of articular cartilage layers and the anisotropy of the meniscus was achieved. The presence of the articular cartilage layers appeared to be of major importance for the load bearing function of the meniscal ring, whereas the effects of the curvature of the tibial surface were minor in the model with soft layers.

The values for the stiffnesses of the soft layers and the bony components differ enormously and therefore the question arises whether it is necessary for the load distribution to take the deformability of the bony components into account. If this deformability does not affect the characteristics, then it is much more efficient to leave it out of the model in future analyses.

In the models with a convex tibial surface ( B and E ) both articular surfaces are convex. A plane of symmetry which is perpendicular to the axis of revolution can be defined when a model with equal curvatures of the femoral and tibial surfaces is considered. For such a model it is sufficient to analyse only one half of the model. Because the curvature of the articular surfaces appeared to have minor effects on the load transmission in the model, besides the deformability of the bony structures, also the necessity for modelling both articular cartilage layers is questioned. In literature several models are presented ( e.g. Hou ( 1989 ) ) comprising only one deformable cartilage layer and both a rigid indenter and a rigid foundation.

A reduced model is introduced here and it is investigated whether the mechanical characteristics with respect to the load distribution  $q$  of the reference model also apply for this reduced model. If this appears to be the case, much more extensive parameter studies can be used to investigate whether these characteristics apply only for a particular set of parameters or also for a wider range of constitutive and geometrical parameters.

Half of the cross-section of the reduced model is shown in Fig. 3.12. The reduced model is similar to the reference model, but the spherical articular surface of the femoral component is considered to be rigid. The articular cartilage on the tibial plateau is a homogeneous cylinder with planar ends, fixed to a rigid foundation.

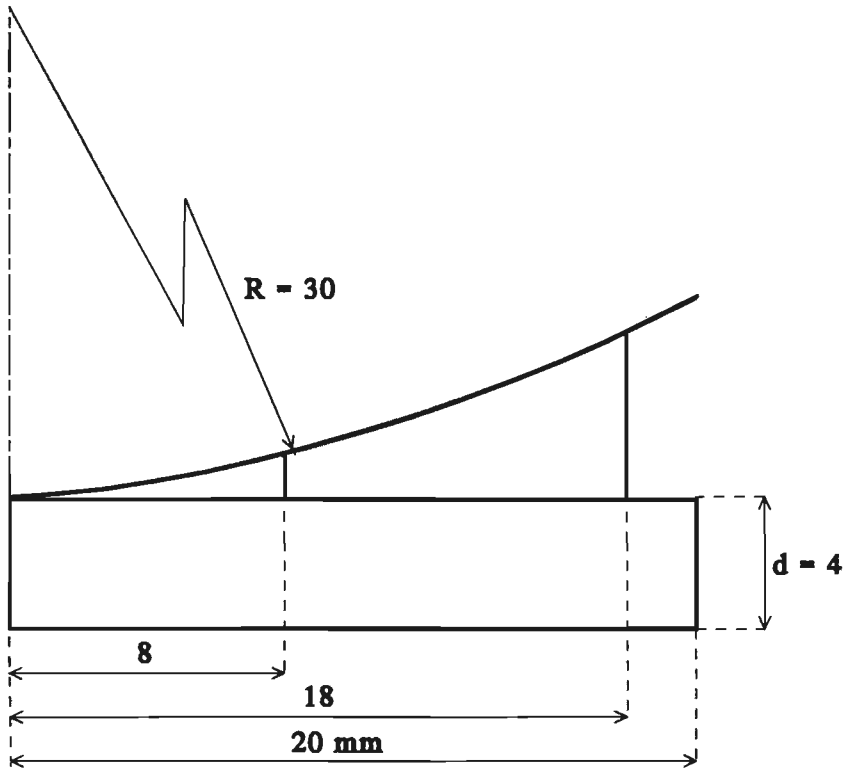


Fig. 3.12 *Half of the cross-section of the axisymmetric reduced model with the parameters  $R$  and  $d$ .*

Frictionless sliding between the rigid femoral sphere, the deformable meniscal ring and the articular cartilage layer is also possible. In Fig. 3.12 the dimensions of the reduced model are indicated. The material of the meniscal ring and the articular cartilage layer is assumed to be isotropic and to behave according to Hooke's law, so that its constitutive relation is given by ( 3.1 ). For both components the Poisson ratio is  $\nu = 0.3$ . The Young modulus of the meniscal ring and the articular cartilage layer are denoted by  $E$  and  $e$ , respectively. Their values are  $E = 20$  MPa and  $e = 10$  MPa.

Parameter studies have been performed with respect to the radius  $R$  ( $R = 20, 30, 40$  and  $60$  mm) of the spherical indenter, the thickness  $d$  ( $d = 0.1, 0.5, 1, 2, 4, 8, 12$  mm) of the articular cartilage layer and the Young modulus  $e$  ( $e = 5, 10, 20, 40$  and  $100$  MPa) of the articular cartilage layer, starting from the reduced model under an axial load of  $500$  N. The results and graphs relating to the part  $q$  of the total load borne by the meniscal ring, the total axial compression  $U$  of the model and the radial displacement  $V$  of the inner side of the meniscal ring as functions of  $R$ ,  $d$  and  $e$  are shown in Fig. 3.13.

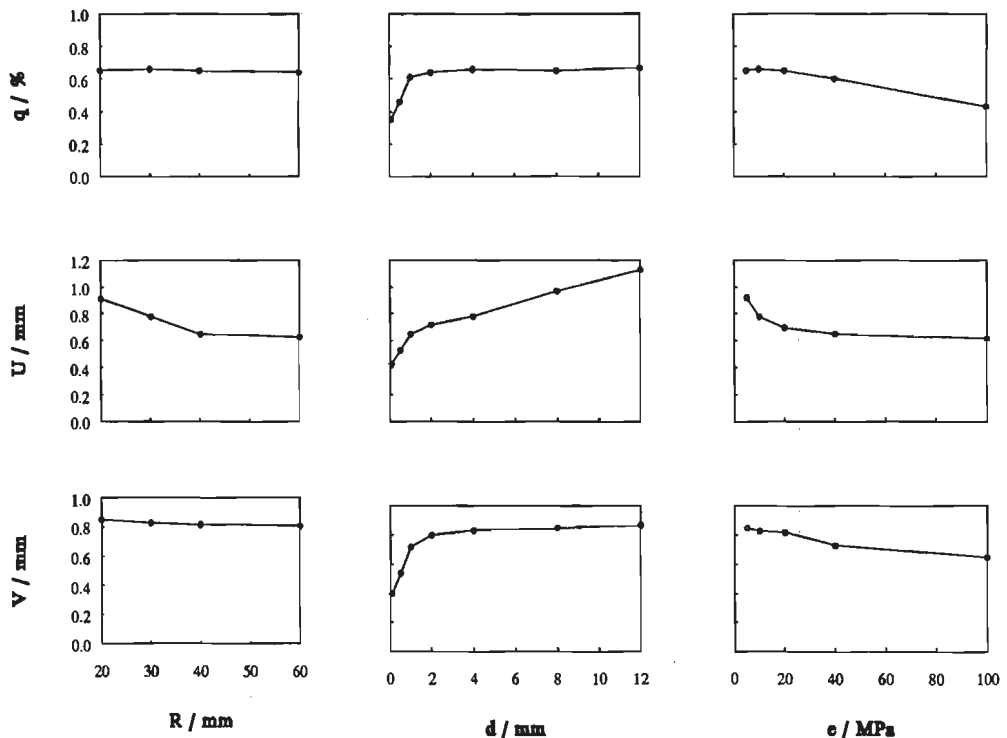


Fig. 3.13

*Results of calculations of the part  $q$  of the total load borne by the meniscal ring, the axial compression  $U$  and the radial displacement  $V$  of the innerside of the meniscal ring with respect to the reduced model for a set of parameters corresponding with  $R = 30$  mm,  $d = 4$  mm and  $e = 10$  MPa. Starting from this set the parameters  $R$ ,  $d$  and  $e$  are varied respectively.*

From the results of these parameter studies the mechanical characteristics with respect to the load distribution  $q$  of the reference model also appear to occur for the reduced model. From these parameter studies it is concluded that  $q$  is between 0.60 and 0.70 for most of the performed analyses and thus virtually independent of  $R$ ,  $d$  and  $e$  in a wide range. However, for  $d < 1$  mm or  $e > 20$  MPa ( Fig. 3.13 ) the meniscal load decreases. A comparison with the reference model shows that for both models the effects of the curvature of the articular surface on the load distribution are small. From analyses with the reduced model this independency of  $q$  for changing  $R$  appears to occur under the conditions that both  $d > 1$  mm and  $e < 20$  MPa. These are important constraints for the choice of the stiffness and thickness of the cartilage layer in future models. The axial compression  $U$  decreases with increasing radius  $R$ , which can be explained by the increasing axial stiffness. The axial stiffness of the cartilage layer depends on its thickness and its Young modulus  $e$ . At larger  $d$  the axial compression increases while it decreases for larger  $e$ . The radial displacement  $V$  shows a similar behaviour as  $q$ .

### *3.5 experimental analysis*

As a first step in the experimental validation process, the reduced model of the tibio-femoral contact complex is considered.

Agreement of results obtained from experimental and physical-mathematical analyses is more valuable if the number of quantities that is compared is larger. With the experimental techniques which are available at this time it is not possible to assess the deformation field or the stress field of the complete system under consideration, because only forces which act at the outer surface of the total system and displacements at the outer circumference of the structure can be measured.

It is advantageous to take the reduced model rather than the reference model as the starting point for the experiments, because in the reduced model one of the contacting components is rigid, whereas both are deformable in the reference model. At contacts of a rigid and a deformable component, the relevant contact stresses / forces can be measured while this is practically impossible in contacts of two deformable components. In the experimental model both the meniscal ring and the articular cartilage layer are made of silicone rubber. Using uniaxial tensile tests, the material characteristics of silicone rubber are determined. These characteristics are used in the

physical-mathematical analyses for the reduced model and the load transmission is calculated. On the other hand experimental analyses are performed for the reduced model and the results obtained from these analyses are compared with those of physical-mathematical analyses.

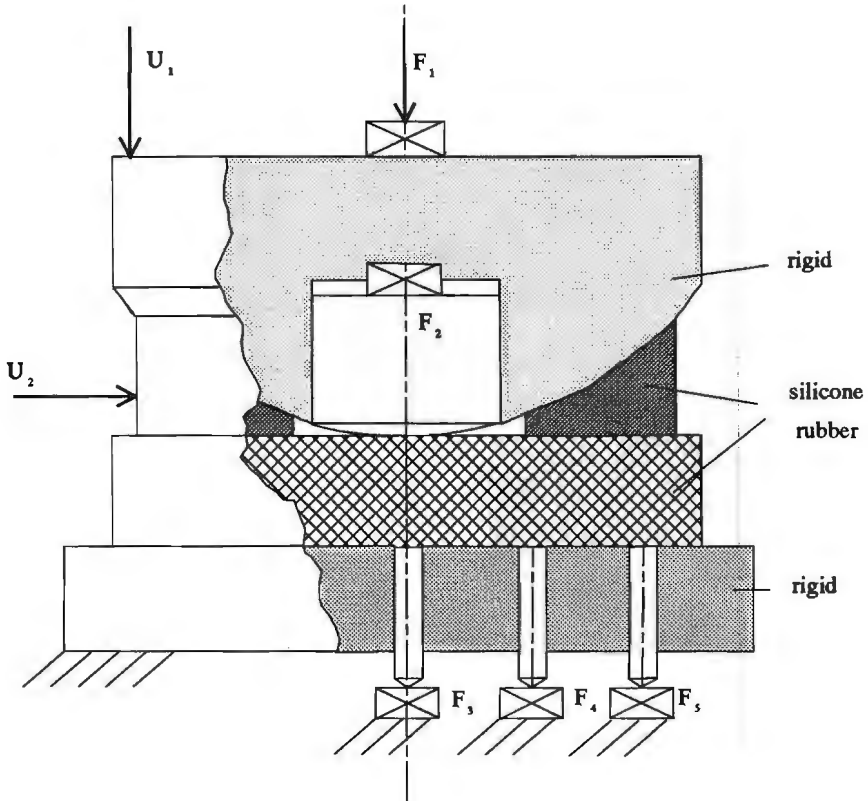


Fig. 3.14 Outline of experimental set-up.

In Fig. 3.14 a schematic outline of the experimental set-up is shown. The rigid spherical femoral component comprises both a cylinder that matches the meniscal ring

and a piston that contacts the articular cartilage layer. The model is resting on a rigid foundation that is spatially fixed. Contrary to the reduced model, as is described in section 3.4, sliding movement of the cartilage layer over the foundation is possible here. Three small cylinders, which are used for measuring the pressure under the cartilage layer, are constructed in this foundation at a distance of 0, 27 and 41 mm from the axis of revolution, respectively, while the outer radius of the cartilage layer is 55 mm.

Five force transducers ( $F_1$ ,  $F_2$ ,  $F_3$ ,  $F_4$  and  $F_5$ ) and two displacement transducers ( $U_1$  and  $U_2$ ) are installed. Using  $F_1$  the total force on the model is measured.  $F_2$  is applied to register the force in the direct contact. Neglecting the friction between the piston and the cylinder in the femoral component, from subtraction of the forces registered by  $F_1$  and  $F_2$  the load of the meniscal ring is established. The inductive displacement transducer  $U_1$  measures the compression of the total system, while the radial displacement of the outer edge of the meniscal component is recorded with the displacement transducer  $U_2$ . The forces on the cylindrical pistons in the rigid foundation are measured by the force transducers  $F_3$ ,  $F_4$  and  $F_5$ . Friction between the pistons and their support appeared to be negligibly small in preliminary experiments.

A two component silicone rubber was used that can be moulded in arbitrary shapes after the curing component is added to the basic component. Model components as well as uniaxial tensile test specimens were prepared from the same mould, as the final material properties depend on the proportion of both basic and curing component in the rubber.

Three different specimens of this silicone rubber are applied, which can be distinguished with respect to their stiffness and their colour ( yellow, green and white ). In appendix B the Mooney-Rivlin material model is fitted on the experimental results of the uniaxial tensile tests. From the fits the stiffness of the yellow, white and green rubber appears to increase in this order.

The experiments which have been performed using the set-up in Fig. 3.14 comprise the combination of a white meniscal ring with a yellow articular cartilage layer and the combination of a white meniscal ring with a green articular cartilage layer. For the first combination the layer is softer than the meniscal ring, while the layer is stiffer for the second combination. To reduce the friction in the contacts, silicone oil of a dynamic viscosity of 12,5 Pas was applied as lubricant.

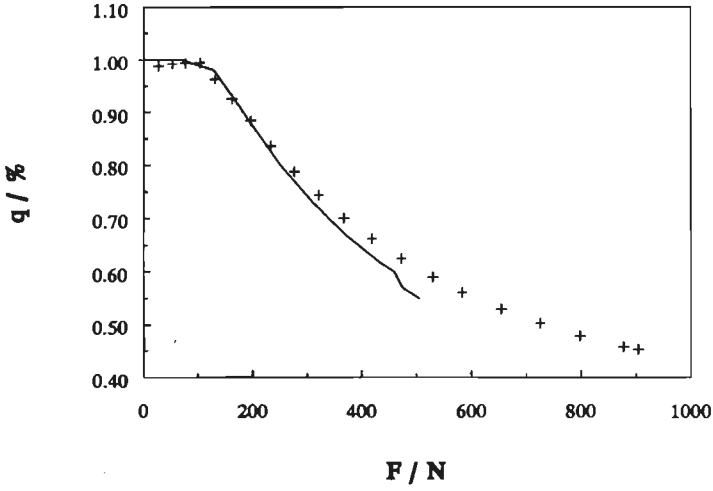


Fig. 3.15a *Part q of the total load borne by the meniscal ring as a function of the total load for the white-green combination.*

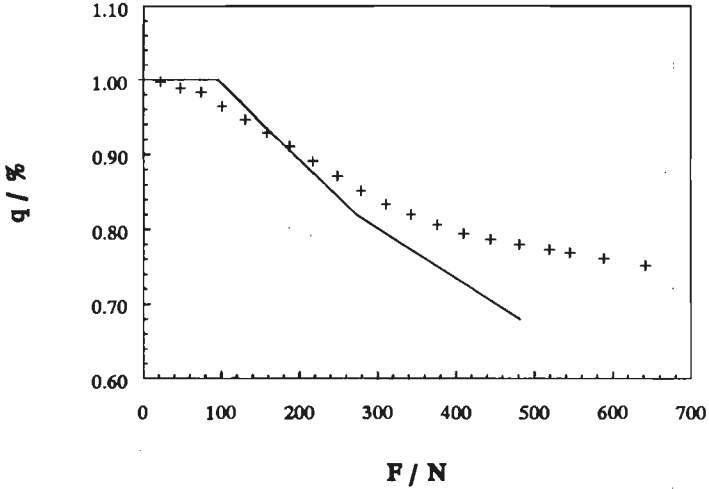


Fig. 3.15b *Part q of the total load borne by the meniscal ring as a function of the total load for the white-yellow combination.*

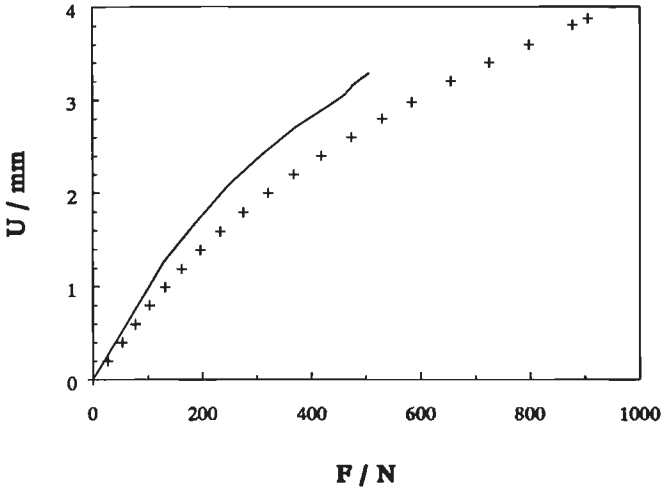


Fig. 3.16a *Axial compression  $U$  of the total model as a function of the total load for the white-green combination.*

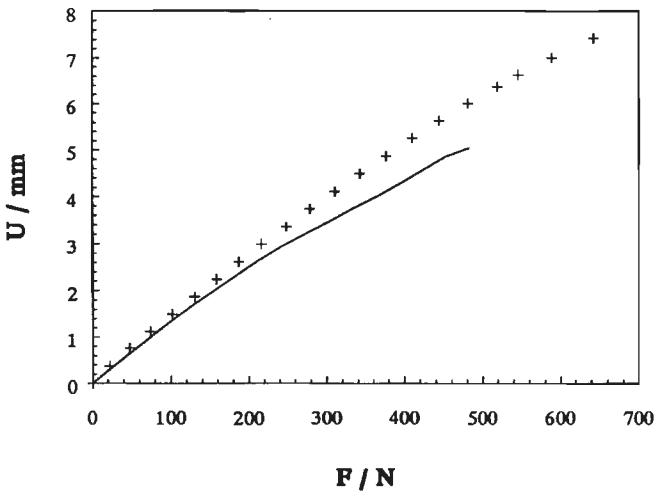


Fig. 3.16b *Axial compression  $U$  of the total model as a function of the total load for the white-yellow combination.*

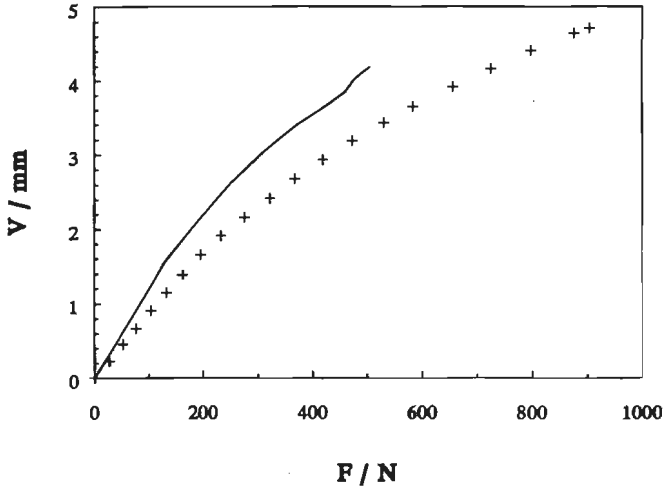


Fig. 3.17a *Radial displacement V of the outer edge of the meniscal ring versus the total load applied on the system for the white-green combination.*

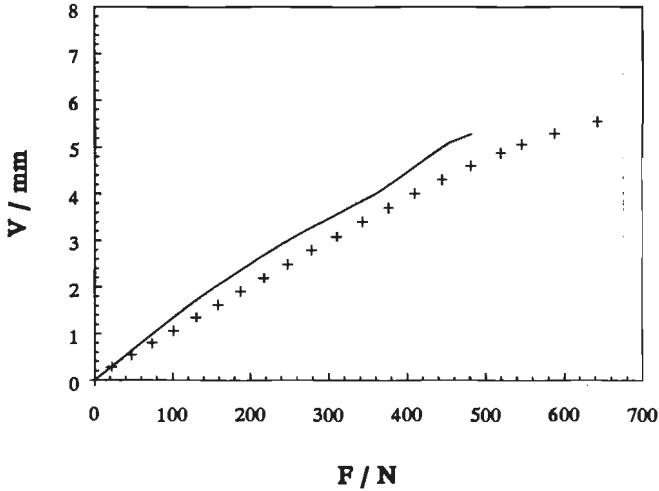


Fig. 3.17b *Radial displacement V of the outer edge of the meniscal ring versus the total load applied on the system for the white-yellow combination.*

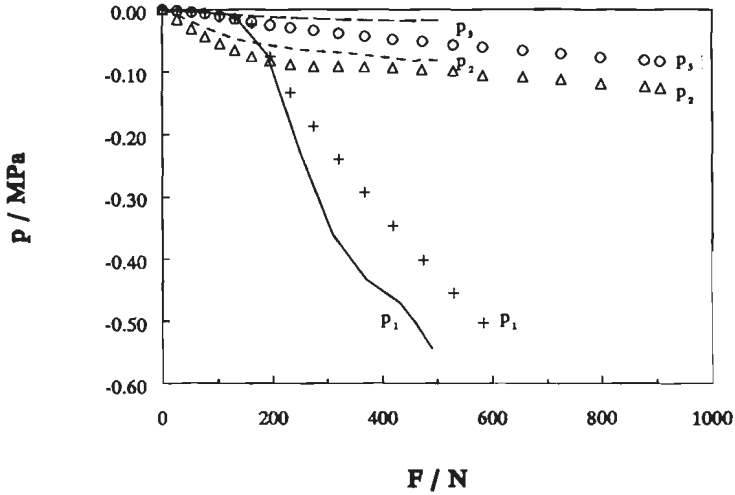


Fig. 3.18a Pressures  $p$  in the contact of tibial component to the rigid underground as a function of the total load applied on the system for the white-green combination.

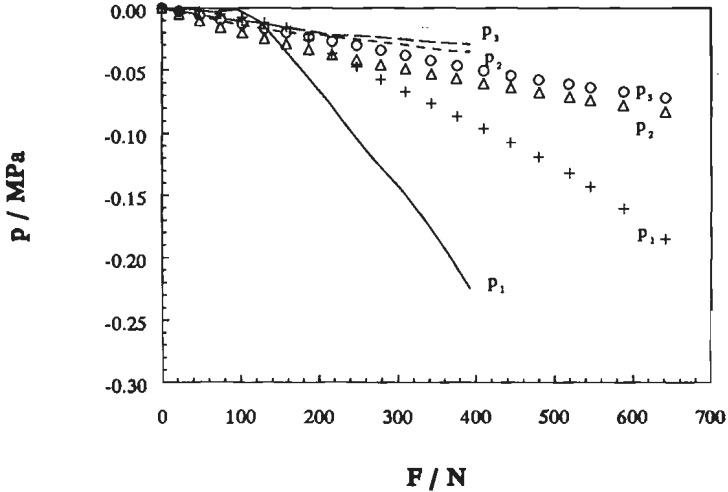


Fig. 3.18b Pressures  $p$  in the contact of tibial component to the rigid underground as a function of the total load applied on the system for the white-yellow combination.

The results of the measurements and of the corresponding numerical analyses are summarized in Figs. 3.15 up to 3.18, where experimental results are indicated by markers while numerical results are represented by drawn lines. Comparison of the experimental and numerical results leads to the following conclusions:

The part  $q$  of the axial load ( Fig. 3.15 ) has a good agreement for the white-green configuration, while for the white-yellow combination the calculated  $q$  is substantially lower than the experimental  $q$ . Further, it is noticed that initially ( up to  $\pm 100$  N ) the total load is borne by the meniscal ring which can be explained by the fact that the meniscal ring is too thick and no initial contact between indenter and articular cartilage layer exists.

For the white-green configuration the experimental  $U$  ( Fig. 3.16 ) is clearly higher than the calculated  $U$ , while for the white-yellow combination a deflection in the opposite direction is found.

The experimental radial displacement  $V$  ( Fig. 3.17 ) of the outer edge of the meniscal ring is lower than the calculated  $V$  for both the white-yellow and the white-green configuration.

For the white-green combination the numerical and experimental pressures in the contact of the articular cartilage layer and the rigid foundation ( Fig. 3.18 ) are qualitatively in agreement, whereas for the white-yellow combination considerable deviations are found. While for  $p_1$  ( at the axis of symmetry ) the numerical results lay underneath the experimental results, the opposite holds for  $p_2$  and  $p_3$ .

The elaboration of the numerical analyses yields problems with respect to the stability of the solution process at loadings of approximately 500 N. These instabilities result from the numerical formulation of the rubber elements. Decreasing the incremental load-size was not helpfull furthermore. However, this shortcoming does not prevent comparison of the numerical and experimental results up to loads of 500 N. Although a qualitative agreement is found, serious differences result, mounting up to  $\pm 20$  % for  $U$ ,  $V$  and  $q$  and up to  $\pm 100$  % for  $p_1$ ,  $p_2$  and  $p_3$ . Although explanations for these deviations can be given, one should keep in mind that to some extent these explanations will have a hypothetical character, because of the limited number of measured quantities. Nevertheless, some explanations are given. The first concerns the friction in the contact between cartilage layer and meniscal ring and the contact of these components to the rigid foundation and the spherical indenter. Suppose that friction in the experimental set-up is not reduced to such a degree that it reasonably

can be considered to be zero. Because no friction is assumed in the physical-mathematical models their  $q$  values will be smaller, while their  $U$  and  $V$  values can be expected to be larger, because moving outward of the meniscal ring is disturbed by the friction. In the physical-mathematical model the cartilage layer is assumed to move without friction along the rigid foundation. Due to friction in the experiment in this contact, the outward movement of the cartilage layer is disturbed and the contact pressure  $p_1$  at the axis of symmetry can be expected to be larger. As a result of this, the contact pressures  $p_2$  and  $p_3$  at larger radii are smaller as the total axial force over the contact surface of the cartilage layer and the rigid foundation is equal for experiments and calculations.

All these deviations can be observed in Figs. 3.15 up to 3.18, except for Fig. 3.16b where the calculated  $U$  is smaller while it is expected to be larger ( due to friction ) than the experimental  $U$ . Another explanation of the differences of experimental and numerical results concerns the yellow moulding of the articular cartilage layer. Close examination of this component by dissection after the experiments revealed that it contained small air bubbles. Therefore its stiffness in the experiment is smaller than in the physical-mathematical model, as in the specimens for the uniaxial tensile test no air bubbles could be noticed. The differences of the values for  $U$  could be explained by the lower stiffness of the yellow cartilage layer. The quantities  $q$ ,  $V$ ,  $p_1$ ,  $p_2$  and  $p_3$  would not be severely affected by a smaller stiffness of the cartilage layer.

### *3.6 summary and conclusions*

An axisymmetric finite element model has been utilized for the analysis of the force transmission in the tibia-meniscus-femur connection. The model assumes linear elastic material properties, static loading and frictionless sliding contact between the components. The study explores the effects of ( a ) tibial surface geometry ( plane, convex, concave ), ( b ) presence of soft layers on the bony components and ( c ) anisotropic properties of the meniscus. Studies with eight combinations of parameters are performed starting from a simple reference model. A reduced model is used to generalize the preliminary findings for a wider range of parameter combinations. This reduced model has also been used for experimental validation.

The important conclusions of the analyses described in this chapter are:

- The soft layers at the ends of femur and tibia, play a considerable role in the force transmission in the models considered. For models with soft layers, the geometry of the tibial plateau seems to have little influence and the load borne by the meniscus increases, as compared to corresponding models without soft layers.
- The stiffness of the meniscus in the circumferential direction is found to be more important for the amount of meniscal load transmission than the stiffness in other directions.
- The parameter studies with the reference model and the reduced model reveal similar effects of the basic parameters as long as soft layers are applied.
- In the range up to 500 N the experimental results in this chapter show qualitatively similar effects as the numerical results. For the displacement quantities and load distribution quantitative deviations up to approximately 20 % occur, while local contact pressures differ up to 100 %. Elucidation of the origin of these deviations can hardly be made, because the experimental measurements are too limited for verifying the proposed explanations.

In the models used for the present study, the material of the components was assumed to be homogeneous and to behave according to Hooke's law. In spite of the viscous, inhomogeneous, and anisotropic nature of bone under certain loading conditions, this assumption is reasonable for the bony structures. For the development of a dynamic knee joint model it will be necessary to model cartilage as a multi-phasic medium ( Mow et al. ( 1984 ) ). In that case it seems also reasonable to consider meniscal tissue as multi-phasic. From the eminent importance of both the presence of soft layers and the circumferential stiffness of the meniscal ring, as found in this study, it is expected that implementation of more appropriate constitutive equations for these parts will undoubtedly yield a more realistic model for the dynamic behaviour of the knee joint.

## FORMULATION OF INTERACTIONS INVOLVING MIXTURES

### *4.1 introduction*

The presence of soft cartilage layers on the articular bone surfaces appears to be very important with respect to the load transmitting function of the meniscal ring in the models discussed in chapter three. These models are based on the assumption that load is fully transmitted by the direct contact between the cartilage layers and the indirect contact via the meniscal ring. All joint components are considered as solids. In reality some of these components are hydrated tissues in a humid environment. Loads acting on these components cause fluid to move in or out. To account for these effects, some components have to be modelled as mixtures. The numerical formulation of solid-solid interaction, as described in chapter two, is adapted in such a way that mixture-mixture interaction and mixture-fluid interaction can be described. Interactions between other combinations of sub-systems can be directly derived from this formulation.

In the following the numerical formulations of a mixture sub-system as well as of a sub-system consisting of an ideal fluid are defined separately. Then, the conditions for the mixture-mixture and mixture-fluid interactions are specified. The numerical formulation will be based on the directly coupled solution strategy.

### *4.2 mixture*

A fictitious continuum is defined, in which each position is occupied by a fluid as well as by a solid. The properties of the resulting continuum are averaged properties and obey the equilibrium and conservation laws ( e.g. Oomens ( 1985 ) ; Mow et al. ( 1984 ) ). In order to describe the averaged properties an elementary volume  $V$  is

used. The characteristic dimensions of the elementary volume are large enough for a fair averaged continuum representation of all discontinuous properties. On the other hand the dimensions have to be much smaller than the characteristic dimensions of the total structure, in such a way that gross inhomogeneities will not be averaged out. The elementary volume comprises a fluid phase and a solid phase

$$V = V_s + V_f \quad (4.1)$$

where the subscripts s and f denote the solid and the fluid, respectively. The corresponding fluid and solid volume fractions are

$$\phi_f = \frac{V_f}{V} \quad ; \quad \phi_s = \frac{V_s}{V} \quad ; \quad \phi_f + \phi_s = 1 \quad (4.2)$$

The balance of mass requires the change of mass to be equal to the mass passing the boundaries of the volume for each phase

$$\frac{\partial \rho_s}{\partial \tau} + \vec{\nabla} \cdot (\rho_s \vec{v}_s) = 0 \quad ; \quad \rho_s = \phi_s \rho_s^* \quad (4.3)$$

$$\frac{\partial \rho_f}{\partial \tau} + \vec{\nabla} \cdot (\rho_f \vec{v}_f) = 0 \quad ; \quad \rho_f = \phi_f \rho_f^* \quad (4.4)$$

with  $\vec{\nabla}$ ,  $\vec{v}_s$  and  $\vec{v}_f$  representing the gradient operator, and the solid and fluid phase velocity, respectively, with respect to a spatially fixed reference. In these equations  $\rho$  is the mass density with respect to the total elementary volume, and  $\rho^*$  is the real mass density of the concerned phase. Both phases in the mixture are assumed to be intrinsically incompressible ( $\rho^* = \text{constant}$ ). Mass transition from one phase to the other is excluded.

Dividing (4.3) and (4.4) by  $\rho_s^*$  and  $\rho_f^*$ , respectively, subsequently adding the results and using (4.2) yields

$$\vec{\nabla} \cdot \phi_f (\vec{v}_f - \vec{v}_s) + \vec{\nabla} \cdot \vec{v}_s = 0 \quad (4.5)$$

From this relation it can be easily derived that, as both phases are intrinsically incompressible, volume changes of the mixture can only occur as a result of relative motion between the fluid and solid phases.

Neglecting inertia effects, the balance of momentum for both phases can be written as

$$\vec{\nabla} \cdot \alpha_s + \vec{r}_s = \vec{0} \quad (4.6)$$

$$\vec{\nabla} \cdot \alpha_f + \vec{r}_f = \vec{0} \quad (4.7)$$

with  $\vec{r}$  representing the specific interaction forces between the solid and fluid phase. Because of the principle of action and reaction

$$\vec{r}_s = -\vec{r}_f \quad (4.8)$$

The material behaviour of a mixture is determined by the behaviour of the phases separately as well as by their interaction.

According to the usual approach of mixture theory the Cauchy stress tensor of the solid and fluid phase are written as

$$\alpha_s = \sigma_{\text{eff}} - \lambda \phi_s \mathbf{I} \quad (4.9)$$

$$\alpha_f = -\lambda \phi_f \mathbf{I} \quad (4.10)$$

where  $\lambda$  is the hydrostatic pressure of the ideal fluid in the mixture and  $\sigma_{\text{eff}}$  is the effective stress. The deformation dependency of the latter will be specified in chapter 5.

Substituting ( 4.9 ) and ( 4.10 ) into ( 4.6 ) and ( 4.7 ), respectively, and subsequently adding the resulting equations leads with ( 4.8 ) to

$$\vec{\nabla} \cdot (\sigma_{\text{eff}} - \lambda \mathbf{I}) = \vec{0} \quad (4.11)$$

The interaction between the phases is described by Darcy's law

$$\vec{v} \cdot \vec{v}_s - \vec{v} \cdot (\mathbf{K} \cdot \vec{v} \lambda) = 0 \quad (4.12)$$

with  $\mathbf{K}$  representing the permeability tensor.

Consider a mixture sub-system  $j$  with volume  ${}_jV$  and outer surface  ${}_jA$ , that is decomposed according to ( 2.2 ) in  ${}_jA_c$  and  ${}_jA_n$ . A weak formulation both for equilibrium of the mixture and for the momentum balance of the fluid phase reads

$$\begin{aligned} & \int_{{}_jV} ({}_j\vec{v} \cdot {}_j\vec{w})^c : {}_j\sigma_{\text{eff}} d{}_jV - \int_{{}_jA_n} {}_j\vec{w} \cdot {}_j\vec{p} d{}_jA - \\ & \int_{{}_jA_c} {}_j\vec{w} \cdot {}_j\vec{p}_c d{}_jA - \int_{{}_jV} {}_j\vec{w} \cdot {}_j\vec{v} \cdot {}_j\lambda d{}_jV + \\ & \int_{{}_jV} {}_jz \cdot {}_j\vec{v} \cdot {}_j\vec{v}_s d{}_jV + \int_{{}_jV} {}_j\vec{v} \cdot {}_jz \cdot {}_j\mathbf{K} \cdot {}_j\vec{v} \cdot {}_j\lambda d{}_jV - \\ & \int_{{}_jA_n} {}_jz \cdot {}_j\vec{n} \cdot {}_j\mathbf{K} \cdot {}_j\vec{v} \cdot {}_j\lambda d{}_jA - \int_{{}_jA_c} {}_jz \cdot {}_j\vec{n} \cdot {}_j\mathbf{K} \cdot {}_j\vec{v} \cdot {}_j\lambda d{}_jA = 0 \end{aligned} \quad (4.13)$$

where  ${}_j\vec{w}$  and  ${}_jz$  are arbitrary weighting functions used in the equilibrium and in the momentum equations, respectively. The vectors  ${}_j\vec{p}$ ,  ${}_j\vec{p}_c$  and  ${}_j\vec{n}$  represent respectively the load vectors on  ${}_jA_n$  and on  ${}_jA_c$  and the unit outward normal vector at  ${}_jA$ .

The term

$${}_j\vec{n} \cdot {}_j\mathbf{K} \cdot {}_j\vec{v} \cdot {}_j\lambda = {}_jq \quad (4.14)$$

can be interpreted as the outward flow per unit area through the surface.

A finite element discretization is applied to both the fields of position vectors and the field of fluid pressures

$${}_j\vec{x} = {}_j\vec{\alpha}^T {}_j\vec{x} \quad ; \quad {}_j\lambda = {}_j\alpha^T {}_j\lambda \quad (4.15)$$

with  ${}_j\vec{x}$  and  ${}_j\lambda$  being the columns of nodal coordinates with respect to the solid phase and nodal hydrostatic pressures, respectively, whereas  ${}_j\vec{\alpha}$  and  ${}_j\alpha$  are columns with vector and scalar interpolation functions. Similar interpolation functions are chosen for the displacement components and for the hydrostatic pressures. Using a Galerkin approach, the weighting functions are written as

$${}_j\vec{w} = {}_j\vec{\alpha}^T {}_j\vec{w} \quad ; \quad {}_jz = {}_j\alpha^T {}_jz \quad (4.16)$$

with the columns  ${}_j\vec{w}$  and  ${}_jz$  defined analogously to  ${}_j\vec{x}$  and  ${}_j\lambda$ , respectively. Using (4.14), (4.15) and (4.16), equation (4.13) can be transformed into

$$\begin{bmatrix} {}_j\vec{w} \\ {}_jz \end{bmatrix}^T \begin{bmatrix} {}_j\vec{f} - {}_j\vec{f} - {}_j\vec{c} - {}_j\vec{t} \\ {}_j\vec{s} + {}_j\vec{b} - {}_j\vec{d} - {}_j\vec{m} \end{bmatrix} = 0 \quad (4.17)$$

with

$${}_j\vec{f} = {}_j\vec{f}({}_j\vec{x}) = \int_{{}_jV} ({}_j\vec{v} \cdot {}_j\vec{\alpha})^c : {}_j\sigma_{\text{eff}} \, d{}_jV \quad (4.18)$$

$${}_j\vec{f} = \int_{{}_jA_n} {}_j\vec{\alpha} \cdot {}_j\vec{p} \, d{}_jA \quad (4.19)$$

$${}_j\vec{c} = \int_{{}_jA_c} {}_j\vec{\alpha} \cdot {}_j\vec{p}_c \, d{}_jA \quad (4.20)$$

$${}_j\vec{t} = {}_j\vec{t}({}_j\lambda) = \int_{{}_jV} {}_j\vec{\alpha} \cdot {}_j\vec{v} \, {}_j\alpha^T {}_j\lambda \, d{}_jV \quad (4.21)$$

$${}_j\vec{s} = {}_j\vec{s}({}_j\dot{x}) = \int_{{}_jV} {}_j\alpha \, {}_j\vec{v} \cdot {}_j\vec{v}_s \, d{}_jV \quad (4.22)$$

$$j\underline{b} = j\underline{b}(j\underline{\lambda}) = \int_{jV} j\underline{\nabla} j\underline{\alpha} \cdot j\underline{K} \cdot j\underline{\nabla} j\underline{\alpha}^T j\underline{\lambda} d_jV \quad (4.23)$$

$$j\underline{n} = \int_{jA_n} j\underline{\alpha} j\underline{q} d_jA \quad (4.24)$$

$$j\underline{m} = \int_{jA_c} j\underline{\alpha} j\underline{q} d_jA \quad (4.25)$$

The columns  $j\underline{f}$ ,  $j\underline{l}$ ,  $j\underline{c}$  and  $j\underline{l}$  comprise the internal nodal forces resulting from the deformation of the solid phase, the external nodal forces applied on  $jA_n$ , the contact forces acting on  $jA_c$  and the internal nodal forces resulting from the hydrostatic pressure, respectively. The columns  $j\underline{s}$ ,  $j\underline{b}$ ,  $j\underline{n}$  and  $j\underline{m}$  contain, respectively, the nodal flows related to the volume change of the mixture, the nodal flows resulting from fluid pressure gradients, prescribed nodal flows on  $jA_n$  and the flow across  $jA_c$ .

The requirement that ( 4.17 ) applies for arbitrary weighting functions results in the system equations

$$\begin{cases} j\underline{f}(j\underline{x}) - j\underline{l} - j\underline{c} - j\underline{l}(j\underline{\lambda}) = \underline{0} \\ j\underline{s}(j\underline{x}) + j\underline{b}(j\underline{\lambda}) - j\underline{n} - j\underline{m} = \underline{0} \end{cases} \quad (4.26)$$

Applying the Houbolt time integration scheme ( Bathe ( 1990 ) ) with constant time-steps  $\Delta t$ , the velocity field is described by

$$j\underline{\dot{x}}(t+\Delta t) = \frac{1}{6\Delta t} [ 11 j\underline{x}(t+\Delta t) - 18 j\underline{x}(t) + 9 j\underline{x}(t-\Delta t) - 2 j\underline{x}(t-2\Delta t) ] \quad (4.27)$$

Now, the discretized formulation of the mixture problem can be written as

$$\begin{cases} j\underline{f}(j\underline{x}) - j\underline{l} - j\underline{c} - j\underline{l}(j\underline{\lambda}) = \underline{0} \\ j\underline{s}(j\underline{x}) + j\underline{b}(j\underline{\lambda}) - j\underline{n} - j\underline{m} = \underline{0} \end{cases} \quad (4.28)$$

where  ${}^{**}j\underline{s}$  comprises the contribution of  $j\underline{x}$  in  $j\underline{s}$  from previous time steps according to the Houbolt time integration scheme and  ${}^*j\underline{s}$  contains the contribution of  $j\underline{x}$  from the actual time step. The degrees of freedom  $j\underline{x}$  and  $j\underline{\lambda}$  of the sub-system satisfy the kinematic boundary conditions, while  $j\underline{r}$  and  $j\underline{u}$  obey the dynamic boundary conditions.

### 4.3 fluid

Again an imaginary sub-system  $j$  with volume  $jV$  and outer surface  $jA_c$  is considered. The sub-system is assumed to be fully enclosed by structure sub-systems and interaction occurs at all points of  $jA_c$ . Let the volume  $jV$  be filled with an ideal fluid, while fluid flow across the outer surface is not allowed. Because the fluid is ideal, two conditions apply. The volume invariance condition is represented by

$$\frac{\partial_j V}{\partial \tau} = 0 \quad (4.29)$$

The stress tensor is given by

$$j\sigma = -j\rho \mathbf{I} \quad (4.30)$$

where  $j\rho$  is the hydrostatic pressure of the fluid, which is equal for all points in  $jV$ . However, if fluid flow across the outer surface is allowed, condition (4.29) has to be replaced by

$$\frac{\partial_j V}{\partial \tau} + \int_{jA_c} j\vec{v}_f \cdot j\vec{n} \, d_j A = 0 \quad (4.31)$$

with  $j\vec{v}_f = \dot{j}\vec{x}_f$  being the fluid velocity vector.

Consider an arbitrary point  $P$  on  $jA_c$  at time  $\tau=t$ . The position vector of  $P$  is expressed as a function of the positions of a number of nodal points on  $jA_c$  in the discretized formulation. When these nodal positions are represented by  $j\underline{x}$ , for the position vector of point  $P$  holds

$$\vec{j}\underline{x}^P(t) = \vec{j}\underline{\alpha}^T(\underline{\xi}^P) \vec{j}\underline{x}(t) \quad (4.32)$$

where  $\vec{j}\underline{\alpha}$  is a column of vector interpolation functions and  $\underline{\xi}^P$  is the column with material coordinates for point P.

The actual volume  ${}_jV$  can be derived from the positions of all nodes on  ${}_jA_c$

$${}_jV = {}_jV({}_j\underline{x}) \quad (4.33)$$

The stress principle of Cauchy-Euler is given by

$$\vec{j}\underline{p}_c = {}_j\underline{\sigma} \cdot {}_j\underline{n} \quad (4.34)$$

Substituting ( 4.30 ) into ( 4.34 ), with the use of ( 2.9 ), the column with nodal contact forces can be expressed as

$$\vec{j}\underline{c} = \vec{j}\underline{c}({}_j\underline{p}) = - {}_j\underline{p} \int_{{}_jA_c} \vec{j}\underline{\alpha} \cdot {}_j\underline{n} d{}_jA \quad (4.35)$$

The flow across the outer surface of the fluid sub-system is distributed over the nodes of the sub-system. The flow related to node P is indicated by  ${}_j\underline{\psi}^P$ , and is positive when fluid flow is leaving the sub-system j. Let the total number of nodes on  ${}_jA_c$  in the fluid sub-system be m. For the present increment or time step the equations ( 4.29 ) and ( 4.31 ) are transformed into

$${}_jV({}^{i+1}{}_j\underline{x}) - {}_jV({}_j\underline{x}) = 0 \quad (4.36)$$

$${}_jV({}^{i+1}{}_j\underline{x}) - {}_jV({}_j\underline{x}) + \Delta t \sum_{k=1}^m ({}^{i+1}{}_j\underline{\psi}^k - {}_j\underline{\psi}^k) = 0 \quad (4.37)$$

respectively, where  $\Delta t$  is the actual time step. In a more concise notation they are formulated as

$$\Delta_j V(\underline{j}\underline{x}) = 0 \quad (4.38)$$

$$\Delta_j V(\underline{j}\underline{x}) + \underline{j}Q = 0 \quad (4.39)$$

where  $\underline{j}Q$  is the total flow leaving the fluid sub-system during the actual increment.

#### 4.4 interface conditions

##### 4.4.4 introduction

In order to formulate the interface conditions between a sub-system consisting of an ideal fluid and mixture sub-systems, it is assumed that the fluid sub-system is enclosed by one or more structure sub-systems. Structure-structure interactions as well as fluid-structure interactions may occur. Whether a material point on  $A_c$  is involved in structure-structure or in fluid-structure interaction is not known a priori, as this depends on the actual deformation of the total system.

Let the nodal contact forces  $\underline{r}\underline{c}$  and the nodal positions  $\underline{r}\underline{x}$  be constituted by a selection from  $\underline{c}$  and  $\underline{x}$  representing the respective columns for the total system. This is expressed by the equations

$$\underline{S}\underline{c} = -\underline{r}\underline{c} \quad (4.40)$$

$$\underline{S}\underline{x} = \underline{r}\underline{x} \quad (4.41)$$

where  $\underline{S}(\underline{x})$  is a selection matrix that selects only those nodes of  $A_c$  that are actually bordering the fluid sub-system.

Three cases are distinguished with respect to interactions involving mixture sub-systems. In the first case fluid flow across the boundaries of the sub-system is not allowed. The surfaces of the interacting mixtures are sealed and impervious. In the second case fluid flow across the boundaries of the sub-systems is allowed. The fluid pressures at both sides of  $A_c$  are equal. In the third case the contact between sealed and not sealed surfaces is considered. These three cases are dealt with in the following sub-sections.

4.4.2 interaction between sealed mixture sub-systems

Starting from the mixture sub-system equations ( 4.28 ), the columns resulting from interaction with other sub-systems have to be defined. These are the columns  $\underline{j}_c$  and  $\underline{j}_m$ , containing the nodal forces and nodal flow at  $\underline{j}A_c$  respectively. When interactions with sealed surfaces are considered fluid flow across  $A_c$  is not permitted while the fluid pressures at both sides of the seal are not necessarily equal. This situation is achieved by assuming the contribution to the column  $\underline{m}$ , comprising nodal fluid flows across  $A_c$  of all contact units, to be zero, hence

$$\underline{m} = \underline{0} \tag{ 4.42 }$$

The fluid sub-system is completely enclosed by impervious sub-system surfaces. Fluid flow in or out of this sub-system is not possible and condition ( 4.38 ) applies. In addition to the contribution of the structure-structure interaction to the column with contact forces  $\underline{c}$ , which is described in chapter two, we now have also a contribution of the fluid-structure interaction that emanates from the pressure of the fluid sub-system. Taking this contribution into account the expression ( 2.29 ) for the column with contact forces is extended according to

$$\underline{c} = \underline{\Delta}(\underline{x}) \underline{k} - \underline{S}(\underline{x}) \underline{r}(\underline{p}) \tag{ 4.43 }$$

The formulation of the interaction between sealed mixture sub-systems and a sub-system consisting of an ideal fluid is represented by

$$\begin{cases} \underline{f}(\underline{x}) - \underline{r} - \underline{c}(\underline{x}, \underline{k}, \underline{p}) - \underline{t}(\underline{\lambda}) = \underline{0} \\ \underline{s}(\underline{x}) + \underline{b}(\underline{\lambda}) - \underline{n} = \underline{s} \\ \underline{h}(\underline{x}, \underline{k}) = \underline{0} \\ \underline{\Delta}_j V(\underline{x}) = 0 \end{cases} \tag{ 4.44 }$$

The system degrees of freedom are denoted by  $\underline{x}$ ,  $\underline{\lambda}$ ,  $\underline{k}$  and  $\underline{p}$ , representing the nodal displacements, hydrostatic pressures, contact forces and the pressure of the fluid sub-system, respectively. When  $n$  is the number of nodes in the total system and  $m$  the number of nodes on  $A_c$ , the equations in ( 4.44 ) represent respectively  $3n$  equilibrium

conditions,  $n$  mass balance conditions for the fluid,  $3m$  contact conditions and 1 condition for the volume invariance of the fluid sub-system. In total (  $4n + 3m + 1$  ) equations and an equal number of system degrees of freedom are used for describing the sealed mixture interaction problem.

#### 4.4.3 *interaction between mixtures which are not sealed*

If mixtures interact that are not sealed, in addition to the conditions for the contact forces, which are equal to the conditions described for interaction between sealed sub-systems, conditions for the fluid flow across  $A_c$  have to be formulated. Therefore, the mixture-mixture and mixture-fluid contact are distinguished. For every node ( contact unit ) on  $A_c$  it is checked whether this node is actually in contact with a structure or with a fluid sub-system. The conditions under which the structure-structure contact is assigned are described in section 2.4.3.

Let  $\phi_P$  be the nodal flow in node P as a result of the interaction in the contact unit defined for P, where  $\phi_P$  is positive for fluid flow leaving the sub-system comprising P. The following conditions apply

- mixture-mixture contact

Because  $\phi_P$  is the flow contribution to node P of the contact unit,  $-\phi_P$  is the flow contribution to a number of other nodes in this contact unit, according to the mass balance of fluid. The distribution of  $-\phi_P$  over these nodes is formally given by

$$\Delta_P \underline{m} = - \underline{d}_P ( \underline{x} ) \phi_P \quad ( 4.45 )$$

where  $\underline{d}_P$  is a distribution column. Then the total contribution to  $\underline{m}$  of the contact unit under consideration is represented by

$$\underline{m}_P = \Delta_P \underline{m} + \underline{l}_P \phi_P = [ - \underline{d}_P + \underline{l}_P ] \phi_P \quad ( 4.46 )$$

with  $\underline{l}_P$  being the appropriate location column. Finally, a condition, taking into account that the hydrostatic pressures at both sides of  $A_c$  are equal, applies for node P. This is formulated by

$$\pi_p(\underline{\lambda}) = 0 \quad (4.47)$$

where  $\pi_p$  is a scalar function of the column of hydrostatic pressures.

- mixture-fluid contact

If the mixture-mixture contact is not active, it is assumed that the concerned material point on  $A_c$  is interacting with a fluid. This can be a fluid sub-system which is enclosed by structure sub-systems, or it can be an environmental fluid with external specified conditions. Here, contact with a fluid sub-system is considered. The nodal flows  $\psi$ , which constitute the total flow  ${}_rQ$  out of the fluid sub-system according to (4.39), are the sum of the components of the results from  $\underline{S} \underline{s}$  and  $-\underline{S} \underline{b}$ . Further, in node P the hydrostatic pressure of the mixture is equal to the pressure in the fluid sub-system

$$\lambda_p = p \quad (4.48)$$

Taking all contact units into account, the problem of interaction between one fluid sub-system and several not sealed mixture sub-systems is characterized by

$$\left\{ \begin{array}{l} \underline{f}(\underline{x}) - \underline{r} - \underline{c}(\underline{x}, \underline{k}, {}_rP) - \underline{t}(\underline{\lambda}) = \underline{0} \\ \underline{s}(\underline{x}) + \underline{b}(\underline{\lambda}) - \underline{n} - \underline{m}(\underline{\phi}) = \underline{s} \\ \underline{h}(\underline{x}, \underline{k}) = \underline{0} \\ \underline{\chi}(\underline{x}, \underline{\lambda}, {}_rP) = \underline{0} \\ \Delta_r \underline{\vartheta}(\underline{x}) + {}_rQ = 0 \end{array} \right. \quad (4.49)$$

with  $\underline{\chi}$  comprising the conditions (4.47) and (4.48) for all contact units. The system degrees of freedom are given by  $\underline{x}$ ,  $\underline{\lambda}$ ,  $\underline{k}$ ,  $\underline{\phi}$  and  ${}_rP$ , representing the nodal displacements, hydrostatic pressures, contact forces, flows across  $A_c$  and the pressure in the fluid sub-system, respectively.

#### *4.4.4 other interactions*

Several other interactions such as solid-fluid and solid-mixture interactions are possible and can be described with the presented formulations.

When the fluid sub-system is enclosed by solid sub-systems, the appropriate formulation can be derived from ( 4.44 ) for the sealed mixtures interaction. All columns of ( 4.44 ), which are related to fluid movement inside the mixture sub-systems, can then be left out of ( 4.44 ). A system of (  $3n + 3m + 1$  ) equations results.

Otherwise, when the fluid is enclosed by solids and mixtures which are not sealed, the formulation is based on ( 4.49 ). A fluid pressure degree of freedom  $\lambda$  is attributed to every node on  $A_c$ . As those degrees of freedom only receive contributions from the interaction with other sub-systems and not directly from mixture elements, these contributions are forced to zero by the system equations. The total number of system degrees of freedom is (  $3n + h + 4m + 1$  ), where  $h$  is the number of nodes in the system which are part of a mixture element or lie on  $A_c$ .

#### *4.5 summary and conclusions*

A mixture sub-system and a sub-system comprising an ideal fluid have been considered. Also the interface conditions for mixture-mixture and fluid-mixture contacts have been defined. With respect to mixtures, sealed and not sealed contact surfaces are distinguished. Concerning the interaction of sealed surfaces the contact forces depend on the actual situation of the total system while the mass-balance conditions for the fluid concern only the quantities of the considered sub-system. When the surfaces are not sealed these mass-balance equations for the several sub-systems are also coupled. For a node on  $A_c$  equations take into account the equilibrium conditions, the mass-balance for the fluid, the impenetrability conditions for the contact and contact conditions for the hydrostatic pressure.



## INCORPORATION OF FLUID AND MIXTURES IN THE TIBIO-FEMORAL CONTACT MODEL

### *5.1 introduction*

Both the articular cartilage layers and the synovial fluid in the tibio-femoral joint are hydrated tissues comprising free fluid that can move through the solid matrix and the hyaluronic acid-protein complex, respectively. In literature the cartilage is often described as a mixture ( Mow et al. ( 1984 ); Spilker et al. ( 1990 ); Spilker and Suh ( 1990 ) ), while the synovia is considered as a viscous fluid ( Droogendijk ( 1984 ) ). A complex interaction between the cartilage layers and the synovial fluid occurs when the joint is loaded. Literature agrees to the importance of the tribological function of the synovia ( Dowson ( 1967 ); Walker et al. ( 1968 ); Dowson et al. ( 1970 ); Armstrong and Mow ( 1980 ) ). Several lubrication mechanisms have been proposed in which the deformability and permeability of the articular cartilage layers are taken into account, but quantitative validation of these mechanisms fails. To achieve insight into the lubrication in the knee joint, the importance of possibly relevant parameters ( such as viscosity of the synovial fluid, permeability and stiffness of the cartilage layers, thickness of the cartilage layers, the presence of menisci and the curvature of the articular surfaces ) have to be investigated.

A very valuable step in this direction has been done by Hou ( 1989 ). He developed a model of squeeze film lubrication. According to this mechanism the load bearing capability of the viscous fluid film is based on the resistance the fluid offers when it is squeezed out of the contact zone. The axisymmetric model comprises a rigid impervious spherical indenter and a plane deformable layer of a fluid-solid mixture, representing the cartilage layer. The layer is fixed to a rigid impervious underground. The complete model is immersed in a Newtonian fluid. With respect to the boundary

conditions for the fluid film, at the solid indenter the no-slip condition applies, while at the cartilage interface the tangential fluid velocity is assumed to be equal to the averaged velocity, weighted by the volume fractions of the fluid and solid phases in the mixture at this place. The coupled differential equations for the infinitesimal deformations of the cartilage layer and the viscous fluid film are solved almost fully analytically for step loadings of 30 N and 300 N, starting at a small initial gap between the cartilage layer and the indenter. The initial gap reduces to zero in the course of time and the fluid pressure in the film has its maximum value at the centre of the contact of indenter and layer and decreases to zero with increasing radius. At the centre of contact a small flow from the film into the cartilage occurs. Under the load of 300 N the deformations of the cartilage are so large that the infinitesimal deformation theory can no more be applied properly. Hou concluded that with the development of finite element models for the mixture and fluid and by using more accurate constitutive relations for the finite deformations, it will be possible to describe the joint function more accurately.

The development of such models is difficult, especially when large relative movements of joint elements such as articular surfaces and menisci are considered. In this chapter a first step of numerical modelling of the fluid-mixture interaction in the tibio-femoral joint is performed, based on the formulations as derived in the chapters two and four. A model is defined using finite deformation mixture elements which are coupled to a sub-system consisting of an ideal fluid.

## 5.2 *description of the model*

The first model in our approach comprising mixture-mixture and mixture-fluid interaction is based on the reduced model as presented in chapter three as far as geometry is concerned. The model ( Fig. 5.1 ) is axisymmetric and contains a planar disc, representing the articular cartilage layer, a spherical indenter, and, in between a toroid with a wedge-shaped cross-section representing the meniscus. In the unloaded situation the upper end plane of the articular cartilage layer is in contact with the indenter only at the axis of symmetry. The lower end plane of the cartilage layer is fixed to a rigid underground. The lower end plane of the meniscal ring rests fully on this layer while the upper surface of the meniscal ring matches the spherical indenter.

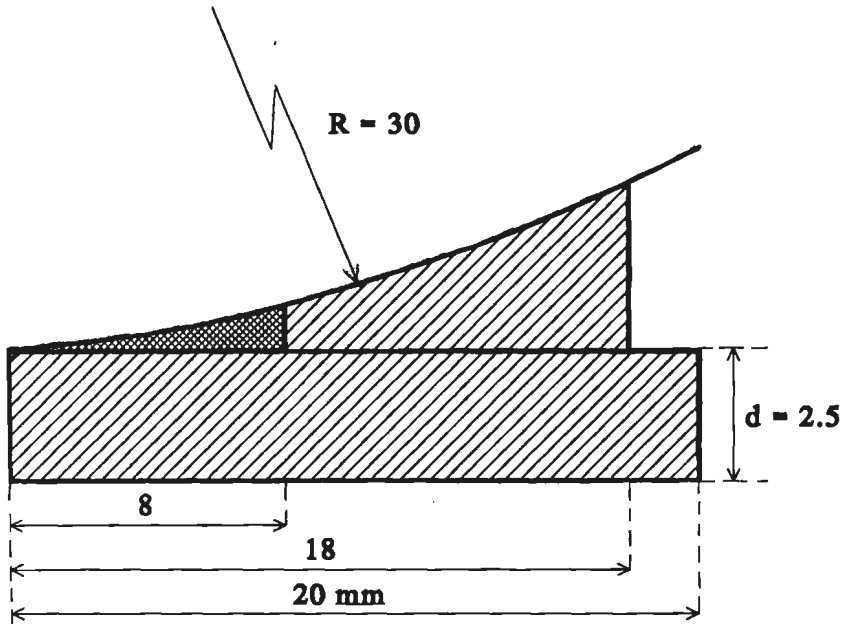


Fig. 5.1 *Half of the cross-section of the axisymmetric model with mixture components ( // ) and fluid component ( XX ).*

Frictionless sliding of the meniscal ring along the articular cartilage layer and the spherical indenter as well as sliding of the articular cartilage layer along the spherical indenter is allowed. Both the articular cartilage layer and the meniscal ring are deformable mixtures of a solid and a fluid, while the spherical indenter and the underground are rigid and impervious. The cavity enclosed by the cartilage layer, the meniscal ring and the rigid sphere is filled with an ideal fluid. In the model this cavity is considerably larger than in the real knee joint, because this is for the time being easier to describe. Fluid flow across the interfaces of the fluid-mixture and mixture-mixture contacts is allowed. The outflow at the outer radius of the meniscal ring and the articular cartilage layer is free while the fluid pressure is assumed to be zero at these places. It is assumed that no fluid layer is present between contacting surfaces. The material behaviour is characterized by a linear coupling between the second

Piola-Kirchhoff stress tensor and the Green-Lagrange strain tensor according to Hooke's law ( equation ( 3.1 ) ) with  $E$  and  $\nu$  representing the Young modulus and Poisson ratio, respectively. The effective Cauchy stress-tensor can be derived directly from the second Piola-Kirchhoff stress tensor. Furthermore, an isotropic constant permeability is assumed with the permeability tensor

$$\mathbf{K} = k \mathbf{I} \quad ( 5.1 )$$

with  $k$  being the permeability coefficient. The numerical values for the material parameters are listed in Table 5.1.

	$E$ ( MPa )	$\nu$ ( - )	$k$ ( mm <sup>4</sup> /Ns )
meniscal ring	20.0	0.3	0.001
articular cartilage	10.0	0.4	0.001

Table 5.1 *values for material parameters*

An axial load of 250 N is applied at  $\tau = 0$  and the response of the model is calculated for the next 25,000 seconds. The articular cartilage layer and the meniscal ring are divided into four-node isoparametric mixture elements with linear interpolation functions for the displacements and hydrostatic pressures.

The problem is solved using the directly coupled solution strategy and this strategy seems to be very effective because no instabilities occurred.

From the performed analysis the load-distribution in this model seems to depend strongly on time. In the reference model, presented in chapter three, the load was borne by both the direct contact between the femoral and tibial component and by the contact through the meniscal ring. In the model which is considered here, a third sub-connection is constituted by the fluid enclosed in the cavity. Fig. 5.2 shows the load-distribution over these three sub-connections as a function of time. Initially, just after the load has been applied, the flow in the mixture components has not yet started and about 75 % of the total load is borne by the fluid sub-system, while the direct and meniscal contact bear 7 and 18 %, respectively. As time proceeds fluid can flow out of the model at the circumferential outer surface of the meniscal ring and the articular cartilage layer and the pressure in the fluid sub-system decreases. Because of the

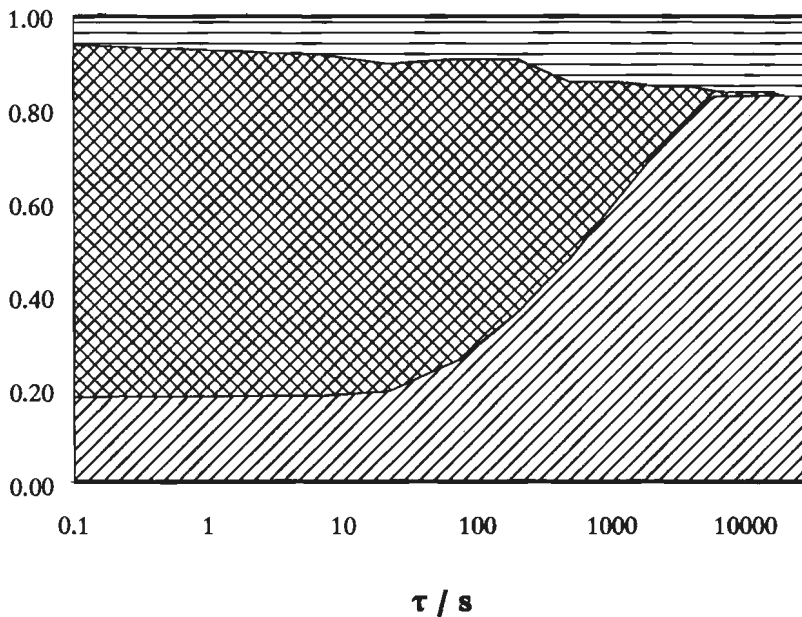


Fig. 5.2 Load-distribution versus time via direct contact ( — ), meniscal ring ( // ) and fluid sub-system ( XX ).

outflow, the compression of the total model increases and the fluid sub-system carries a continually decreasing part of the total load. Finally, after 10,000 seconds the hydrostatic pressure is approximately zero all over the model and the load is borne only by the direct contact ( 16 % ) and the meniscal ring ( 84 % ). Flow across the upper surface of the cartilage layer only occurs when the concerned node is contacting the fluid sub-system or the meniscal ring. When it is contacting the impervious spherical indenter, the outflow ceases in this node.

Because of electrolytes are soluted in the fluid phase of the articular cartilage and the proteoglycan aggregates of the solid matrix are ionized, local concentrations of electrical loadings are created by forcing the fluid to move out of the model. Therefore, the time that elapses until no further changes, resulting from the applied load, occur will be probably smaller in reality.

The meniscal ring has a dual function in this model. Initially, just after the load is applied the enclosure of the fluid cavity by the meniscal ring results in a pressure building up in the cavity, while finally, when fluid pressure approximates zero, the meniscal ring carries the larger part of the total load.

### 5.3 *parameter studies*

#### 5.3.1 *introduction*

In comparison with the models presented in chapter three, in the preceding section an additional function for the meniscal ring with respect to the building up of pressure in the cavity is found. To get some more insight into this function, parameter studies have been performed with respect to the interface conditions and the load which is applied to the model, respectively. In the following the consequences of the transition from the solid material models in chapter three to the mixture material models in this chapter are studied systematically.

#### 5.3.2 *interface conditions*

The interface conditions with respect to the fluid flow are considered in this sub-section. Higginson and Norman ( 1974 ) questioned the necessity of taking into account the cartilage components in the tibio-femoral joint as mixtures because of their very low permeability. Both meniscus and cartilage layer comprise a dense network of fibres at their outer surfaces and it might be speculated that this layer hampers the fluid flow across these surfaces.

Five models are considered which differ from each other with respect to the boundary conditions for the hydrostatic pressure. Two basic parameters are considered. First, there is the presence or absence of fluid in the joint cavity. The other concerns the fluid flow. Next to models in which fluid flow across the outer surfaces of components is allowed, also models with sealed mixture components and models with solid components are considered. In model A ( Fig. 5.3 ) the meniscal ring and articular cartilage layers consist of solid material while the cavity is empty. Model B is similar

to model A, with the cavity being filled by an ideal fluid. The models C and D are similar to the models A and B, respectively, except that the meniscal ring and articular cartilage layers are mixtures being sealed at their outer surfaces. Finally, model E is the model presented in the previous section, which is identical to model D apart from the fact that the outer surfaces are not sealed. The model which is similar to model C but without sealed surfaces is not taken into account here. The reason for this is that it

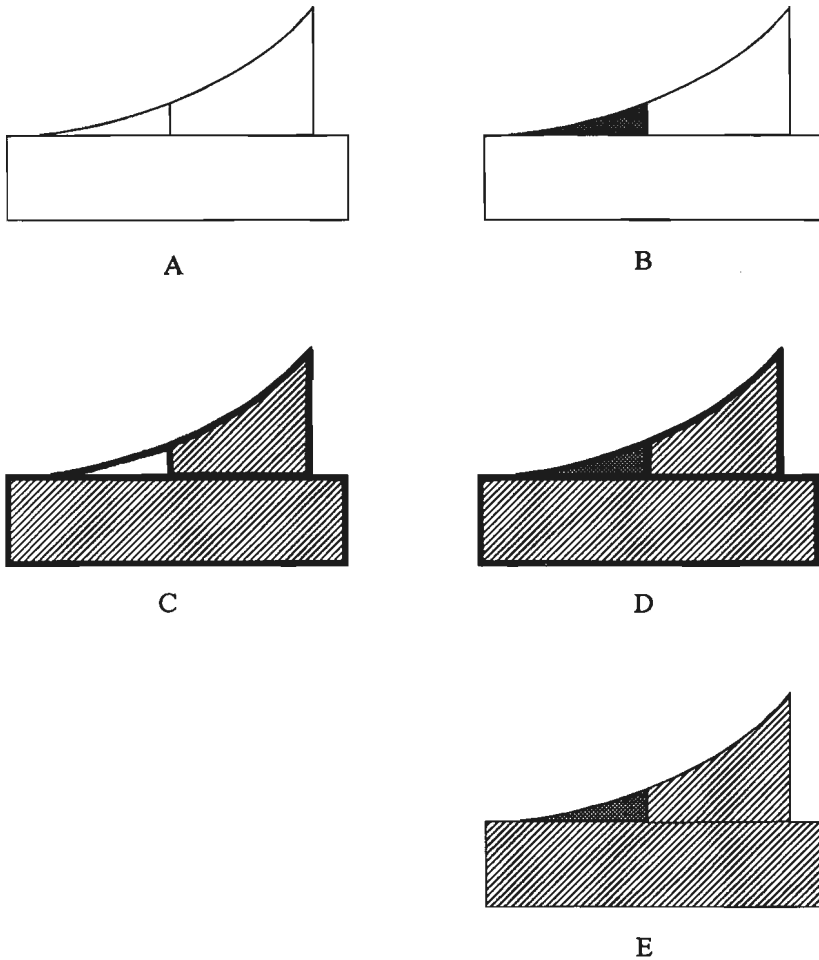


**Fig. 5.3** *Half of the cross-sections of models A to E, where fluid sub-systems ( gray ), mixture components ( dashed ) and solid components ( white ) are indicated. Impervious outer surfaces are indicated by fat lines.*

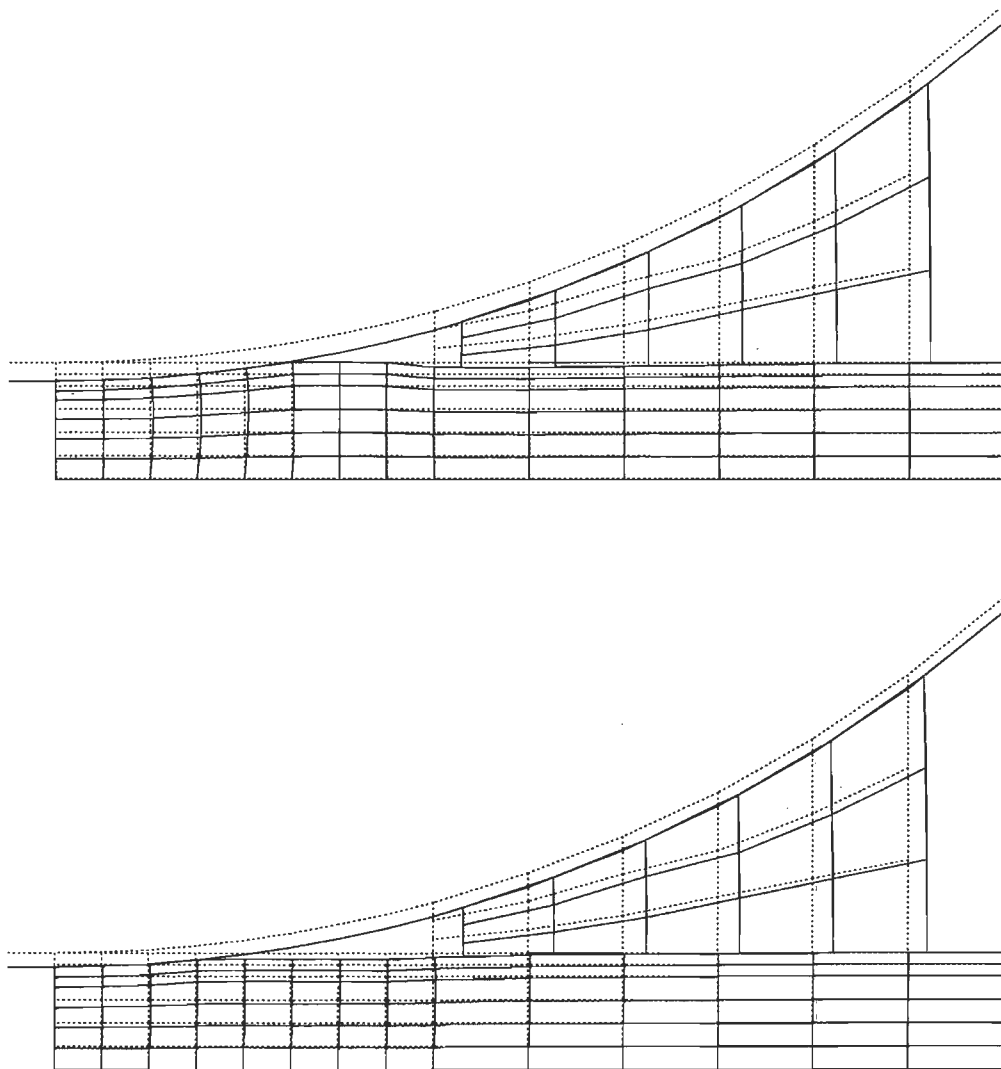


Fig. 5.4      *Finite element mesh of undeformed ( dashed ) and deformed ( drawn ) geometry of model A ( a ) and model B ( b ), respectively.*

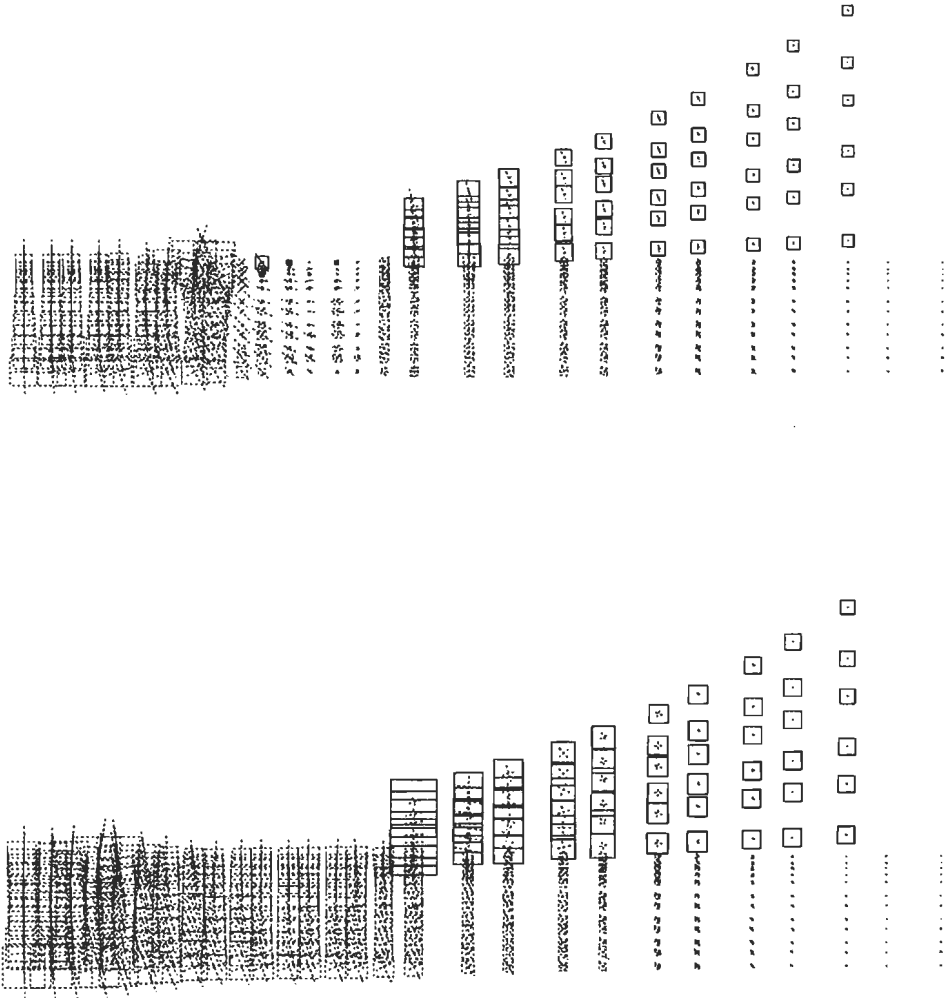


Fig. 5.5 *Principal stresses in integration points for model A ( a ) and model B ( b ), respectively. See text for further explanation.*

is considered to be a non-realistic model as no pressure is built up in the cavity although the space is enclosed. The constitutive behaviour of all models is the same as that of the model described in the previous section on the understanding that the models A and B have zero permeability.

In Figs. 5.4a and 5.4b the undeformed and deformed element meshes for the models A and B are shown. The axial compression of both models is clearly visible and larger for model A than for model B. The contact area between the rigid sphere and the tibial component is larger for model A than for model B. These effects can be deduced from the larger axial stiffness of model B as a result of the load bearing capacity of the fluid in the cavity. The volume of the cavity remains unchanged in model B while it is reduced with increasing load for model A.

The Figs. 5.5a and 5.5b represent the principal stresses related to the Cauchy stress tensor for the models A and B in the integration points. The stresses in the  $r$ - $z$ -plane are indicated by crosses while the circumferential stresses are represented by squares. Dashed figures correspond to compressive stresses, while tensile stresses are indicated by solid lines. For both models the stresses in the meniscal ring are mainly directed circumferentially. In model B (cavity filled) at the inner side of the meniscal ring the larger compressive stresses in the  $r$ - $z$ -plane are mainly radially directed, while for model A they are more axially oriented at this place.

Figs. 5.6 and 5.7 show the axial compression and the fraction of the total load that is transmitted by the meniscal ring, respectively, versus time for all five models. Because fluid flow is absent in the models A and B, their behaviour is constant in time. From Fig. 5.6 the axial stiffness for the models with a fluid filled cavity ( B, D and E ) appears to be larger than for the models with an empty cavity ( A and C ), because the fluid bears part of the load. For the former models the loading of the meniscal ring is smaller. Initially, the curves of model E are very close to the curves of model D, but as time proceeds more and more fluid is squeezed out and at the end the hydrostatic pressure equals zero everywhere, yielding the same conditions as in model A.

From these analyses it can be concluded that:

- The application of the mixture theory on the model of the tibio-femoral contact complex only leads to significant effects if the outer surfaces of the components are not sealed.

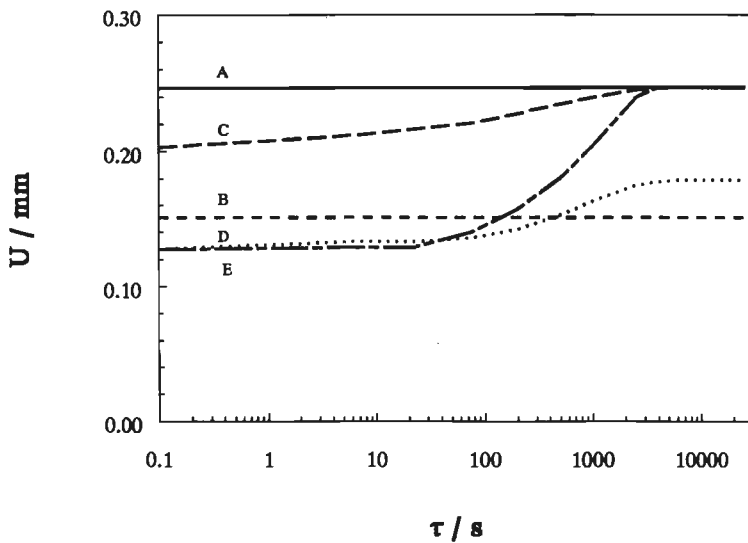


Fig. 5.6 *Axial compression of the models A to E versus time for a load step of 250 N at  $\tau = 0$  s.*

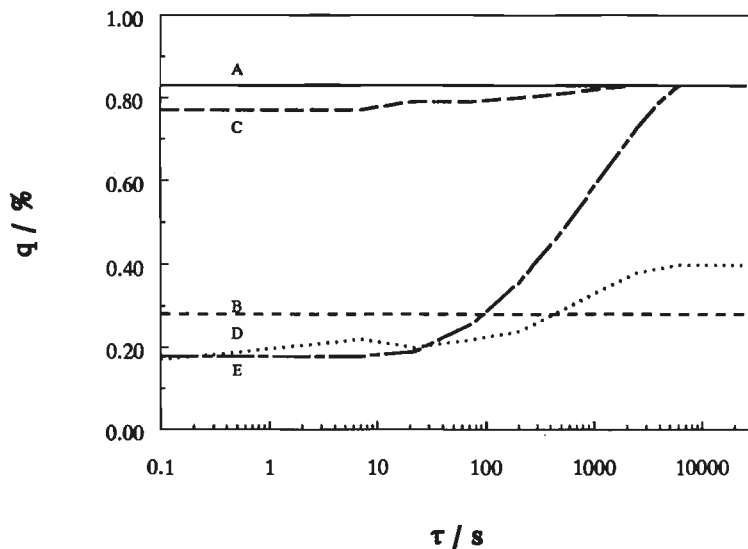


Fig. 5.7 *Part of the load borne by the meniscal ring for the models A to E versus time for a load step of 250 N at  $\tau = 0$  s.*

- If these surfaces are not sealed the load distribution depends on the load-history in such a way that the time that elapses until no further changes resulting from the applied load occur, is rather large for the parameter values.
- The fluid-filled cavity carries a large part ( up to 75 % ) of the total load applied on the model and this fraction decreases to zero when the fluid is being squeezed out of the model.

### 5.3.3 *loadings*

In the parameter studies described in chapter three, the joint load ranged from 0 to 1000 N. The load distribution appeared to depend on this load. In the preceding section all analyses were done for a step change of the load from 0 to 250 N. The influence of the magnitude of the step is still unknown. Two possible effects are proposed beforehand. The first effect concerns an increasing total compression of the model for larger loads. Thus more fluid has to be squeezed out of the model, resulting in a larger time to elapse until no further changes occur as a result of the step change of the load. In the following this period is called the relaxation time. The other effect implies an increase of the initial pressure in the cavity for larger loads. The resulting fluid velocities will increase so that the relaxation time is expected to be smaller.

Taking these contradictory effects into account it cannot be predicted whether the relaxation time will increase or decrease for larger loads. Therefore, the effect of the magnitude of the load is investigated by performing an additional analysis for a loading step of 500 N.

In Fig. 5.8 the pressure in the cavity is given as a function of time. Fig. 5.9 shows the fraction of the load transmitted by the meniscal ring versus time for both loadings. From both figures it can be seen that the relaxation time for the loading of 500 N is approximately half of the relaxation time for the loading of 250 N.

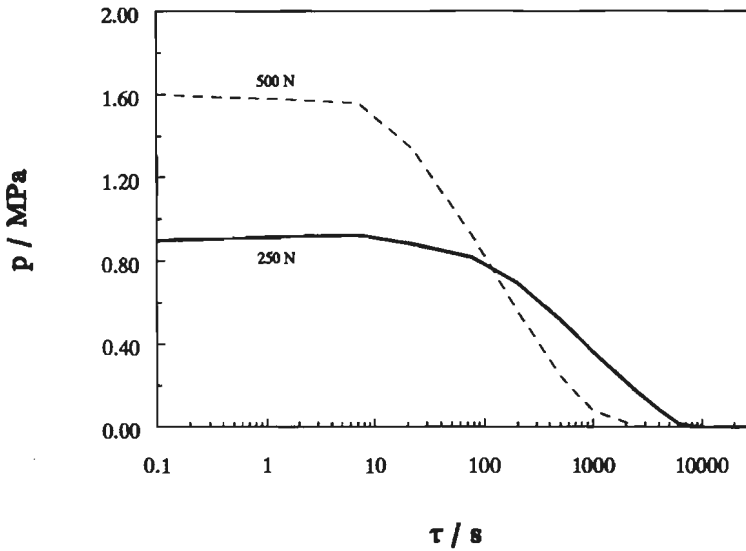


Fig. 5.8 Pressure in the cavity versus time for model E under load steps of 250 N and 500 N at  $\tau = 0$  s.

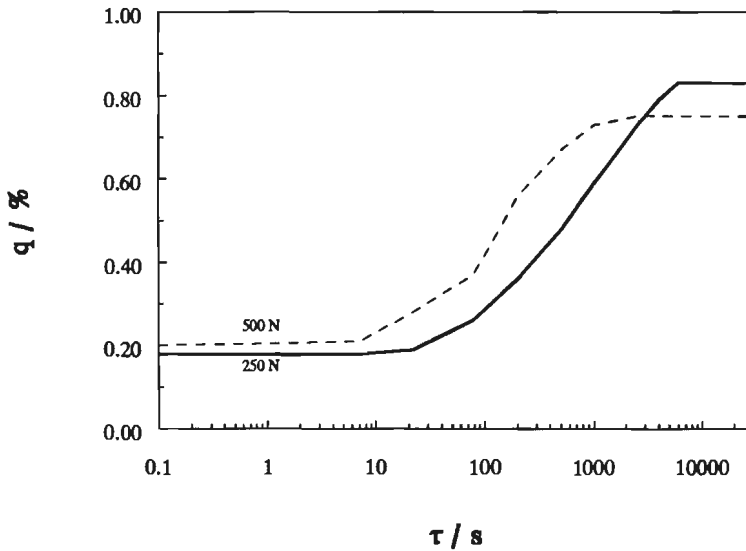


Fig. 5.9 Part of the load borne by the meniscal ring versus time for model E under load steps of 250 N and 500 N at  $\tau = 0$  s.

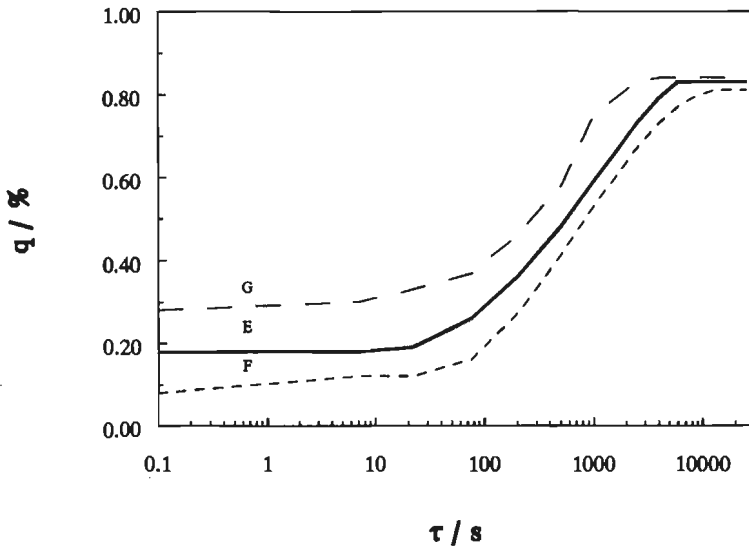


Fig. 5.10 *Part of the load borne by the meniscal ring versus time for the models E, F and G under a load step of 250 N at  $\tau=0$  s.*

#### 5.3.4 surface geometry

Both for the reference model and for the reduced model, presented in chapter 3, the curvature of the contact surface(s) appeared to have only minor effects on the load distribution in the models when the contact surfaces are covered by soft layers. This is an important characteristic for the mechanical behaviour on the tibio-femoral contact complex. Therefore, we want to know whether it also applies when mixture materials are used and the cavity is filled with fluid. Starting from model E, two models with different curvatures of the rigid spherical indenter are defined. These models are indicated by F and G and their radius is 20 mm and 60 mm, respectively. Thus, in model G the wedge of the meniscal ring and the cavity are smaller while for model F they are larger. To both models a step change of the load from 0 to 250 N is applied. After load is applied, some time elapses until only the solid materials bear load. Then, the load distribution in these models is similar to the load distribution in the reduced models in section 3.4, and the fraction of the load borne by the meniscal ring can be expected to be approximately the same for the models E, F and G. Whether this is the

case for the initial response, when fluid bears part of the load, is not clear on forehand. In Fig. 5.10 the part of the load borne by the meniscal ring versus time for the models E, F and G are shown as results of the performed numerical analyses. From this Figure the initial loadings of the meniscal ring appear to differ for the three models up to 10 %. The relaxation time for the model G, with the larger radius, is smaller, while the relaxation time for the model F with the smaller spherical radius is larger in comparison with model E.

#### *5.4 summary and conclusions*

An axisymmetric finite element model is formulated which comprises a meniscal ring and an articular cartilage layer, both considered as mixture materials which are interacting with an ideal fluid sub-system.

From parameter studies it is concluded that the application of the mixture theory in comparison with solid modelling only leads to significant effects when the outer surfaces of the components are not sealed. The load-distribution seems to change enormously during relaxation of the models. Initially the largest fraction of the load is borne by the fluid in the cavity, while at the end, when the system has reached its final configuration, the meniscal ring bears the major part of the load. Further, the relaxation time appears to depend on the magnitude of the step change of the load. Finally, the curvature of the spherical indenter appears to have significant effects on the loading of the meniscal ring, just after the step changes of load are applied and these effects disappear when the fluid is leaving the models.



## CONCLUSIONS AND RECOMMENDATIONS

### *6.1 conclusions*

For the investigations reported in this thesis, conclusions with respect to the modelling strategy as described in section 1.2, and conclusions concerning the mechanical behaviour of the tibio-femoral contact complex, are distinguished.

The modelling strategy is characterized by a stepwise approach. Successive models take more and more aspects of the mechanical behaviour of the tibio-femoral contact complex into account. The material behaviour is assumed to be physically linear and homogeneous over the joint components. Structural refinements of the materials are applied, such as the application of mixture models for the cartilage components and accounting for anisotropy in the fibrous meniscal ring. However, refinements concerning physical non-linear behaviour, material inhomogeneities or a three-dimensional geometry are left out of consideration and more priority is given to a proper description of the interaction of the several components. From the results presented in this thesis, the interaction between the components appears to be an important aspect of the load transmission in the knee joint.

The model formulation is based on the finite element method and is easily adaptable for application of more detailed and more complex material descriptions or for extension to three-dimensional models. An important aspect of the numerical formulation concerns the interaction of the different joint components. These interaction problems are solved using the directly coupled solution strategy, as described in the chapter two. This appears to be a very effective method because of the stability of the solution process.

Another important aspect of the modelling strategy is the validation of numerical results by experiments on physical models. Experimental and numerical results have to be compared with respect to a large number of quantities related to the important aspects of the actual step in the modelling process. The search for explanations for differences between experimental and numerical results is facilitated when the number of quantities, that is compared, is larger. Measuring enough quantities for this purpose is difficult.

The most important problem with respect to deformable solid and mixture components is the fact that no techniques are available for a real three-dimensional experimental registration of the deformation inside the components. Such techniques are necessary for both a reliable registration of the deformation of the physical model and the characterization of frictional and material behaviour of the real knee joint.

The mechanical characteristics, which are explored by parameter studies on the different models, are lined up and the developments of the successive models are described. Because of the abstraction of the actual models, one has to be very careful translating these characteristics to the real knee joint. However it is supposed that the effects of basic parameters in the tibio-femoral contact complex are properly described.

Starting from the reference model, as described in section 3.2, especially the presence of soft layers on the articular surfaces of femur and tibia appears to be very important for the load distribution in the joint. When such a layer is applied, variations with respect to the curvature of the tibial plateau have only minor effects on the loading of the meniscal ring. Taking these characteristics into account, the reduced model is derived from the reference model. Therefore, the bony components are left out of consideration and only one cartilage layer is modelled. The model components are structurally refined by application of mixture materials. The cavity enclosed by the meniscal ring and the articular surfaces is filled by an ideal fluid and bears a considerable part of the total load. Possibilities of this fluid to flow out of the model have to be investigated into more detail.

## *6.2 recommendations*

The most general recommendation for modelling the tibio-femoral joint is to continue the similar strategy, with a stepwise evolution of models, as applied in this thesis. Although the investigated mechanical characteristics seem to be sometimes trivial, they are not because they cannot be predicted. To keep the several effects distinguishable, it is advisable for every step in the modelling process to add or change only a very limited number of parameters.

As long as only concise data are available with respect to the mechanical characteristics of the real tibio-femoral joint, stepwise unravelling of mechanical characteristics is performed in successive modelling steps. The characteristics for a certain modelling stage are used as a guide-line for choosing subsequent modelling steps.

A possible way to arrive at a model for the complete joint is as follows. First, attention has to be focussed on the interaction of mixture components with a Newtonian fluid. Then squeeze film effects in both the direct and indirect contact area have to be investigated. This aspect could cause the relaxation time of the model to decrease considerably. Next, the application of more complex loading patterns, such as harmonic axial loads, can be performed. When a three-dimensional formulation is applied also bending of the knee may be simulated. Finally, more detailed descriptions of the material and geometry of the real joint can be accounted for in the model. In this stage e.g. physical non-linear material behaviour and effects resulting from moving electrical loadings in the articular cartilage can be taken into account. At the end, the model of the tibio-femoral contact complex has to be integrated with or extended to other sub-connections and a model of the complete joint results.



## REFERENCES

- Ahmed, A.M. and Burke, D.L. ( 1983 ) In-vitro measurements of static pressure distribution in synovial joints, *J. of Biomech. Engng.*, **105**, 216-225.
- Armstrong, C.G. and Mow, V.C. ( 1980 ) Friction, lubrication and wear of synovial joints, *Sc. Foundations of Orthop. and Traumatology*, edited by R.Owen, J. Goodfellow and P. Bulloughs, W. Heinemann Medical Books Ltd, Londen.
- Aspden, R.M. ( 1985 ) A model for the function and failure of the meniscus, *Engng. in Medicine*, **14**, 119-122.
- Aspden, R.M., Yarker, Y.E. and Hukins, D.W.L. ( 1985 ) Collagen orientations in the meniscus of the knee joint, *J. of Anatomy*, **140**, 371-380.
- Baaijens, F.P.T. ( 1987 ) On a numerical method to solve contact problems, *Ph.D.-thesis Eindhoven University of Technology, The Netherlands*.
- Bathe, K.J. ( 1990 ) Finite-Elemente-Methoden, *Springer Verlag, New-York Berlin Heidelberg Paris Tokyo*.
- Bathe, K.J. and Chaudhary, A. ( 1985 ) A solution method for planar and axisymmetric contact problems, *Int. J. for Num. Meth. in Engng.*, **21**, 65-88.
- Bullough, P.G., Munera, L., Murphy, L. and Weinstein, A.M. ( 1970 ) The strength of the menisci of the knee as it relates to their fine structure, *J. of Bone and Joint Surg.*, **52B**, 564-570.
- De Lange, A., Jaspers, P., Huiskes, R. and Van Rens, Th.J.G. ( 1979 ) A rheologic model of the menisci in static and dynamic load transmission, *Proc. of 7th Int. Congress on Biomech.*, Warsaw, Poland.
- De Keizer, G. ( 1976 ) On synovial fluid, joint lubrication and osteoarthritis, *Ph.D.-thesis State University of Utrecht, The Netherlands*.
- DIANA finite element analysis ( 1990 ) User manual, *T.N.O. Institute for Building Materials and Structures, Rijswijk, The Netherlands*.
- Dortmans, L.J.M.G. ( 1988 ) Aspects of the dynamic behaviour of the human knee joint, *Ph.D.-thesis Eindhoven University of Technology, The Netherlands*.
- Dortmans, L., Jans, H., Sauren, A., and Huson, A. ( 1991<sup>a</sup> ) Non-linear dynamic behaviour of the human knee joint. Part I: Post-mortem frequency domain analyses, *accepted for publication in J. of Biomech. Engng.*

- Dortmans, L., Jans, H., Sauren, A., and Huson, A. ( 1991<sup>b</sup> ) Non-linear dynamic behaviour of the human knee joint. Part II: Time-domain analyses: effects of structural damage in post-mortem experiments, *accepted for publication in J. of Biomech. Engng.*
- Dowson, D. ( 1967 ) Modes of lubrication in human joints, *Engng. in Medicine*, 181, 3J.
- Dowson, D., Unsworth, A. and Wright, V. ( 1970 ) Analysis of boosted lubrication in human joints, *J. of Mech. Engng Sc.*, 12, 364.
- Droogendijk, L. ( 1984 ) On the lubrication of synovial joints, *Ph.D.-thesis Twente University, The Netherlands.*
- Fahmy, N.R.M., Williams, E.A. and Noble, J. ( 1983 ) Meniscal pathology and osteoarthritis of the knee, *J. of Bone and Joint Surg.*, 65B, 24-28.
- Fairbank, T.J. ( 1948 ) Knee joint changes after meniscectomy, *J. of Bone and Joint Surg.*, 30B, 664-670.
- Guerra, F.M. and Browning, R.V. ( 1983 ) Comparison of two slideline methods using Adina, *Computers and Structures*, 17, 819-834.
- Hayes, W.C. ( 1986 ) Bone mechanics: From tissue mechanical properties to an assessment of structural behaviour, *in Frontiers in Biomechanics, eds. by G.W. Schmid-Schoenbein, S.L.-Y. Woo and B.W. Zweifach, Springer-Verlag, New York Berlin Heidelberg Tokyo.*
- Hefzy, M.S. and Zoghi M. ( 1988 ) The menisci: a finite element model, *Proc. of 34th Ann. Meeting Orthop. Research Soc.*, 149.
- Hendriks, M.A.N. ( 1991 ) Identification of the mechanical behaviour of solid materials, *Ph.D.-thesis Eindhoven University of Technology, The Netherlands.*
- Higginson, G.R. and Norman, R. ( 1974 ) The lubrication of porous elastic solids with reference to the functioning of human joints, *J. of Mech. Engng. Sc.*, 16, 250-257.
- Holmes, M.H. and Mow, V.C. ( 1990 ) The nonlinear characteristics of soft gels and hydrated connective tissues in ultrafiltration, *J. of Biomech.*, 23, 1145-1156.
- Horsten, J.B.A.M. ( 1990 ) On the analysis of moving heart valves, *Ph.D.-thesis Eindhoven University of Technology, The Netherlands.*
- Hou, J. ( 1989 ), Formulation of synovial fluid-articular surface interface conditions and asymptotic and numerical analyses of squeeze film, *Ph.D.-thesis, Rensselaer Polytechnic institute, United States.*

- Hou, J.S., Holmes, M.H., Lai, W.M. and Mow, V.C. ( 1989 ) Boundary conditions at cartilage-synovial fluid interface for joint lubrication and theoretical verifications, *J. of Biomech. Engng.*, 111, 78-87.
- Hughes, Th.J.R., Taylor, R.L., Sackman, J.L., Curnier, A. and Kanoknukulchai, W. ( 1976 ) A finite element method for a class of contact-impact problems, *Comp. Meth. in Appl. Mech. and Engng.*, 8, 249-276.
- Huiskes, R., Kremers, J., De Lange, A., Woltering, H. and Van Rens, T. ( 1985 ) An analytical stereo-photogrammetric method to determine the three dimensional geometry of articular surfaces, *J. of Biomech.*, 18, 559-570.
- Jans, H.W.J, Dortmans, L.J.M.G., Sauren, A.A.H.J. and Huson, A. ( 1988 ) An experimental approach to evaluate the dynamic behavior of the human knee, *J. of Biomech. Engng.*, 110, 69-73.
- Jaspers, P., De Lange, A., Huiskes, R. and Van Rens, Th.J.G. ( 1980 ) The mechanical function of the meniscus, experiments on cadaveric pig knee-joints, *Acta Orthop. Belgica*, 46, 663-668.
- Jaspers, P. ( 1982 ) De mechanische functie van de menisci in het kniegewricht ( in Dutch ), *Ph.D.-thesis, University of Nijmegen, The Netherlands.*
- Kurosawa, H., Fukubayashi, T. and Nakajima, H. ( 1980 ) Load-bearing mode of the knee joint, *Clin. Orthop. and Rel. Res.*, 149, 283-290.
- Mac Conaill, M.A. ( 1932 ) The function of intra-articular fibro-cartilages, with special reference to the knee and inferior radio-ulnar joints, *J. of Anatomy*, 68, 210-227.
- Minns, R.J. and Steven, F.S. ( 1977 ) The collagen fibril organization in human cartilage, *J. of Anatomy*, 123, 437-457.
- Mow, V.C., Holmes, M.H. and Lai, W.M. ( 1984 ) Fluid transport and mechanical properties of articular cartilage: a review, *J. of Biomech.*, 17, 337-394.
- Oomens, C.W.J. ( 1985 ) A mixture approach to the mechanics of skin and subcutis, *Ph.D.-thesis, Twente University, The Netherlands.*
- Op de Camp, O. ( 1990 ) Experimentele analyses aan een eenvoudig model van de knie, *Eindhoven University of Technology, The Netherlands, internal report W.F.W 90.029.*
- Radin, E.L. and Paul, I.L. ( 1971 ) Response of joints to impact loading, *Arthritis and Rheumatics*, 14, 356-362.

- Radin, E.L. and Paul, I.L. ( 1972 ) A consolidated concept of joint lubrication, *J. of Bone and Joint. Surg.*, 54A, 607-616.
- Sauren, A.A.H.J., Huson, A. and Schouten, R.Y. ( 1984 ) An axisymmetric finite element analysis of the mechanical function of the meniscus, *Int. J. of Sports and Medicine*, 5, 93-95.
- Schouten, J. ( 1990 ) Constitutief gedrag van elastisch materiaal, *Eindhoven University of Technology, The Netherlands, internal report W.F.W 90.008*.
- Schreppers, G.J.M.A., Sauren, A.A.H.J. and Huson, A. ( 1990 ) A numerical model of the load transmission in the tibio-femoral contact area, *J. of Engng. in Medicine*, 204, 53-59.
- Seedhom, B.B. and Hargreaves, D.J. ( 1979 ) Transmission of the load in the knee joint with special reference to the role of the menisci, *J. of Engng. in Medicine*, 8, 207-228.
- Snijders, H. ( 1989 ) personal communication, *State University Limburg, The Netherlands*.
- Spilker, R.L., Suh, J.-K. and Mow, V.C. ( 1990 ) Effects of friction on the unconfined compressive response of articular cartilage: a finite element analysis, *J. of Biomech. Engng.*, 112, 138-146.
- Spilker, R.L. and Suh, J.-K. ( 1990 ) Formulation and evaluation of a finite element model for the biphasic model of hydrated soft tissues, *Computers and Structures*, 35, 425-439.
- Starmans, F.J.M. ( 1989 ) On friction in forming, *Ph.D.-thesis Eindhoven University of Technology, The Netherlands*.
- Swann, A.C. and Seedhom, B.B. ( 1989 ) Improved techniques for measuring the indentation and thickness of articular cartilage, *J. of Engng. in Medicine*, 203, 143-150.
- Tissakht, M., Farinaccio, R. and Ahmed, A.M. ( 1989 ) Effect of ligament attachments on the response of the knee menisci in compression & torsion: a finite-element study, *Proc. of 35th Ann. Meeting Orthop. Research Soc.*, 203.
- Walker , P.S., Dowson, D., Longfield, M.D. and Wright, V. ( 1968 ) Boosted lubrication in synovial joints by fluid entrapment and enrichment, *Ann. rheum. Dis.*, 27, 512-520.
- Walker, P.S. and Erkman, M.J. ( 1975 ) The role of the menisci in force transmission across the knee, *Clin. Orthop. and Rel. Res.*, 109, 184-192.

- Walker, P.S. and Hajek, J.V. ( 1972 ) The load-bearing area in the knee joint, *J. of Biomech.*, 5, 581-589.
- Wismans, J., Veldpaus, F., Janssen, J., Huson, A. and Struben, P. ( 1980 ) A three dimensional mathematical model of the knee-joint, *J. of Biomech.*, 13, 677-685.
- Zhong, Z. and Nilsson, L. ( 1990 ) A contact searching algorithm for general 3-D contact-impact problems, *Computers and Structures*, 34, 327-335.

appendix A

## DIRECTLY AND ITERATIVELY COUPLED SOLUTION METHODS

The direct fully coupled and the iteratively coupled solution strategies are illustrated using a simple system. This system comprises two linear spring elements with stiffnesses  $K_1$  and  $K_2$ , which are both considered to be sub-systems.

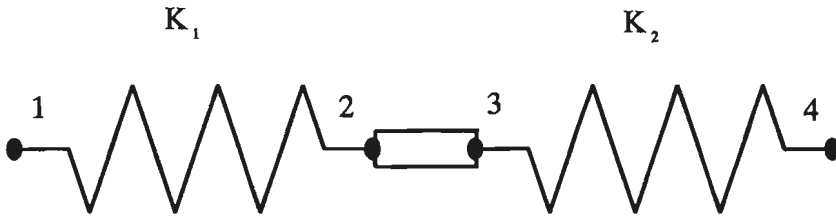


Fig. A.1 *One-dimensional system comprising two structures.*

The springs connect node 1 to 2 and 3 to 4 ( Fig. A.1 ). The system is one-dimensional. The nodal displacements, the internal nodal forces, external nodal forces and nodal contact forces of node P are indicated by  $u^p$ ,  $f^p$ ,  $r^p$  and  $c^p$ , respectively. It is assumed that the nodes 2 and 3 are fixed to each other which results in the contact conditions

$$u^2 = u^3 \quad \text{and} \quad c^2 = -c^3 \tag{A.1}$$

Prescribing the displacement of node 1 and suppressing the displacement of node 4

yields the boundary conditions

$$u^1 = u \quad \text{and} \quad u^4 = 0 \quad (\text{A.2})$$

The equilibrium equation is applied to all four nodes

$$\begin{cases} f^1 - r^1 = 0 \\ f^2 - c^2 = 0 \\ f^3 - c^3 = 0 \\ f^4 - r^4 = 0 \end{cases} \quad (\text{A.3})$$

direct fully coupled solution strategy

Both sub-systems are assembled in one matrix equation

$$\begin{bmatrix} -K_1 & K_1 & 0 & 0 \\ K_1 & -K_1 & 0 & 0 \\ 0 & 0 & -K_2 & K_2 \\ 0 & 0 & K_2 & -K_2 \end{bmatrix} \begin{bmatrix} u^1 \\ u^2 \\ u^3 \\ u^4 \end{bmatrix} = \begin{bmatrix} r^1 \\ 0 \\ 0 \\ r^4 \end{bmatrix} + \begin{bmatrix} 0 \\ c^2 \\ c^3 \\ 0 \end{bmatrix} \quad (\text{A.4})$$

Using the contact and boundary conditions, by substituting  $u^3$  and  $c^3$  by  $u^2$  and  $-c^2$ , respectively, this equation is transformed into

$$\begin{bmatrix} -K_1 & K_1 & 0 \\ K_1 & -(K_1+K_2) & K_2 \\ 0 & K_2 & -K_2 \end{bmatrix} \begin{bmatrix} u \\ u^2 \\ 0 \end{bmatrix} = \begin{bmatrix} r^1 \\ 0 \\ r^4 \end{bmatrix} \quad (\text{A.5})$$

from which it easily can be derived that

$$u^2 = \frac{K_1}{K_1+K_2} u \quad (\text{A.6})$$

iteratively coupled solution strategy

Let a first estimate be

$$u^2 = 0 \quad (\text{A.7})$$

From the equations concerning the first sub-system

$$\begin{bmatrix} -K_1 & K_1 \\ K_1 & -K_1 \end{bmatrix} \begin{bmatrix} u \\ 0 \end{bmatrix} = \begin{bmatrix} r^1 \\ 0 \end{bmatrix} + \begin{bmatrix} 0 \\ c^2 \end{bmatrix} \quad (\text{A.8})$$

it is calculated that

$$c^2 = K_1 u \quad (\text{A.9})$$

Because  $c^3 = -c^2$ , now an estimate of the contact force of the second sub-system is known and from the equation concerning the second sub-system

$$\begin{bmatrix} -K_2 & K_2 \\ K_2 & -K_2 \end{bmatrix} \begin{bmatrix} u^3 \\ 0 \end{bmatrix} = \begin{bmatrix} 0 \\ r^4 \end{bmatrix} + \begin{bmatrix} -K_1 u \\ 0 \end{bmatrix} \quad (\text{A.10})$$

it is calculated that

$$u^3 = \frac{K_1}{K_2} u \quad (\text{A.11})$$

Using  $u^2 = u^3$ , from ( A.11 ) a second estimate for  $u^2$  is obtained and the iterative solution process is continued. The iterative change of  $u^2$  after the  $i$ -th iteration stroke is given by

$${}^i u^2 - {}^{i-1} u^2 = - \left( - \frac{K_1}{K_2} \right)^i u \quad (\text{A.12})$$

From ( A.12 ) it is concluded that the iteration process will converge to the solution ( A.6 ) only if  $K_1 < K_2$ .



appendix B

## CONSTITUTIVE BEHAVIOUR OF SILICONE RUBBER

For three different silicone rubbers ( white, yellow and green ) the constitutive parameters are established using the uniaxial tensile test. Therefore, four or five specimens of every material of approximately 110 x 10 x 1 mm are prepared and loaded in the uniaxial tensile test where the force is measured for different elongations. The tested specimens seemed not to be fully elastic but some stress-relaxation occurred. The elongation is prescribed in steps of 4 mm while every step 150 seconds it is waited before the related force is noted. Following this procedure, for every step the relaxed state is considered, because after this time the force does hardly change anymore. With respect to the experiments of the knee model equivalent strain steps are prescribed while displacements and loading are measured after similar relaxation periods. Let  $t$  be the second Piola-Kirchhoff stress tensor and  $B$  the left Cauchy-Green tensor, then the Mooney-Rivlin constitutive relation for incompressible materials is formulated as

$$t = \alpha \frac{dI_B}{dB} + \beta \frac{dII_B}{dB} \quad (B.1)$$

where  $\alpha$  and  $\beta$  are material parameters and  $I_B$  and  $II_B$  are the first and second invariants with respect to  $B$ , respectively. For the uniaxial tensile test, equation ( B.1 ) can be transformed into

$$F = \alpha A_0 \left( \lambda - \frac{1}{\lambda^2} \right) + \beta A_0 \left( 1 - \frac{1}{\lambda^3} \right) \quad (B.2)$$

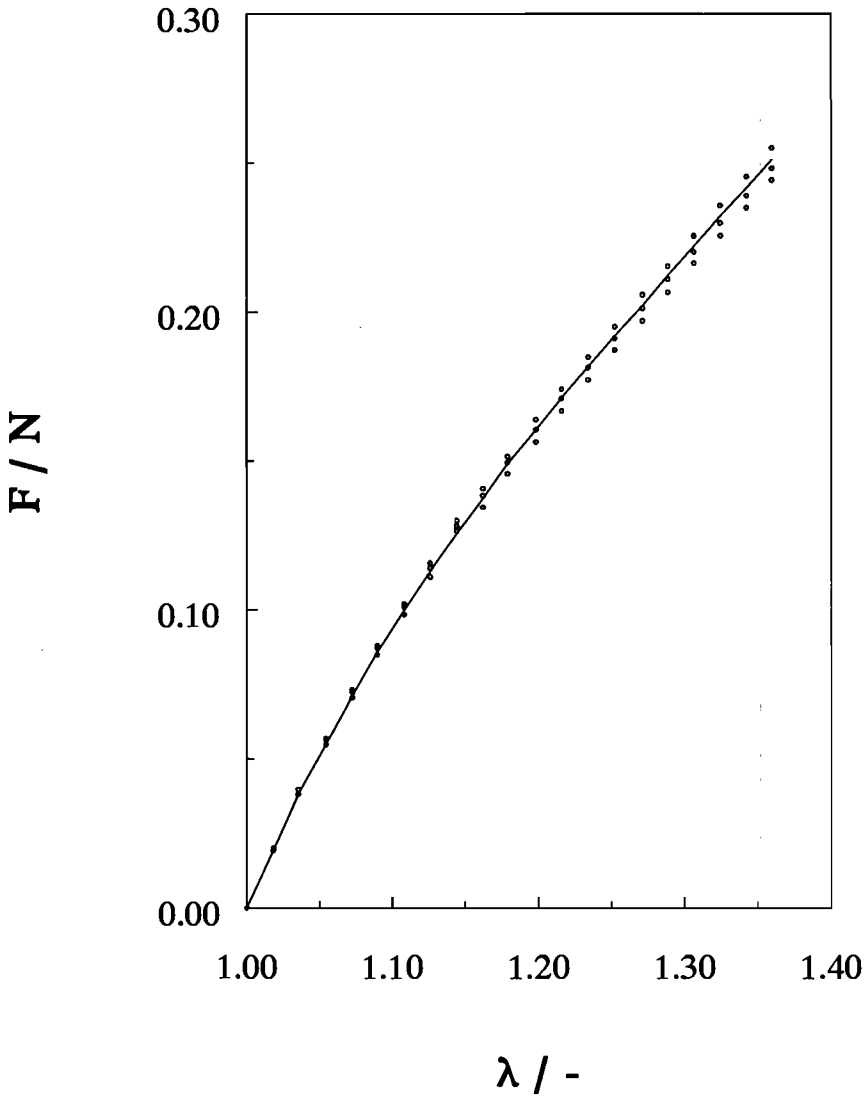


Fig. B.1 *Force - elongation diagram for the white rubber, where markers represent experimental measurements and the drawn line represents the fitted Mooney-Rivlin equation.*

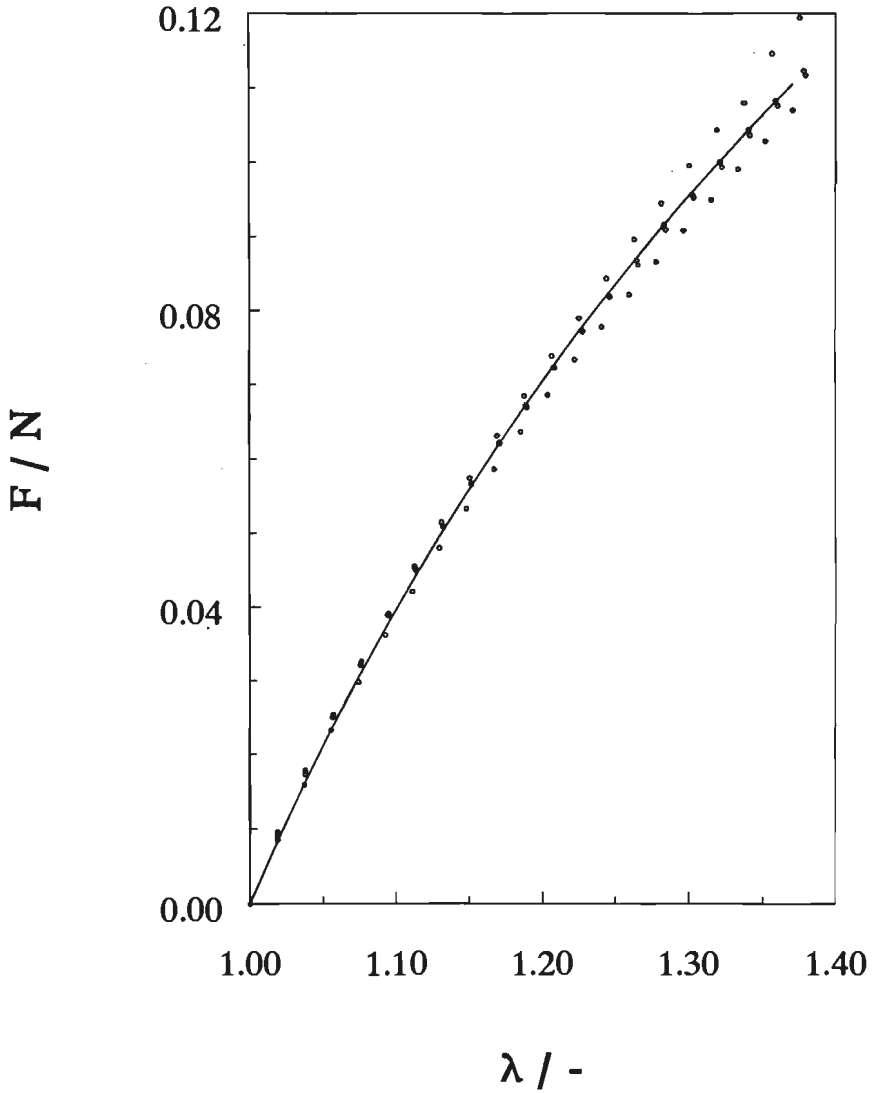


Fig. B.2 *Force - elongation diagram for the yellow rubber, where markers represent experimental measurements and the drawn line represents the fitted Mooney-Rivlin equation.*

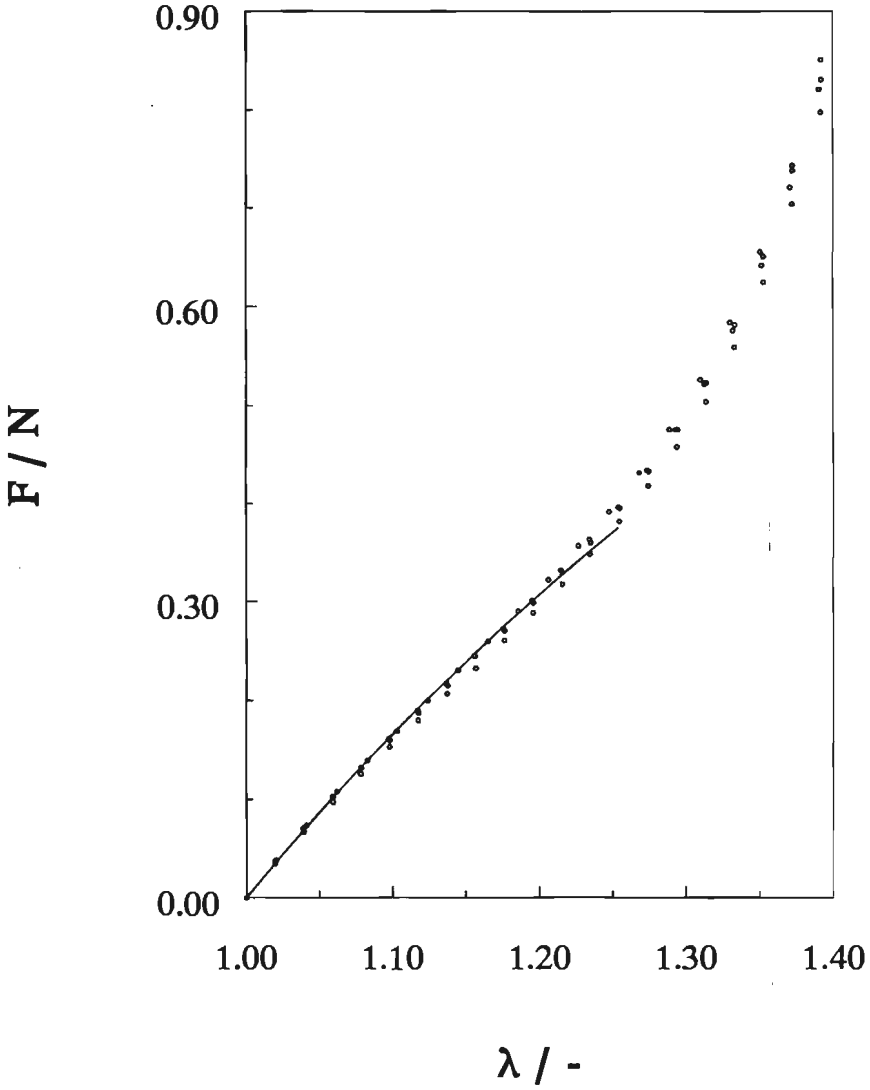


Fig. B.3 *Force - elongation diagram for the green rubber, where markers represent experimental measurements and the drawn line represents the fitted Neo-Hookean equation.*

with  $F$  representing the tensile force and  $\lambda$  being the elongation factor. Here,  $A_0$  is the area of the cross-section of the specimen perpendicular to the stress direction in the unloaded situation. Using regression analysis  $\alpha$  and  $\beta$  are deduced from equation ( B.2 ) which fits best to the measurements. In Figs. ( B.1 ), ( B.2 ) and ( B.3 ) these measurements and the appropriate Mooney-Rivlin model are shown for the white, yellow and green rubber, respectively. The related material coefficients are given by

	white	yellow	green
$\alpha$	0.15	0.08	0.61
$\beta$	0.21	0.07	0.00

table B.1     *Material coefficients.*

Because the best fitted Mooney-Rivlin equation for the green rubber is not thermodynamically allowable (  $\beta < 0$  ), it is prescribed that  $\beta = 0.00$  and Neo-Hookean behaviour results. As the green rubber is stiffer, for the deformation range we are interested in only the smaller  $\lambda$ 's can be taken into account and doing so the increase of  $F$  for  $\lambda > 1.25$  will not disturb the fitting.



## SAMENVATTING

Het doel van dit onderzoek is om het inzicht in de mechanische functie van de gewrichtsonderdelen in het contact gebied van femur en tibia te vergroten. De beschouwde onderdelen zijn femur, tibia, kraakbeenlagen, menisci en synoviaal vloeistof. De mechanische functies van de gewrichtsonderdelen zijn afhankelijk van hun interacties met andere onderdelen. Er wordt uitgegaan van een stapsgewijze modelontwikkeling waarbij wordt begonnen met eenvoudige modellen. In iedere stap worden parameterstudies uitgevoerd om de functies van de relevante onderdelen te onderzoeken. Numerieke analyses worden uitgevoerd met behulp van de eindige elementen methode en de geldigheid van de resultaten wordt getoetst door experimenten met fysische modellen. Contactproblemen zijn gedefinieerd door de balansvergelijkingen voor de afzonderlijke onderdelen en de contactcondities. Deze condities en de contactkrachten zijn in het algemeen afhankelijk van de posities en de deformaties van alle onderdelen in het beschouwde systeem. Voor vaste stof/vaste stof interacties met grote slip wordt een probleemformulering uitgewerkt waarbij de wrijving nul is verondersteld. Dit algoritme blijkt voor het oplossen van algemene contactproblemen goed te functioneren. Een rotatie-symmetrisch model is gebruikt om de belastingdoorleiding in het contact tussen femur, tibia en meniscus te analyseren. Dit model gaat uit van lineair elastisch materiaalgedrag, statische belastingen en wrijvingsloze slip in de contacten tussen de componenten. Het onderzoek is gericht op de effecten van de geometrie van het tibiale oppervlak, de aanwezigheid van zachte lagen op botcomponenten en anisotrope eigenschappen van de meniscus op de belastingdoorleiding. Studies met acht combinaties van parameters zijn uitgevoerd, uitgaande van een eenvoudig referentiemodel. De aanwezigheid van kraakbeenlagen en de stijfheid van de meniscus in de omtrekrichting blijken van groot belang te zijn voor de belastingverdeling. Vervolgens wordt de probleemformulering zodanig uitgebreid dat modelcomponenten kunnen worden beschouwd als een mengsel van een vaste stof en een vloeistof. Interacties tussen mengsels onderling en interacties tussen mengsels en vloeistof kunnen gesimuleerd worden. In het model worden de kraakbeenlaag en de meniscus als mengsels beschouwd. Deze componenten interacteren met een ideale vloeistof die de synovia representeert. Slip zonder wrijving in de contacten is mogelijk. De responsie van het model ten gevolge van een stap belasting wordt berekend. Effecten van de permeabiliteit van buitenoppervlakken en van verschillende belastingen worden onderzocht. De belastingverdeling in het model blijkt aanzienlijk te variëren in de tijd.

## STELLINGEN

behorende bij het proefschrift

### FORCE TRANSMISSION IN THE TIBIO-FEMORAL CONTACT COMPLEX

1. Voor de experimentele validatie van resultaten van analyses met sterk geschematiseerde fysisch-mathematische modellen van het kniegewricht is het gebruik van niet-biologische structuren zinvol.  
( dit proefschrift, hoofdstukken 1 en 3 )
2. De volledig gekoppelde directe oplossingsstrategie kan leiden tot een stabiel algoritme voor problemen waarbij interactie optreedt tussen een vaste stof en een vloeistof.  
( dit proefschrift, hoofdstukken 2 en 5 )
3. De menisci in het tibio-femorale gewricht dragen in belangrijke mate bij tot een gelijkmatige belastingverdeling in het gewricht. Dit geldt voor schokbelastingen en statische belastingen.  
( dit proefschrift, hoofdstukken 3 en 5 )
4. In vergelijking met fenomenologische materiaalmodellen bieden structurele materiaalmodellen meer perspectief bij het verkrijgen van inzicht in mechanische karakteristieken van ingewikkelde structuren.
5. Om praktische redenen verdient een gesegmenteerde programma-opbouw de voorkeur bij het ontwikkelen en testen van grote software-systemen.
6. Het beschikbaar zijn van snelle computers werkt inefficiënt gebruik ervan in de hand.
7. Multi-disciplinair werken weerspiegelt te vaak de statistische wetmatigheid van regressie naar het gemiddelde.

8. De begrippen centripetaalkracht, centrifugaalkracht en Corioliskracht worden vaak gebruikt als vlaggen om een niet begrepen lading te dekken.
9. Het gebruik van 'schijnkrachten' om een dynamisch probleem tot een 'schijnbaar' statisch probleem te transformeren doet geen recht aan het feit dat een echt statisch probleem een bijzonder geval is van een dynamisch probleem. Bovendien kan deze werkwijze leiden tot oneigenlijke en foute beschouwingen.
10. Wat inspanning en beloning betreft zijn er veel overeenkomsten tussen amateur-topsporters en assistenten in opleiding.

Eindhoven, juni 1991

Gerd-Jan Schreppers